1-1-1995

Test and analysis methods for resolving fan/motor vibration problems in air-conditioning units

Xiaolei Teng
University of Nevada, Las Vegas

INFORMATION TO USERS

This manuscript has been reproduced from the microfilm master. UMI films the text directly from the original or copy submitted. Thus, some thesis and dissertation copies are in typewriter face, while others may be from any type of computer printer.

The quality of this reproduction is dependent upon the quality of the copy submitted. Broken or indistinct print, colored or poor quality illustrations and photographs, print bleedthrough, substandard margins, and improper alignment can adversely affect reproduction.

In the unlikely event that the author did not send UMI a complete manuscript and there are missing pages, these will be noted. Also, if unauthorized copyright material had to be removed, a note will indicate the deletion.

Oversize materials (e.g., maps, drawings, charts) are reproduced by sectioning the original, beginning at the upper left-hand corner and continuing from left to right in equal sections with small overlaps. Each original is also photographed in one exposure and is included in reduced form at the back of the book.

Photographs included in the original manuscript have been reproduced xerographically in this copy. Higher quality 6" x 9" black and white photographic prints are available for any photographs or illustrations appearing in this copy for an additional charge. Contact UMI directly to order.

UMI

A Bell & Howell Information Company
300 North Zeeb Road, Ann Arbor, MI 48106-1346 USA
313/761-4700 800/521-0600

TEST AND ANALYSIS METHODS FOR RESOLVING FAN/MOTOR VIBRATION PROBLEMS IN AIR-CONDITIONING UNITS

by

Xiaolei Teng

A thesis submitted in partial fulfillment

of the requirements for the degree of

Master of Science

in

Mechanical Engineering

Department of Mechanical Engineering

University of Nevada, Las Vegas

August 1995

The Thesis of Xiaolei Teng for the degree of Master of Science in Mechanical Engineering is approved.

Chairperson, Douglas D. Reynolds, Ph.D.

Co-Chairperson, Mohamed ~~B.E.~~ Trabia, Ph.D.

Examining Committee Member, Georg F. Mauer, Ph.D.

Examining Committee Member, Woosoon Yim, Ph.D.

Graduate Faculty Representative, Samaan Ladkany, Ph.D., PE.

Interim Dean of the Graduate College, Cheryl L. Bowles, Ed.D.

University of Nevada, Las Vegas

August 1995

ABSTRACT

This thesis deals with part of ASHRAE Research Project No. 685-RP: Test and Analysis Methods for Resolving Fan/Motor Vibration Problems in Air-Conditioning Units. The objective of the ASHRAE Research Project No. 685-RP: Test and Analysis Methods for Resolving Fan/Motor Vibration Problems in Air-Conditioning Units, is to develop the basic analytical models and experimental procedures that can be used to find the vibration modes associated with fan impeller, motor and motor mount in air-conditioning units that are excited by fan impeller unbalance, taking into account the gyroscopic effect of the rotating fan impeller.

Two air-conditioning units were investigated in the project. They were designated as test units #1 and #2. For the test unit #1 and test unit #2, the vibration problems associated with fan impeller, motor and motor mount system that are excited by fan impeller unbalance taking into account the gyroscopic effect of the rotating fan impeller were investigated. It was proved, both theoretically and experimentally, that the gyroscopic effect of the rotating fan impeller did have significant effect on the forward vibration modes of the system. The classical approach and energy approaches were used in the three dimensional lumped parameter model development, in which the gyroscopic effect of rotating fan impeller was included. In the classical approach, the gyroscopic effect of the rotating fan impeller gave an additional damping matrix. In the energy approaches, additional terms were added to the stiffness matrix due to the gyroscopic effect of the rotating fan impeller. All these additional terms, either in the damping matrix

or in the stiffness matrix, represent the modal coupling between the motions in the two different planes. The model from classical approach and the model from energy approach gave very good predictions about the forward rocking mode, which is the most important vibration mode in this work.

Both non-rotating and rotating tests were conducted in this work. The non-rotating tests were used to measure the vibration modes associated with fan impeller, motor and motor mount system and to identify the parameters used in the analytical models. The rotating tests were used to measure the vibration mode shifting due to the gyroscopic effect of the rotating fan impeller and to locate the resonance speeds corresponding to both the forward and backward rocking modes. The results from analytical models agreed very well with the experimental results both for the non-rotating and rotating tests.

TABLE OF CONTENTS

LIST OF FIGURES

LIST OF TABLES

NOMENCLATURE

f_x = The resonance frequency of the swaying mode in the x direction, Hz.
f_y = The resonance frequency of the swaying mode in the y direction, Hz.
f_z = The resonance frequency of the translational mode in the z direction, Hz.
$f_{\theta x}$ = The resonance frequency of the rocking mode in the xz plane, Hz.
$f_{\theta y}$ = The resonance frequency of the rocking mode in the yz plane, Hz.
F' = The force measured from the load cell, N.
F = The force between the tip and the impact surface, N.
a = The acceleration, g.
g = The acceleration of gravity, g = 9.81 m/s^2.
E'_f = The voltage of the load cell of the impact hammer, Volt.
E_a = The voltage of the accelerometer, Volt.
S_f = The sensitivity of the load cell of the impact hammer, mV/N.
S_a = The sensitivity of the accelerometer, mV/g.
H(f) = The true frequency response of the calibration system, m/Ns^2.
H'(f) = The measured frequency response of the calibration system, m/Ns^2.
$C_a(f)$ = The calibration factor for the testing instrument.
m = The mass used to do calibration, Kg.
m_o = The mass of the test object in the tri-filar pendulum, Kg.
R = The distance from the center of the tri-filar pendulum to each of the wires, mm.
L = The length of the wires of the tri-filar pendulum, mm.
τ = The period of the tri-filar pendulum, second.
I_{cc} = The mass moment of inertia of the test object in the tri-filar pendulum, $Kg\text{-}m^2$.
I_{pl} = The mass moment of inertia of the platform in the tri-filar pendulum, $Kg\text{-}m^2$.
K_x = The equivalent stiffness of the unit in the x direction, N/m.
K_y = The equivalent stiffness of the unit in the y direction, N/m.
K_z = The equivalent stiffness of the top of the unit in the z direction, N/m.
$K_{\theta x}$ = The equivalent rocking stiffness of the top of the unit in the xz plane, N-m/rad.
$K_{\theta y}$ = The equivalent rocking stiffness of the top of the unit in the yz plane, N-m/rad.
M_x = The equivalent mass of the unit in the x direction, Kg.
M_y = The equivalent mass of the unit in the y direction, Kg.
M_z = The equivalent mass of the top of the unit in the z direction, Kg.
I_x = The equivalent mass moment of inertia of the top of the unit in the xz plane, $Kg\text{-}m^2$.
I_y = The equivalent mass moment of inertia of the top of the unit in the yz plane, $Kg\text{-}m^2$.
M_3 = The mass of the motor, Kg.
M_4 = The mass of the fan impeller/circular disk, Kg.
M_a = The added mass in motor and circular disk test and motor and fan test,

$M_a = M_3 + M_4$, Kg.

M_b = The added mass in the one mass test, Kg.

I_3 = The mass moment of inertia of the motor about the axis which is through the mass center and perpendicular to its rotating axis, Kg-m^2.

$I_{4(d)}$ = The mass moment of inertia of the fan impeller/circular disk about one of its diameter which is perpendicular to its rotating axis, Kg-m^2.

I_b = The mass moment of inertia of the added mass in one mass test, Kg-m^2.

I_a = The mass moment of inertia of the fan impeller/circular disk through its rotating axis, Kg-m^2.

I_{add} = The added mass moment of inertia in motor and circular disk test and motor and test, $I_{add} = I_3 + I_4 + M_3L_3^2 + M_4L_4^2$, Kg-m^2.

$I_{tx(y)}$ = The mass moment of inertia, $I_{tx(y)} = I_{x(y)} + I_3 + I_4 + M_3L_3^2 + M_4L_4^2$, Kg-m^2.

L_3 = The distance from the mass center of the motor to the top, mm.

L_4 = The distance from the mass center of the fan impeller/the circular disk to the top, mm.

L_b = The distance from the mass center of the added mass to the top, mm.

x, y, z = The displacement in the x, y, and z directions, mm.

θ_x = The rocking displacement in the xz plane, rad.

θ_y = The rocking displacement in the yz plane, rad.

x_3, x_4, y_3, y_4 = The displacement of the mass centers of the motor and fan impeller/ circular disk in the x and y directions respectively, mm.

V = The potential energy of the system, N-m.

T = The kinetic energy of the system, N-m.

ω = The whirling speed of the fan impeller/circular disk, rad/sec.

Ω = The rotating speed of the motor rotor and fan impeller/circular disk, RPM.

T_x and T_y = The gyroscopic moments of the rotating fan impeller, N-m.

ψ = The angle between z axis and the deflected shaft axis, degree.

r = The position vector of the mass centers of motor and fan impeller, mm.

f_{x1}, ω_{x1} = The resonance frequency of the swaying mode in the x direction of the frame only test or the one mass test, Hz.

f_{x2}, ω_{x2} = The resonance frequency of the swaying mode in the x direction of the motor and circular disk test or the motor and fan test, Hz.

$f_{\theta x1}$, $\omega_{\theta x1}$ = The resonance frequency of the rocking mode in the xz plane of the frame only test or the one mass test, Hz.

$f_{\theta x2}$, $\omega_{\theta x2}$ = The resonance frequency of the rocking mode in the xz plane of the motor and circular disk test or the motor and fan test, Hz.

f_{y1}, ω_{y1} = The resonance frequency of the swaying mode in the y direction of the frame only test or the one mass test, Hz.

f_{y2}, ω_{y2} = The resonance frequency of the swaying mode in the y direction of the motor and circular disk test or the motor and fan test, Hz.

$f_{\theta y1}$, $\omega_{\theta y1}$ = The resonance frequency of the rocking mode in the yz plane of the frame only test or the one mass test, Hz.

$f_{\theta y2}$, $\omega_{\theta y2}$ = The resonance frequency of the rocking mode in the xz plane of the motor and

circular disk test or the motor and fan test, Hz.

f_{z1} = The resonance frequency of the translational mode in the z direction of the frame only test, Hz.

f_{z2} = The resonance frequency of the translational mode in the z direction of the motor and circular disk test or the motor and fan test, Hz.

D_x = The static deflection in the x direction, mm.

F_x = The force in the x direction, N.

D_y = The static deflection in the y direction, mm.

F_y = The force in the y direction, N.

a_1 , b_1 , c_1 and a_2 , b_2 , c_2 = The coefficients of the eigenvalue equations.

ACKNOWLEDGMENTS

When something is achieved, however small it may be, you need to think about it and thank the people who gave you help and made it possible.

I would like to thank Dr. Douglas D. Reynolds and Dr. Mohamed B.E. Trabia, who are my advisors and the principle investigators of this project, for providing me valuable advice and funding me in my masters program here at University of Nevada, Las Vegas.

I would like to thank Dr. Peter K. Baade, who is the Chairman of Project Monitoring Sub-Committee, and other committee members for giving me a lot of comments and inputs in this research work.

I would like to thank my teachers, both here in U.S. and in China, for bringing me the knowledge to finish this work and other jobs in the future.

Finally, I would like to thank my wife, Zhu Meng, my parents and other family members for their love and support.

CHAPTER 1

INTRODUCTION

Because of frequent reports of propeller fan failures in air conditioning units, heat pumps, and similar heating, ventilating and air conditioning equipment, a symposium on propeller fan vibration was held at the 1973 ASHRAE Annual Meeting in Louisville [1]. As a result of this activity, ASHRAE Standard Project Committee 87.1P was formed. In 1980, ASHRAE funded Research Project No. 266 - Propeller Fan Dynamics. The reports and ASHRAE papers that were published as a result of this project formed the technical bases for ASHRAE Standard 87.1 - 1983: Method of Testing Dynamic Characteristics of Propeller Fan - Aerodynamically Excited Fan Vibrations and Critical Speeds [2-4].

Users of ASHRAE Standard 87.1 identified the fact that the procedures outlined in the standard for determining fan resonance frequencies and corresponding critical fan speeds did not accurately take into account the effects of centrifugal blade stiffening. This turned out to be an important factor when transforming from the resonance frequencies determined from static, non-rotating fan tests to the corresponding critical speeds that were anticipated to exist when the fan was rotating.

In 1985, ASHRAE funded Research Project No. 477 - Development of a Method to Predict Vibration Response of Propeller Fans under Actual Operation Conditions. The reports and papers that resulted from this project provided the technical bases for revi-

sions in ASHRAE Standard 87.1 - 1983 which more accurately incorporated the effects of centrifugal blade stiffening when converting from measured fan resonance frequencies to corresponding fan critical speeds [5-8].

The results of ASHRAE Research Projects Nos. 266 and 477 and ASHRAE Standard 87.1 cover propeller fan vibration that is associated only with fan impeller vibration caused by aerodynamic forces acting on the impeller. Experience has shown that fan failures occur as a result of vibration modes associated with the interaction between the fan impeller and the fan motor and the motor structural support system. Several of these vibration modes were identified in a Seminar on Fan Vibration at the 1986 ASHRAE Annual Meeting in Ottawa. These modes are associated with fan unbalance, aerodynamic forces, motor torque pulsations, and blade flutter. In general, these modes can not be identified using the test and analysis procedures outlined in ASHRAE Standard 87.1. Also, to properly identify these vibration modes, it is usually necessary to analyze the fan assembly. The assembly usually consists of fan impeller, motor, and motor mount structure.

In response to developing information and forming a new ASHRAE Standard relative to the vibration modes described above, ASHRAE has issued a new Research Project No. 685-RP - Test and Analysis Methods for Resolving Fan/Motor Vibration Problems in Air-Conditioning Units. The objectives of this research work are:

(1) Develop and perfect the experimental procedures that can be used to measure and quantify the vibration modes associated with the fan impeller, motor and motor mount of small (< 36 in diameter fan impeller) direct-drive propeller fans that are excited by fan impeller unbalance, taking into account the gyroscopic effect of the rotating fan impeller.

(2) Develop the basic analytical models that can be used to predict the vibration modes described in (1), especially the gyroscopic effect of the rotating fan impeller on the system.

(3) Provide reports and papers that can be used as the technical basis of the new ASHRAE Standard.

Two air-conditioning units were investigated in this project. They were designated as test units #1 and #2.

In these test units, the vibration problems associated with fan impeller, motor and motor mount that were excited by fan impeller unbalance taking into account the gyroscopic effect of the rotating fan impeller were investigated. It was proved, both theoretically and experimentally, that the gyroscopic effect of the rotating fan impeller did have significant effect on the vibration modes of the systems. Chapter 2 through Chapter 6 in this thesis summarized these investigations. Both theoretical models and experimental efforts were included.

CHAPTER 2

THE TEST PROCEDURES

2.1 The investigated air conditioning units

Two air conditioning units were investigated in the first phase of this project. They were designated as test unit #1 and test unit #2.

Figure 2-1 shows the schematic of the test unit #1. The top of the unit is a radially louvered discharge grille supporting the fan motor. The side panels are louvered sheet metal that covers the condenser coil. The total mass of the unit, including the top, is 78.05 Kg. The mass of the top is 10.48 Kg. Because the compressor was not present in this unit, 23.58 Kg of additional mass was added to the bottom of the unit to compensate for the mass of the compressor.

Figure 2-2 shows the schematic of the test unit #2. The structure of the top of the unit is the same as test unit #1. A wire grille is used to protect the condenser coil. The total mass of the unit, including the top and compressor, is 85.60 Kg. The mass of the top is 5.35 Kg.

Following vibration modes of interest for the test units, as shown in Figure 2-3, were investigated in this first phase.

Swaying modes: There are two swaying modes: f_x in the x direction and f_y in the y direction. Figure 2-3 shows the swaying mode in the x direction, f_x. It is the mode in which the top, motor, fan impeller and the part of side panels vibrate relative to the base

in the x direction. The swaying mode in the y direction, f_y, is the mode in which the top, motor, fan impeller, and part of the side panels vibrate relative to the base in the y direction.

Rocking modes: There are two rocking modes: $f_{\theta x}$ in the xz planes and $f_{\theta y}$ in the yz plane. Figure 2-3 shows the rocking mode in the xz plane, $f_{\theta x}$. This is the mode in which the part of the top, motor and fan impeller rock relative to the side panel in the xz plane. It is same for $f_{\theta y}$.

Translational mode: There is one mode in the z direction, f_z. This is the mode in which the part of the top, motor and fan impeller vibrates up and down in the z direction.

The indicated points on both units are the points at which mobility measurements were made. Points 1, 2, 3 and 4 are at the edges of the tops of both units. Point 1', 2'(2"), 3' and 4' on test unit #1 are at the middle of its each side panel. Mobility measurements made at these points were used to identify the swaying modes in the x and y directions. Points 5, 6, 7, 8 and 9 are located on the tops of each unit. Mobility measurements made at these points were used to identify the rocking modes in the xz and yz planes and also the translational mode in the z direction.

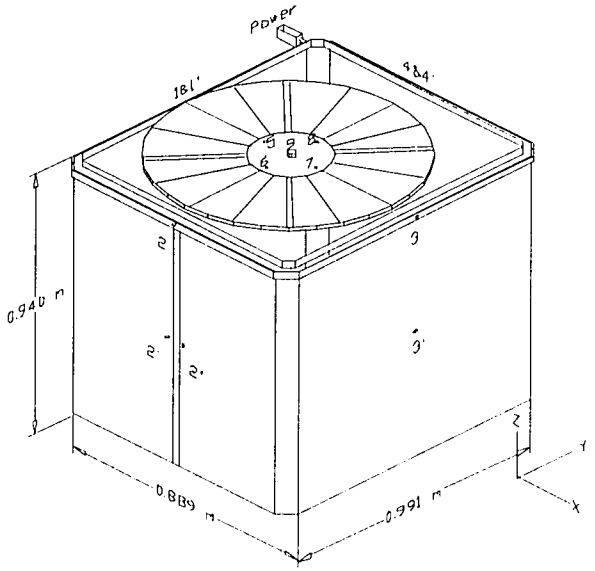

Figure 2-1 The schematic of test unit #1 and measurement points

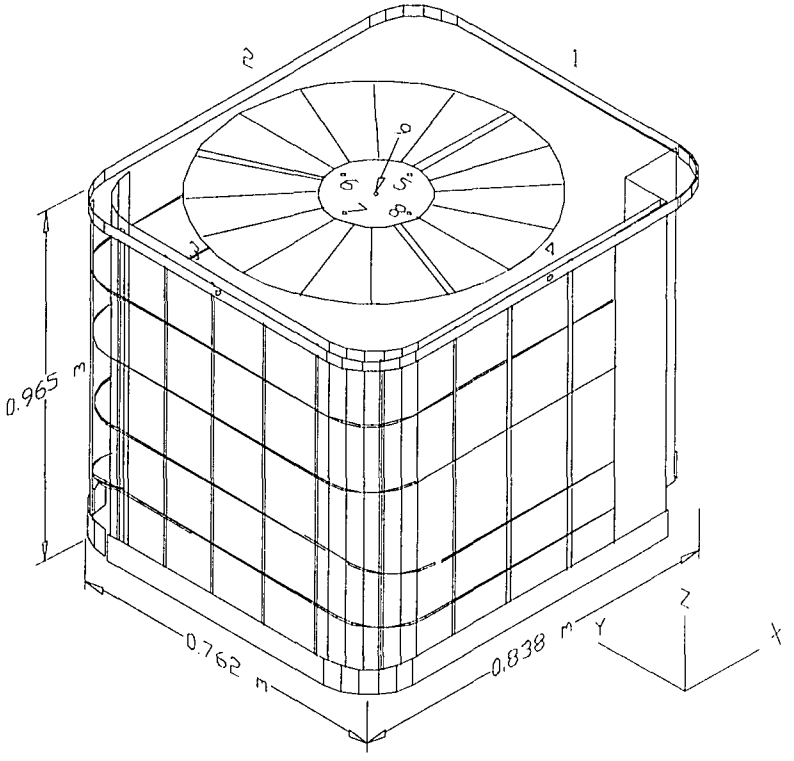

Figure 2-2: The schematic of test unit #2 and measurement points

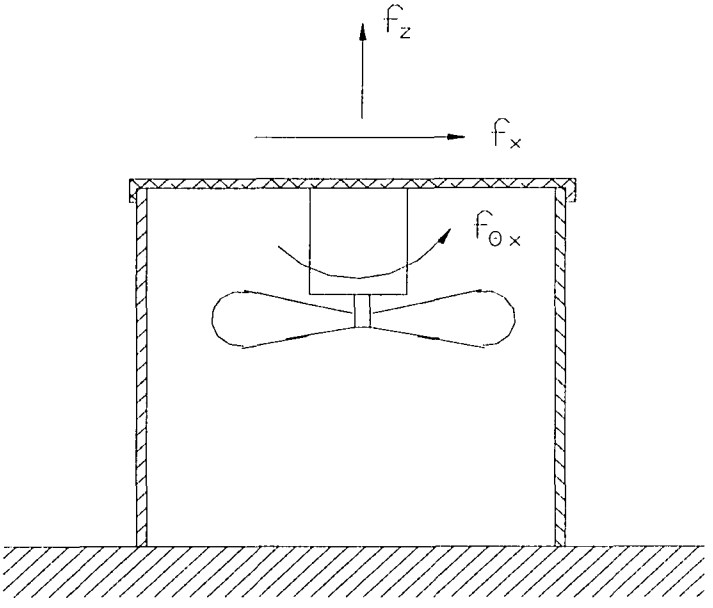

Figure 2-3: The major modes of interest in the test units #1 and #2

2.2 Instrumentation and calibration

One of the objectives of this project is to develop experimental procedures that can be used to measure and quantify the vibration modes associated with the fan impeller, motor, and motor mount. A summary of the test equipment and procedures used for the tests on unit #1 and unit #2 is presented. The following equipment was used in the tests.

- A PC-based 486 portable computer.
- A pair of WavePak boards -- two channel FFT analyzer.
- 086C20 Impulse Force Hammer.
- 303M07 Accelerometer.
- 480D06 Power Unit.
- Oscillator, Signal Generator
- Cables, Force Gauge and Dial Indicator.

Figure 2-4 shows a layout of the instrumentation used in the tests. To obtain accurate and reliable results, the instrumentation was properly calibrated before a series of tests. The calibration procedure is described in details in ISO Standard 7626-2:1990. Here, a short review of this procedure for the calibration of the accelerometer, impact hammer and the FFT analyzer is presented.

There are two types of calibration. One is to calibrate only the impact hammer

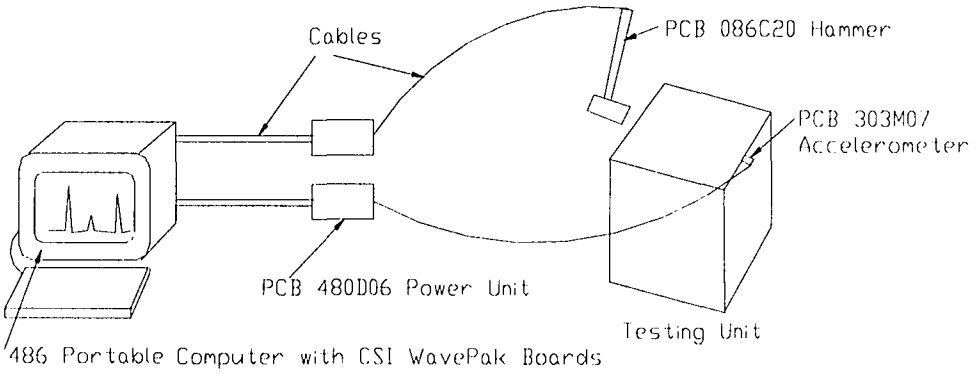

Figure 2-4: The layout of the instrumentation used in the tests

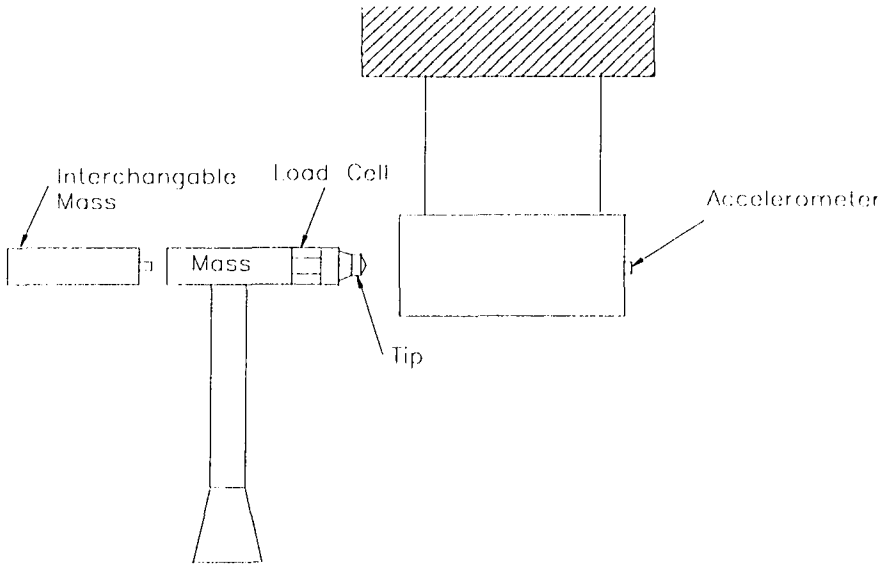

Figure 2-5: The schematic of the calibration system

used in the tests. The other is to calibrate the measurement system. Only the second calibration method was used. To do this, an inertia block of known mass was used and the whole system was calibrated by measuring the accelerance of the mass.

The mass was suspended as a pendulum from two long strings, as shown in Figure 2-5. The purpose for this setup was to ensure that the system resonance frequency was very low. The accelerometer was mounted on one end of the mass. The other end was impacted with the impact hammer. The following procedures were used to obtain the accelerance calibration factor, $C_a(f)$. If the impact force applied by impact hammer is through the mass center, the force is given by:

$$F = ma \tag{2-1}$$

The true frequency response of the system is:

$$H(f) = \frac{a}{F} = \frac{1}{m} \tag{2-2}$$

The measured force, F', which is the force acting on the force transducer of the impact hammer, is different from the force, F, transmitted to the system. Thus, the measured

voltage ratio is:

$$H'(f) = \frac{E_a}{E_f'} \tag{2-3}$$

where E'_f and E_a are the measured voltages from the force transducer in the impact hammer and from the accelerometer. H'(f) is a function of the sensitivities of the sensors. The relationship between the frequency response H(f) and the voltage ratio H'(f) is:

$$H(f) = \frac{H'(f)}{C_a(f)} \tag{2-4}$$

where $C_a(f)$ is the accelerance calibration factor of the measurement system. It is defined as:

$$C_a(f) = \frac{S_a}{S_f} \tag{2-5}$$

where S_f and S_a are the sensitivities of the force transducer and the accelerometer. From equation (2-4), this accelerance calibration factor can be calculated as:

$$C_a(f) = \frac{S_a}{S_f} = \frac{H'(f)}{H(f)} = m\frac{E_a}{E_f'} \tag{2-6}$$

A 303M07 and a 302A accelerometers, 086C20 impact hammer, and two channel FFT analyzer were calibrated using the above procedures. Table 1 gives the calibration factors of the given accelerometers, hammer and FFT analyzer. The hammer tip used in the calibration and the test was the medium tip (red). The mass used in the calibration was m = 18.32 Kg.

Table 1: The calibration factors of Accelerometers, Impact Hammer and FFT Analyzer

Accelerometers	$H'(f)=E_a/E'_f$	$C_a(f)=mH'(f)$
303M07	0.301	5.50
302A	0.570	10.40

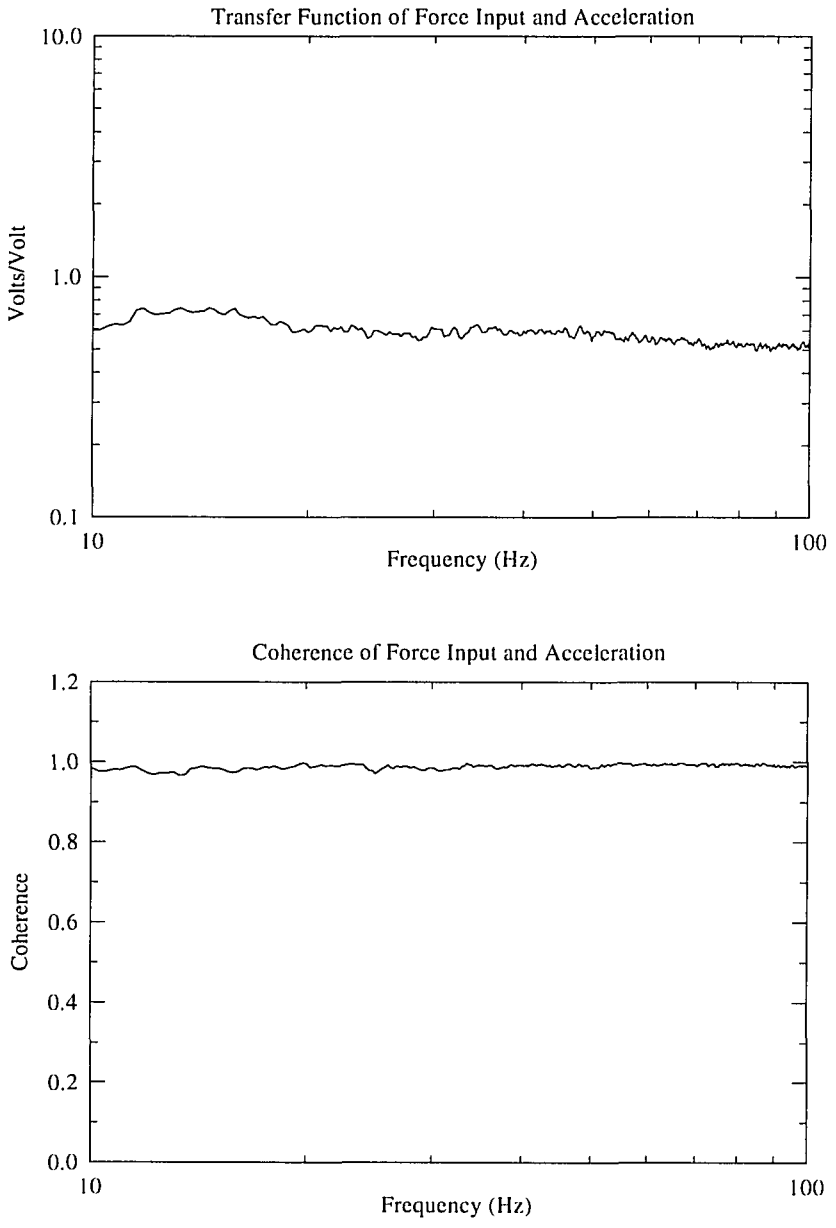

Figure 2-6: The calibration accelerance for 302A accelerometer and 086C20 impact hammer

Figure 2-6 is a typical calibration curve for 302A accelerometer, 086C20 impact hammer. The direct readout was the measured voltage ratio, $H'(f) = E_a/E'_r$. To obtain an uniform calibration factor in the frequency range of interest, the data from the flat portion of the calibration curve were used to calculated the average H'(f) in this range. The frequency range used in the calculation of calibration factors was from 10 Hz to 100 Hz. The values of H'(f) given in Table 1 are these average values.

2.3 Tri-filar pendulum

A tri-filar pendulum was used to measure the mass moment of inertia of fan impellers, circular disk and motors. Figure 2-7 shows the layout of the tri-filar pendulum.

The objects to be measured is suspended by three wires with the same length, 'L'. The three wires are spaced equally with radius, R, and the angles between wires are 120 degree. If the period, τ, of torsional oscillation of the test object about the vertical axis C-C passing through the center of gravity is measured, the mass moment of inertia of the object can be calculated using the following equation:

$$I_{cc} = \frac{m_o g R^2 \tau^2}{4\pi L} - I_{pl} \qquad (2\text{-}7)$$

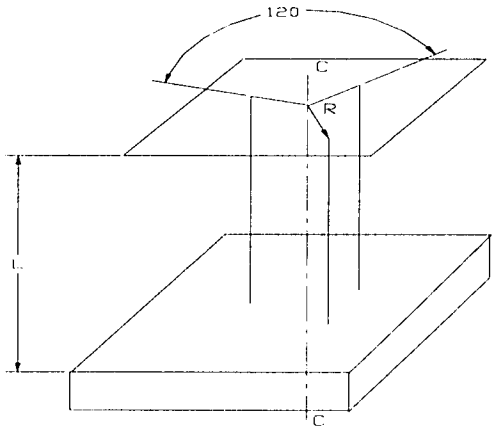

Figure 2-7: The principle of tri-filar pendulum

Table 2: The measured mass, mass center and mass moment of inertia

Name	Mass	Mass Center	Axial Mass Moment of Inertia	Transverse Mass Moment of Inertia
Unit	Kg	m	Kg-m^2	Kg-m^2
Circular Disk	1.52	0.140	0.0394	0.0207
U#1 60843301 Fan	1.43	0.140	0.0376	0.0206
U#1 60799501 Fan	1.45	0.140	0.0378	0.0205
U#1 1/3 HP Motor	7.44	0.064	0.0234	0.0188
U#1 1/4 HP Motor	5.90	0.059	0.0173	0.0138
U#2 IRA025A Fan	0.98	0.133	0.0192	0.0106
U#2 203020-A Fan	0.98	0.133	0.0193	0.0108
U#2 203020-B Fan	0.98	0.133	0.0193	0.0108
U#2 203020-C Fan	0.97	0.133	0.0192	0.0108
U#2 203020-D Fan	0.97	0.133	0.0192	0.0108
U#2 203020-E Fan	0.97	0.133	0.0192	0.0107
U#2 203020-F Fan	0.97	0.133	0.0192	0.0107
U#2 Motor	4.63	0.056	0.0133	0.00985
Added Mass	3.95	0.0335	N/A	0.00518

where, I_{cc} is the mass moment of inertia of the test object, m_o is the mass of the test object, g is the gravitational acceleration, R is the distance from the center of the pendulum to each of the wires, L is the length of wires, τ is the period of oscillation of the pendulum and I_{pl} is the mass moment of inertia of the platform on which the measured objects are placed.

Table 2 gives the measured mass moment of inertia for the fan impellers and the motors used in the tests. In Table 2, fan impellers 203020-A and B have Projected Width Difference (PWD) of 6.35 mm and unbalance of 0.0 g-mm; fan impellers 203020-C and D have PWD of 0.0 mm and unbalance of 0.0 g-mm; fan impellers 203020-E has PWD of 0.0 mm and unbalance of 93.6 g-mm; fan impeller 203020-F has PWD of 0.0 mm and unbalance of 187.2 g-mm.

2.4 Test setups

The following static tests were conducted to experimentally identify the vibration modes of interest and to estimate the parameters in the analytical models,.

(1) **Frame only test.** This test was conducted with both the motor and the fan impeller removed, as shown in Figure 2-8.

(2a) **Motor and circular disk test.** This test was conducted with the motor and a

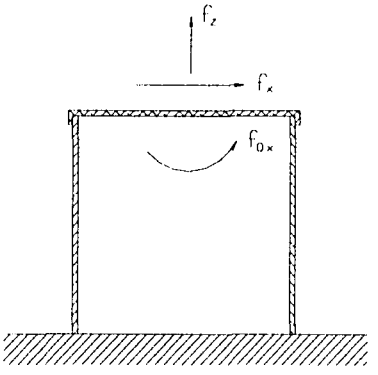

Figure 2-8: The schematic of frame only test

circular disk, which had the same mass and mass moment of inertia as the fan impeller, attached to the top of the unit, as shown in Figure 2-9. The circular disk was used instead of the fan impeller to eliminate the dynamic and aerodynamic effects associated with the flexibility of the fan impeller on the system.

(2b) **Motor and fan test.** This test was conducted with the motor and fan impeller attached to the top of the unit, as shown in Figure 2-10. Because the lowest vibration modes of the fan impeller are usually greater than 30-40 Hz and the modes of interest in the test units are less that 30 Hz, it is practical to directly use the fan impeller both in static and dynamic tests.

(3) **One mass test.** This test was conducted with both the motor and the fan

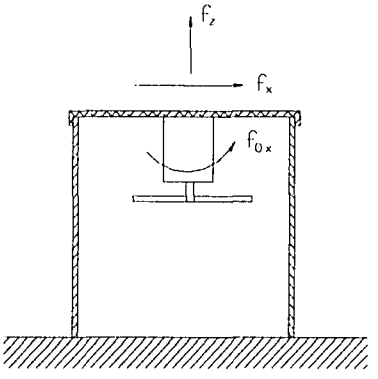

Figure 2-9: The schematic of motor and circular disk test

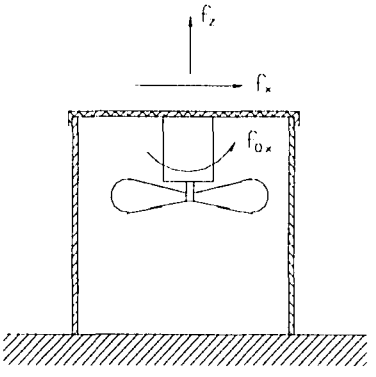

Figure 2-10: The schematic of motor and fan test

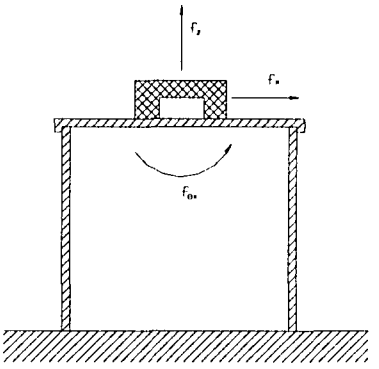

Figure 2-11: The schematic of one mass test

impeller removed, but an additional mass was attached to the top of the unit, as shown in Figure 2-11. The mass used in the tests was a lead brick of dimension 4" x 4" x 2" with blank hole of 3.5" diameter and 1.15" depth at the center of the brick to fit the top of the test unit. The physical parameters of the mass are: M_b = 3.95 Kg, I_b = 0.00518 Kg-m^2 and L_b = 0.0335 m.

For test unit #1, **the frame only test** and the **motor and circular disk test** were conducted to identify the parameters used in the analytical model. The **one mass test** was abandoned because it did not give clear information about the two swaying modes.

For test unit #2, the **frame only test, one mass test** and the **motor and fan test** were used. The additional **one mass test** was needed because the **frame only test** did not give clear information about the two rocking modes.

2.5 Test procedures

To accurately identify the vibration modes of interest on the air conditioning units shown in Figures 2-1 and 2-2, two things were considered: (1) the location where the accelerometer is mounted and (2) the point at which the impact force is applied. It was decided not to use any locations inside the unit since such locations might be inaccessible in some unit designs or in a field test. Figures 2-12 and 2-13 showed a detailed layout of

all the points at which the accelerometer was attached and at which the impact force was applied for the test units #1 and #2.

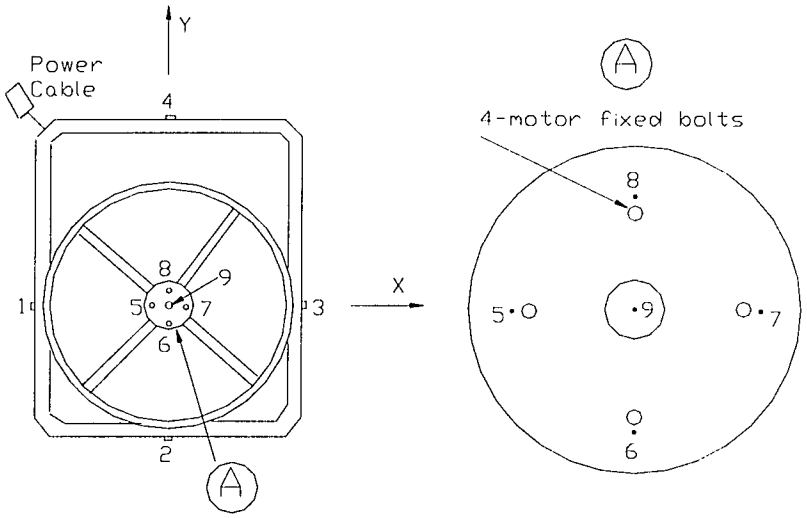

Figure 2-12: The points for mounting the accelerometer and applying the impact force for test unit #1 (not for scale)

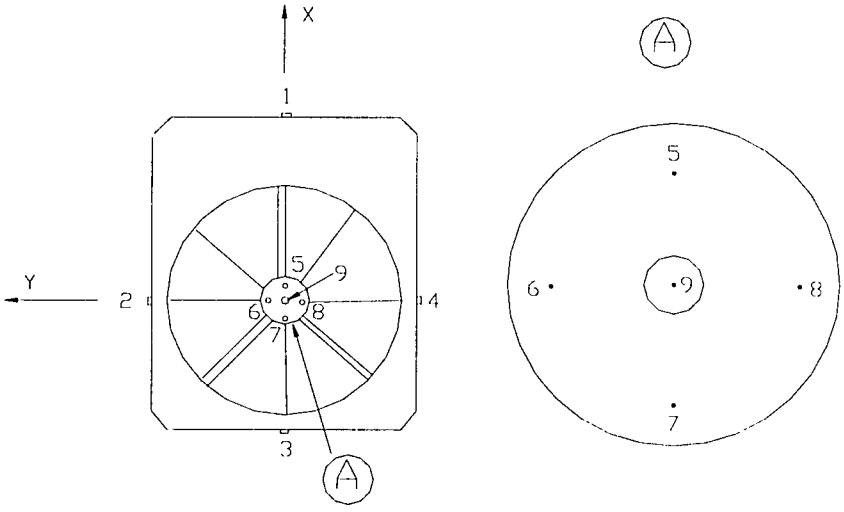

Figure 2-13 The points for mounting the accelerometer and applying the impact force for test unit #2 (not for scale)

2.5.1 The swaying mode in the x direction, f_x

Test unit #1:

Location of accelerometer: Test results indicated the best location to mount the accelerometer for measuring the swaying modes in the x and y directions for test unit #1 was at point 9 (Figures 2-1 and 2-12). Figure 2-14 showed how the accelerometer was mounted at point 9 in the x direction for the different tests. An angle, with dimension 0.75" x 0.75" x 0.86" and thickness 0.125", was glued to the top of the unit. The accelerometer was mounted on the angle in the x direction as close as possible to where the motor was attached to the top of the unit. The purpose of this was to eliminate or minimize the presence of the rocking modes in the xz and yz planes and the translational mode in the z direction when the swaying modes were measured.

Location of impact: Referring to Figures 2-1 and 2-12, the impact force was applied to either point 1 or point 3.

Discussion: When an impact force was applied to point 1 or point 3, in addition to the swaying mode in the x direction being excited, the modes of the side panels were also excited. The excitation of the side panel modes made it very difficult to identify the swaying mode. To solve this problem, the panel modes which were excited were

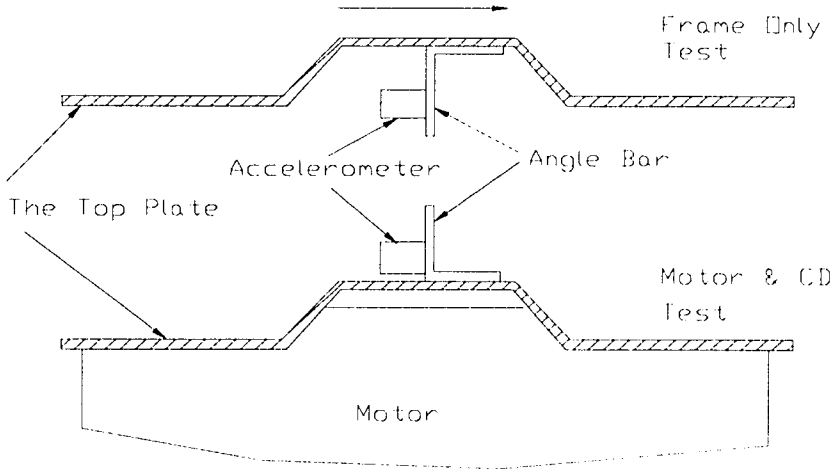

Figure 2-14: The location for accelerometer fixed in the x direction

measured. This was accomplished by applying an impact force at the points 1', 2', 3' and 4' in the middle of each panel. The accelerometer was mounted at point 9 as indicated in Figure 2-14. Next, all the screws that attached the top and side panels together were loosened to eliminate the panel modes when an impact force was applied at point 1 or point 3. When this was done, the swaying mode was the only prominent mode that was excited. Because the boundary conditions of the system were changed by loosening the screws, the swaying mode that was measured occurred at a different frequency as compared to when the screws were tightened. However, this yielded information relative to the frequency range of the swaying mode. This was very helpful in distinguishing the swaying mode from the panel modes.

Test unit #2: Both **location of accelerometer** and **location of impact** were the same as the test unit #1. It was not necessary to measure the swaying mode in the x direction by loosening the screws because there were no side panel modes for unit #2.

Figure 2-15 is a typical mobility plot of the swaying mode in the x direction, f_x, of test unit #1 with 1/4 HP motor and circular disk. Figure 2-16 is a typical mobility plot of the loosened-screw swaying mode in the x direction of test unit #1 with 1/4 HP motor and circular disk.

2.5.2 The swaying mode in the y direction, f_y

Test unit #1:

Location of accelerometer: The location for mounting the accelerometer for measuring the swaying mode in the y direction was also at point 9. The only change in Figure 2-14 was that the angle and accelerometer was fixed in y direction.

Location of impact: Referring to Figures 2-1 and 2-13, the impact force was applied to either point 2 or point 4.

Discussion: When an impact force was applied to point 2 or point 4, both the swaying and the panel modes were excited. The side panel modes were identified using

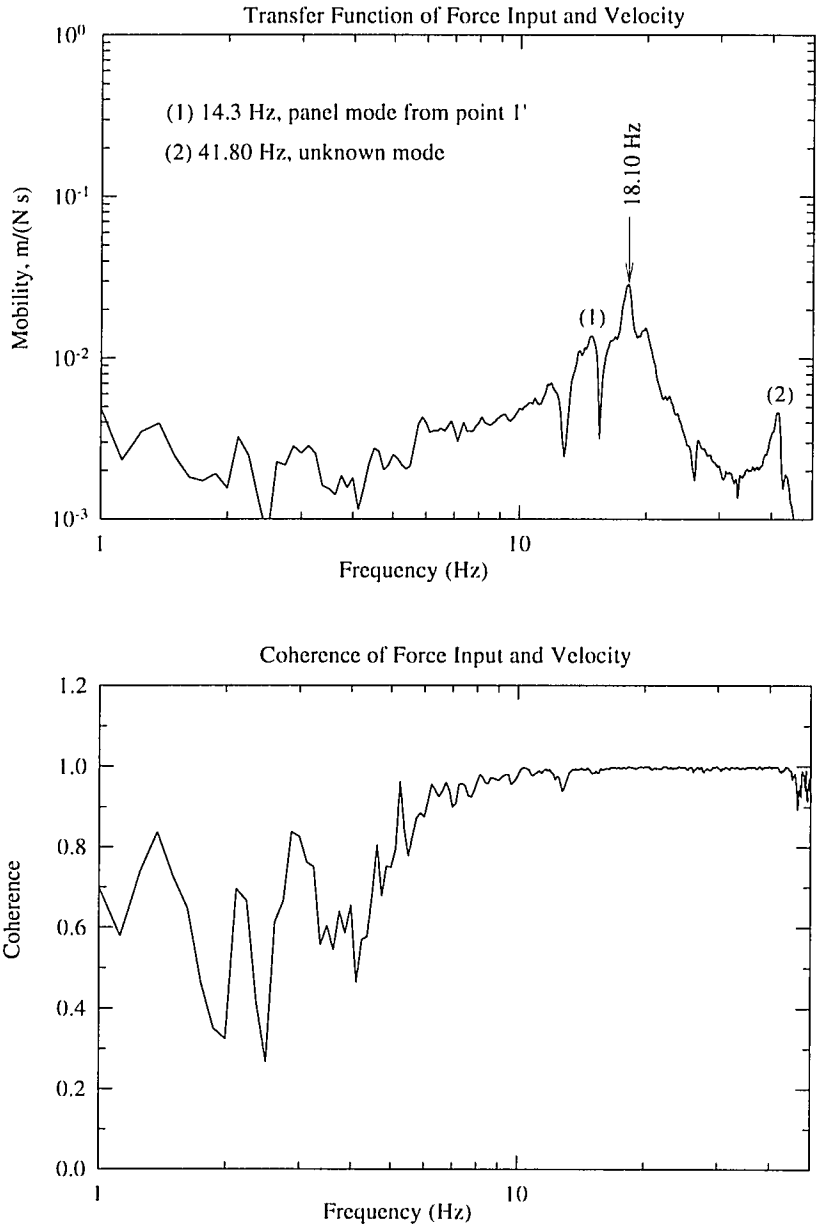

Figure 2-15: The mobility of the swaying mode in the x direction, f_x, of test unit #1 on case with 1/4 HP motor and circular disk, f_x = 18.10 Hz

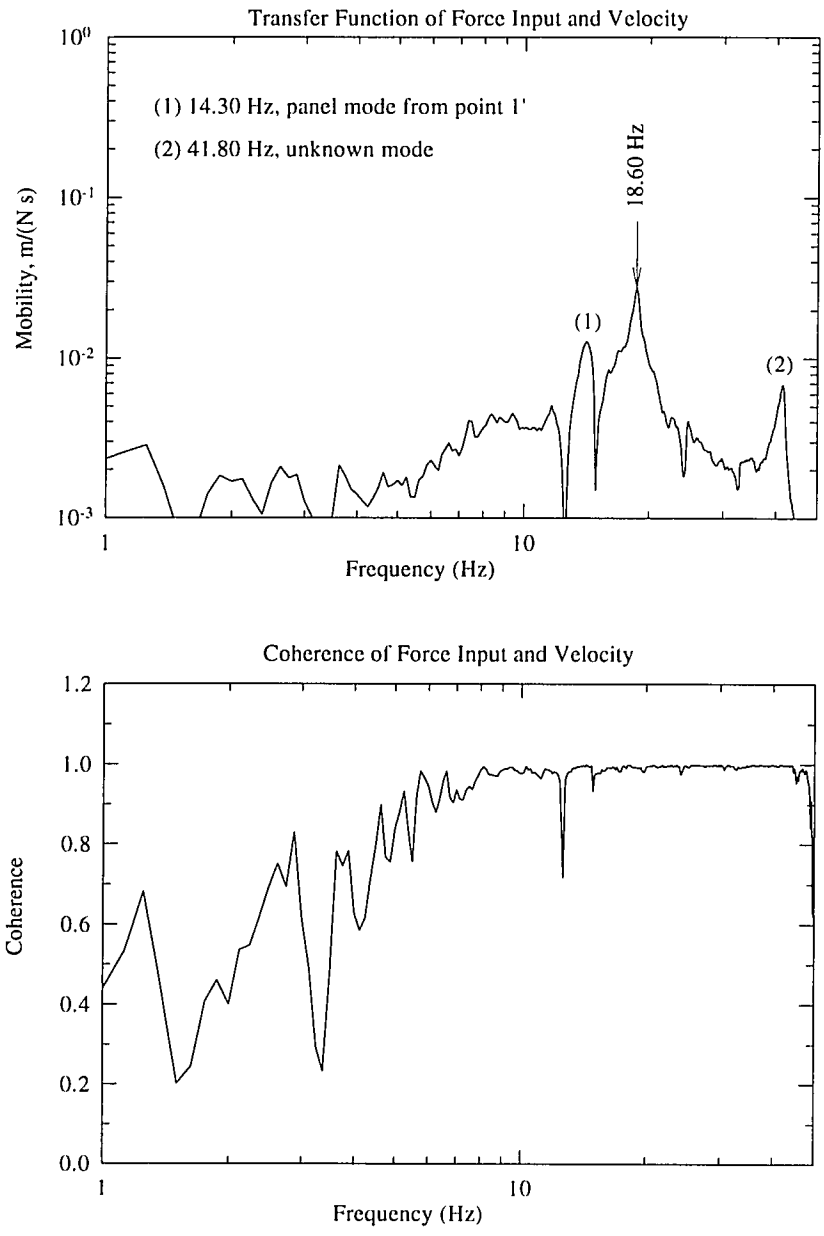

Figure 2-16: The mobility of the swaying mode in the x direction, f_x, of test unit #1 on case with 1/4 HP motor and circular disk and loosened-screw, f_x = 18.60 Hz

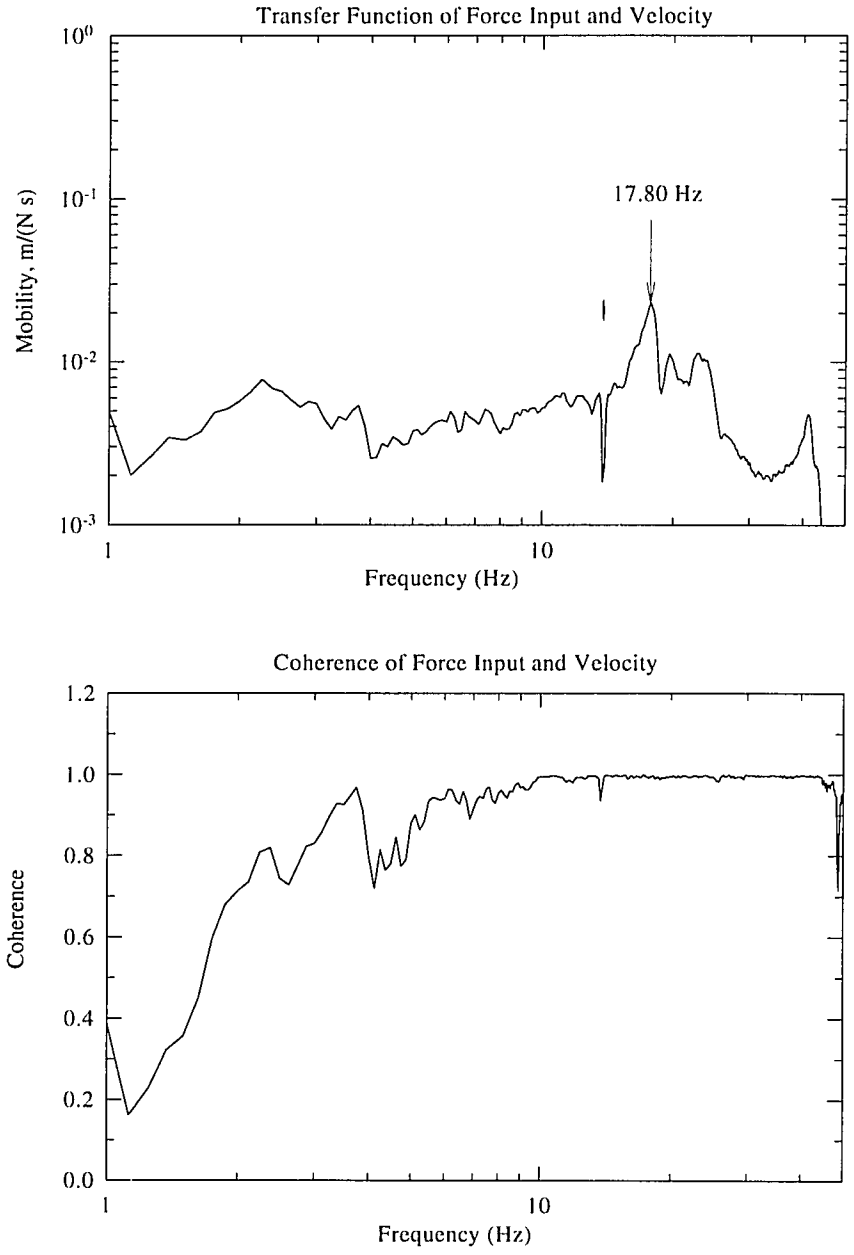

Figure 2-17: The mobility of the swaying mode in the y direction, f_y, of test unit #1 on case with 1/4 HP motor and circular disk, f_y = 17.80 Hz

the same procedures that were used for the x direction.

Test unit #2: Both **location of accelerometer** and **location of impact** were the same as for test unit #1. It was not necessary to measure the swaying mode in the y direction by loosening screws because there were no side panel modes for unit #2.

Figure 2-17 is a typical mobility plot of the swaying mode in the y direction, f_y, of test unit #1 with 1/4 HP motor and circular disk.

2.5.3 The translational mode in z direction, f_z

Test unit #1:

Location of accelerometer: The top of the unit can be visualized as a beam with its ends simply supported, as shown in Figure 2-18. The translational mode, f_z, corresponds to the first vibration mode of the beam. Thus, the best location for mounting the accelerometer was at point 9 in the z direction. In this case, the accelerometer was mounted directly to the top of the unit in the z direction.

Location of impact: To prevent the excitation of the rocking modes in the xz and yz planes, the impact point should be at the center of the beam shown in Figure 2-18. Thus, the best impact point for f_z was at point 9. When the accelerometer was mounted and impact force was applied properly, the translational mode in the z direction, f_z, was the only prominent peak in the mobility measurement.

Test unit #2: Both **location of accelerometer** and **location of impact** were the

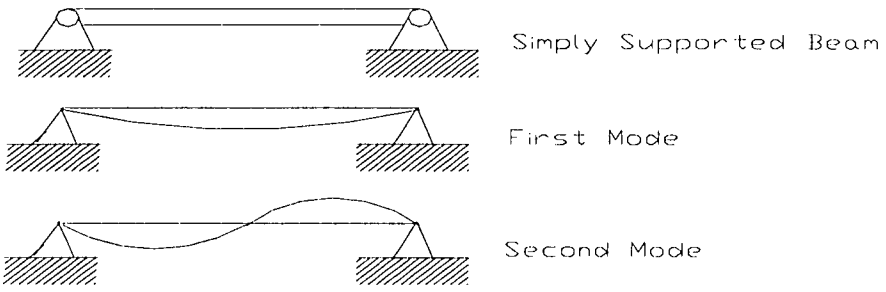

Figure 2-18: The beam model for the top with two ends simply supported

same as the test unit #1.

Figure 2-19 is a typical mobility plot of the translational mode in the z direction, f_z , of test unit #1 with 1/4 HP motor and circular disk.

2.5.4 The rocking mode in the xz plane, $f_{\theta x}$

Test unit #1:

Location of accelerometer: As discussed in Section 2.5.3, the top of the unit can be visualized as a beam with two ends simply supported, as shown in Figure 2-18. The rocking mode, $f_{\theta x}$, in the xz plane (and the rocking mode, $f_{\theta y}$, in the yz plane which will be discussed in Section 2.5.5) corresponds to the second vibration mode of the beam. Because of symmetry, the best location for mounting the accelerometer was at a point near the bolts which were used to attach the motor to the top of the unit. For the rocking mode in the xz plane, $f_{\theta x}$, the best location for mounting the accelerometer was point 5 or point 7 in the z direction, as shown in Figure 2-12.

Location of impact: For the reasons similar to those discussed above, the best impact point was also at point 5 or point 7. When the accelerometer was mounted at point 5, the impact force was applied at point 7, or vice versa.

Discussion: When the accelerometer was mounted at point 5 and the impact force applied at point 7 (or vice versa), not only the rocking mode in the xz plane, $f_{\theta x}$, was excited, but also the translational mode, f_z, in the z direction was excited. Sometimes, the rocking mode in the yz plane, $f_{\theta y}$, was excited too. However, the peaks at both f_z and $f_{\theta y}$ were less prominent than that at $f_{\theta x}$. Comparing the results with those in Sections 2.5.3 and 2.5.5, $f_{\theta x}$ was easily identified.

Test unit #2: Both **location of accelerometer** and **location of impact** were the same as the test unit #1.

Figure 2-20 was a typical mobility plot of the rocking mode in the xz plane, $f_{\theta x}$, of test unit #1 with 1/4 HP motor and circular disk.

2.5.5 The rocking mode in the yz plane, $f_{\theta y}$

Test unit #1: This mode was very similar to $f_{\theta x}$. All the discussions about f_{qx} were applicable to $f_{\theta y}$.

Test unit #2: Both **location of accelerometer** and **location of impact** were the same as the test unit #1.

Figure 2-21 was a typical mobility plot of the rocking mode in the yz plane, $f_{\theta y}$, of test unit #1 with 1/4 HP motor and circular disk.

2.6 The discussion

Two things are very important relative to experimentally identifying the modes of interests: (a) the location where the accelerometer was mounted and (b) the point at which the impact force was applied, as discussed in Section 2.5. There are also some other minor issues which must be considered when conducting the tests.

(1) The method of the accelerometer fixing. The accelerometer was fixed by using petro wax from the accelerometer manufacturer. In this work, 080A24 petro wax from PCB was used.

(2) The location of the accelerometer. For identifying the rocking modes in the xz and yz planes, points 5, 6, 7 and 8 were the locations where the accelerometer was mounted, as shown in Figures 2-12 and 2-13. In this test, the position of, for example, point 5 was carefully adjusted to obtain the optimum position at which only the rocking mode in the xz plane, $f_{\theta x}$, was measured or its peak was dominant in the measurement. The same procedure was true for points 6, 7 and 8. For identifying the swaying modes in the x and y directions, the discussion in Section 2.5.1 should be followed. For identifying translational mode in the z direction, the accelerometer was fixed at the center of motor mount.

(3) The impact force. For identifying the rocking modes in the xz and yz planes,

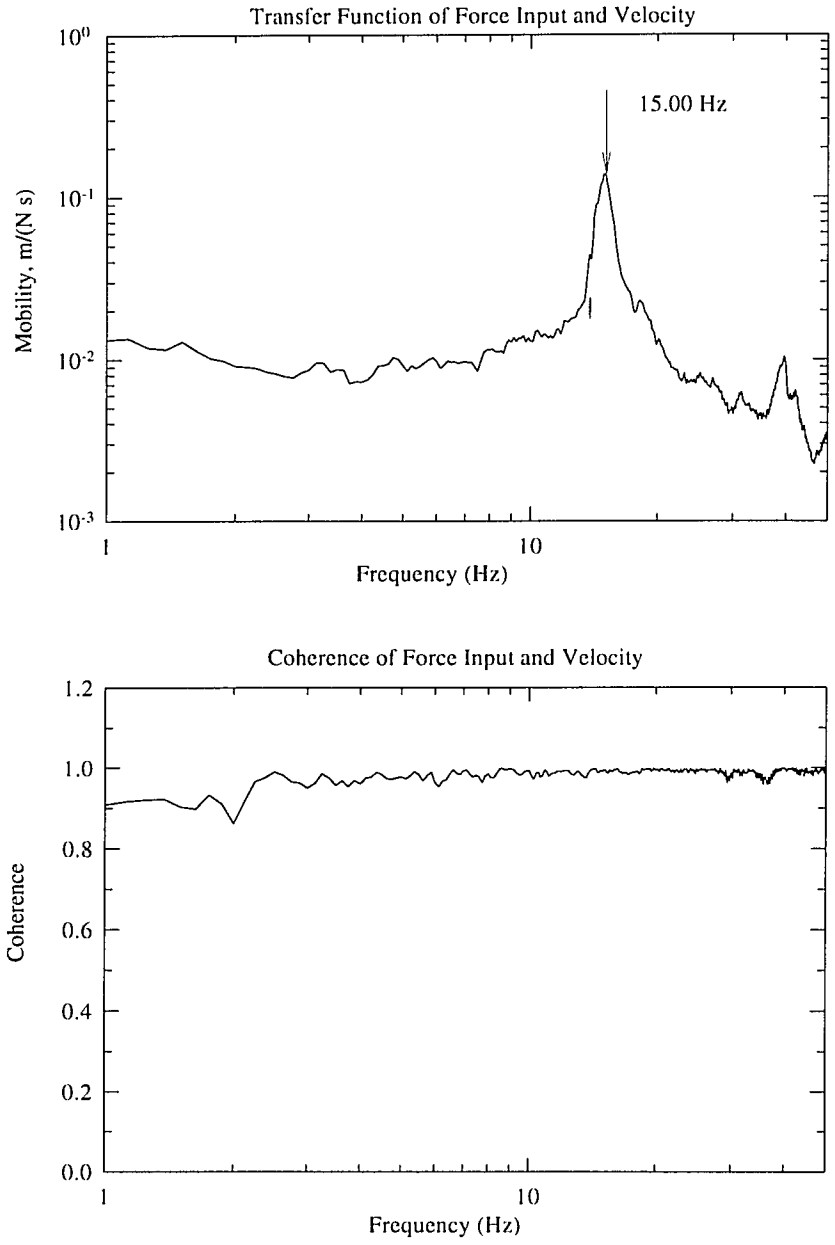

Figure 2-19: The mobility of the translational mode in the z direction, f_z, of test unit #1 on case with 1/4 HP motor and circular disk, f_z = 15.00 Hz

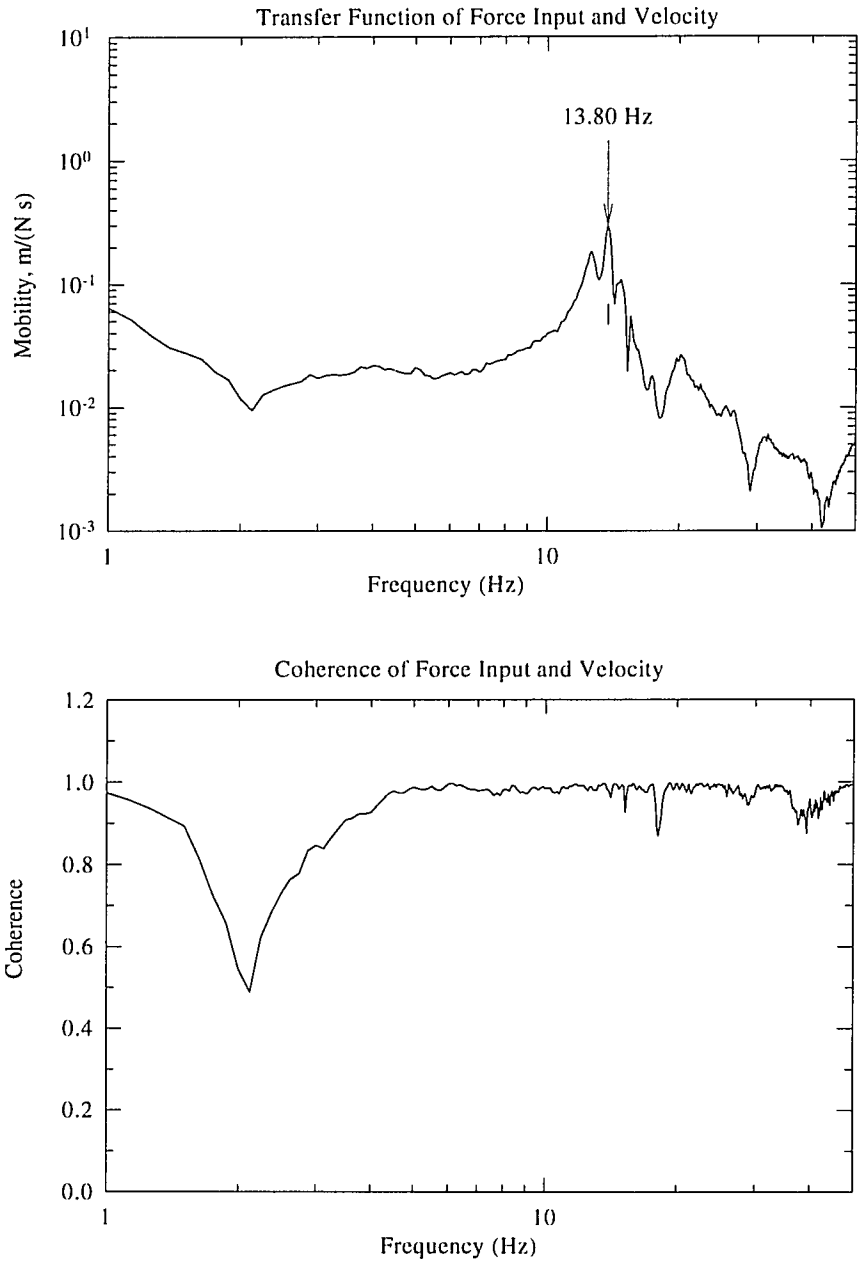

Figure 2-20: The mobility of the rocking mode in the xz plane, f_{0x}, of test unit #1 on case with 1/4 HP motor and circular disk, f_{0x} = 13.80 Hz

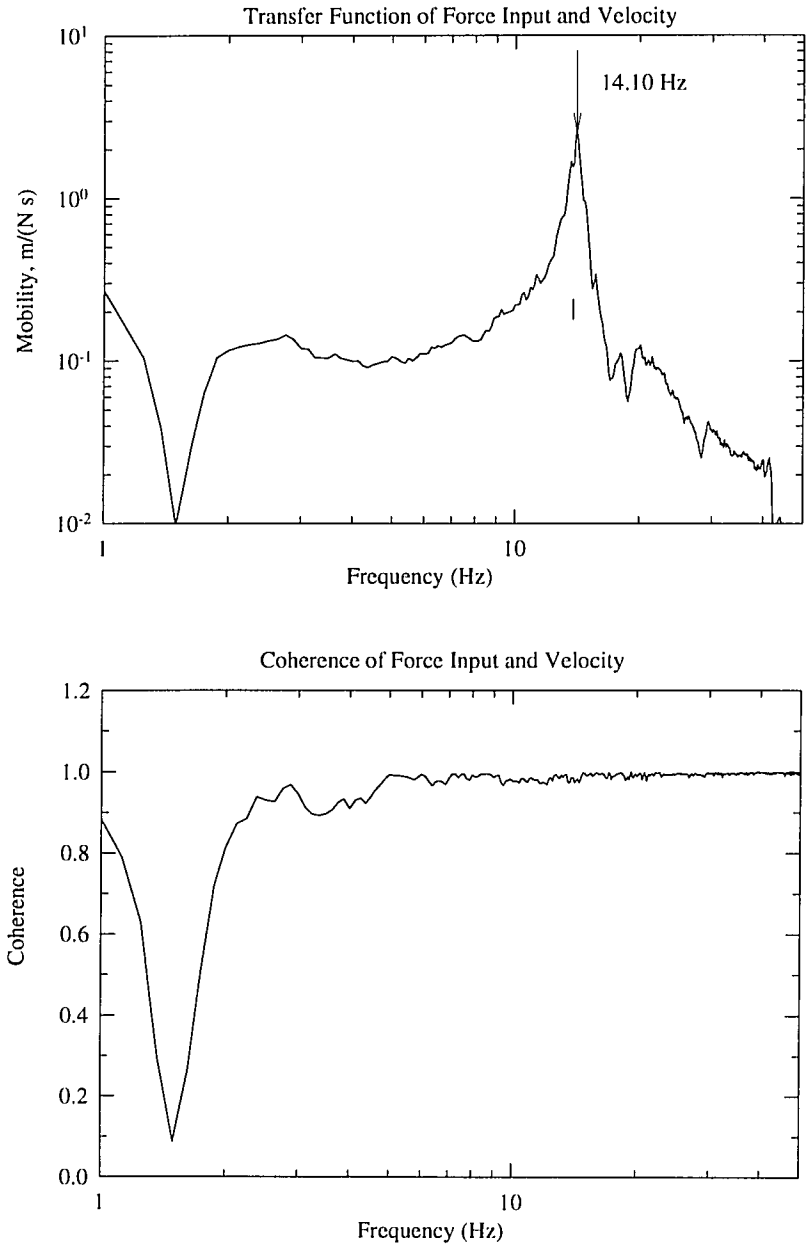

Figure 2-21: The mobility of the rocking mode in the yz plane, $f_{\theta y}$, of test unit #1 on case with 1/4 HP motor and circular disk, $f_{\theta y}$ = 14.10 Hz

the impact forces were applied to points 5, 6, 7 and 8. In test unit #1, these points were selected near the bolts which were used to attach the motor to the top of the unit. The points for applying the impact force should be located away from the bolts far enough to ensure the impact force was applied directly on the top. In test unit #2, the impact force was directly applied to the selected points. For identifying the swaying modes in the x and y directions, the impact force must be applied to the edge of the top of the unit, not to the side panel, at the selected points. For identifying translational mode in the z direction, a small steel bar (D = 0.5", L = 5") was used to ensure the impact force applied to the top of the unit was close enough to the point 9 where the accelerometer was fixed because of limited space at this point 9. For all these cases, the impact force must be perpendicularly applied to the impact surfaces.

(4) The side panel modes. For the test units which have sheets metal side panels like test unit #1, the side panel vibration modes can be excited and superimposed on the swaying mode measurements. Thus, the side panel modes must be measured separately. To measure the side panel modes, the accelerometer was fixed at the center of each side panel, i.e. points 1', 2', 3' and 4' as shown in Figure 2-1. The impact force were applied to both the points 1', 2', 3' and 4' and the points 1, 2, 3 and 4 to ensure that the correct side panel modes were measured and identified.

(5) Test setups. In the four different test setups discussed in Section 2.4, the motor and fan test should be conducted first, then, the frame only test. If any vibration modes of interest are not clear identified in the frame only test, the one mass test should be conducted. The motor and circular disk test is an optional test. It can be used to validate the test results from the motor and fan test.

(6) After conducting any two different test setups, the two-degree-of-freedom parameter estimating method discussed in Section 4-3 should be first used to estimate the system equivalent parameters. If the two-degree-of-freedom parameter estimating method does not work because the non-linear characteristics of the tested unit, the static stiffness

measurement as discussed in Section 4-2 should to be conducted. Then, the one-degree-of-freedom parameter estimating methods discussed in Sections 4-1 and 4-2 are used to obtain system equivalent parameters.

CHAPTER 3

ANALYTICAL MODELS

The vibration modes associated with the fan impeller, motor, and motor mount that are excited by fan impeller unbalance were investigated in two stages. The first stage was to develop the test procedures for making mobility measurements on the unit and for identifying all the modes of interest. The second stage was to develop a lumped parameter model for calculating the resonance frequencies associated with each mode. The test procedures were presented in Chapter 2. The development of the lumped parameter model and the corresponding equations of motion are discussed in this Chapter.

Following are basic assumptions that were made in the model development.

(1) When the fan impeller and motor is non-rotating, the motions in the xz and yz planes are both dynamically and statically uncoupled, and the motion in the z direction is both dynamically and statically uncoupled with other motions in the xz and yz planes.

(2) Comparing with the rocking stiffness of the top of the units, the bending stiffness of the motor rotor and shaft is significant larger. The bending deflection of the motor rotor and shaft is neglected.

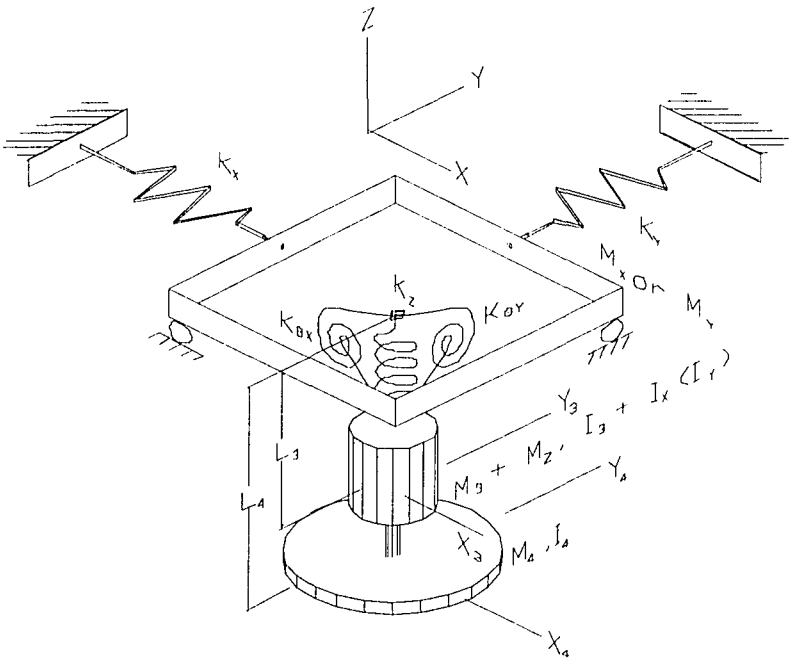

Figure 3-1: The three dimensional model with fan impeller not rotating

3.1 Three dimensional analytical model for non-rotating test

The units shown in Figures 2-1 and 2-2 are continuous systems which are impractical to model exactly. For simplicity, a lumped parameter model was used to approximate the continuous systems. For the motor and fan impeller not rotating, the lumped parameter model is shown in Figure 3-1.

In this three dimensional model, M_x and M_y represent the mass of the top of the unit and the equivalent mass from the unit frame in the x and y directions, respectively. The stiffness of the frame in the x and y directions are represented by K_x and K_y, respectively. Similarly, I_x and I_y are the effective mass moments of inertia and K_{0x} and K_{0y} are the effective rocking stiffness of the top of the unit in the xz and yz planes, respectively. Note that M_x is not necessarily the same as M_y because the test units are not exactly symmetrical. The same applies to K_x, K_y, I_x, I_y, K_x and K_y. M_z is the effective mass and K_z is the effective stiffness of the central part of the top of the unit in the z direction.

Masses M_3 and M_4 in Figure 3-1 are the masses of the motor and the circular disk/

or fan impeller, respectively. I_3 and I_4 are the mass moments of inertia of the motor and circular disk/or fan impeller, respectively, along the axis which is perpendicular to the rotation axis and through their mass centers.

3.1.1 The equations of motion

The velocity components of the mass centers of fan impeller and the motor associated with rocking motions in the xz and yz planes and the translational motions in the x, y and z directions are:

$$\begin{aligned} v_{3x} &= L_3\dot{\theta}_x + \dot{x} \\ v_{3y} &= L_3\dot{\theta}_y + \dot{y} \\ v_{3z} &= \dot{z} \end{aligned} \tag{3-1}$$

$$\begin{aligned} v_{4x} &= L_4\dot{\theta}_x + \dot{x} \\ v_{4y} &= L_4\dot{\theta}_y + \dot{y} \\ v_{4z} &= \dot{z} \end{aligned} \tag{3-2}$$

The potential energy of the system is:

$$V = \frac{1}{2}K_x x^2 + \frac{1}{2}K_y y^2 + \frac{1}{2}K_z z^2 + \frac{1}{2}K_{\theta x}\theta_x^2 + \frac{1}{2}K_{\theta y}\theta_y^2 \tag{3-3}$$

The kinetic energy of the system is:

$$\begin{aligned} T = &\frac{1}{2}m_x\dot{x}^2 + \frac{1}{2}m_y\dot{y}^2 + \frac{1}{2}m_z\dot{z}^2 + \frac{1}{2}I_{tx}\dot{\theta}_x^2 \\ &+ \frac{1}{2}I_{ty}\dot{\theta}_y^2 + ml(\dot{x}\dot{\theta}_x + \dot{y}\dot{\theta}_x) \end{aligned} \tag{3-4}$$

where:

$$
\begin{aligned}
I_{tx} &= I_3 + I_4 + M_3 L_3^{\,2} + M_4 L_4^{\,2} + I_x \\
I_{ty} &= I_3 + I_4 + M_3 L_3^{\,2} + M_4 L_4^{\,2} + I_y \\
ml &= M_3 L_3 + M_4 L_4 \\
m_x &= M_3 + M_4 + M_x \\
m_y &= M_3 + M_4 + M_y \\
m_z &= M_3 + M_4 + M_z
\end{aligned}
\tag{3-5}
$$

There is no external force on the system. Thus, the virtual work of the system is equal to zero:

$$\delta W = 0 \tag{3-6}$$

The equations of motion of the system are derived using Lagrange equation as following.

In the x direction:

$$
\begin{aligned}
&\frac{d}{dt}\left(\frac{\partial T}{\partial \dot{x}}\right) - \frac{\partial T}{\partial x} + \frac{\partial V}{\partial x} = 0 \\
&m_x \ddot{x} + ml\ddot{\theta}_x + K_x x = 0
\end{aligned}
\tag{3-7}
$$

In the θ_x direction:

$$
\begin{aligned}
&\frac{d}{dt}\left(\frac{\partial T}{\partial \dot{\theta}_x}\right) - \frac{\partial T}{\partial \theta_x} + \frac{\partial V}{\partial \theta_x} = 0 \\
&I_{tx}\ddot{\theta}_x + ml\ddot{x} + K_{\theta x}\theta_x = 0
\end{aligned}
\tag{3-8}
$$

In the y direction:

$$
\begin{aligned}
&\frac{d}{dt}\left(\frac{\partial T}{\partial \dot{y}}\right) - \frac{\partial T}{\partial y} + \frac{\partial V}{\partial y} = 0 \\
&m_y \ddot{y} + ml\ddot{\theta}_y + K_y y = 0
\end{aligned}
\tag{3-9}
$$

In the θ_y direction:

$$\frac{d}{dt}\left(\frac{\partial T}{\partial \dot{\theta}_y}\right)-\frac{\partial T}{\partial \theta_y}+\frac{\partial V}{\partial \theta_y}=0$$
$$I_{ty}\ddot{\theta}_y+ml\ddot{y}+K_{0y}\theta_y=0 \tag{3-10}$$

z direction:

$$\frac{d}{dt}\left(\frac{\partial T}{\partial \dot{z}}\right)-\frac{\partial T}{\partial z}+\frac{\partial V}{\partial z}=0$$
$$m_z\ddot{z}+K_z z=0 \tag{3-11}$$

In the matrix form, equations (3-7) through (3-11) are expressed as:

$$[M]\{\ddot{X}\}+[K]\{X\}=\{0\} \tag{3-12}$$

where:

$$[M]=\begin{bmatrix} M_x+M_3+M_4 & M_3L_3+M_4L_4 & 0 & 0 & 0 \\ M_3L_3+M_4L_4 & I_{tx} & 0 & 0 & 0 \\ 0 & 0 & M_y+M_3+M_4 & M_3L_3+M_4L_4 & 0 \\ 0 & 0 & M_3L_3+M_4L_4 & I_{ty} & 0 \\ 0 & 0 & 0 & 0 & M_z+M_3+M_4 \end{bmatrix} \tag{3-13}$$

$$[K]=\begin{bmatrix} K_x & 0 & 0 & 0 & 0 \\ 0 & K_{\theta x} & 0 & 0 & 0 \\ 0 & 0 & K_y & 0 & 0 \\ 0 & 0 & 0 & K_{\theta y} & 0 \\ 0 & 0 & 0 & 0 & K_z \end{bmatrix} \tag{3-14}$$

$$\{\ddot{X}\} = \begin{Bmatrix} \ddot{x} \\ \ddot{\theta}_x \\ \ddot{y} \\ \ddot{\theta}_y \\ \ddot{z} \end{Bmatrix} \tag{3-15}$$

$$\{X\} = \begin{Bmatrix} x \\ \theta_x \\ y \\ \theta_y \\ z \end{Bmatrix} \tag{3-16}$$

3.1.2 Discussion

The equations of motion indicate the motion in the z direction is uncoupled from the motions in other directions. The motions in the xz plane are uncoupled from the motions in the yz plane. The coupled motions are the swaying motion in the x direction with the rocking motion in the xz plane and the swaying motion in the y direction with the rocking motion in the yz plane.

3.2 Analytical models including the gyroscopic effect of rotating fan impeller, model 1 - classical approach

When the fan impeller is rotating at speed, Ω, because of the flexibility of the top of the unit, the rocking motions of the fan impeller in the xz and yz planes will induce a whirling motion of the fan impeller about the non-rotating axis, or called spin axis. This whirling motion of the fan impeller will cause additional inertial moments acting on the system. These additional inertial moments are called gyroscopic moments. The phenomenon is called gyroscopic effect of the rotating fan impeller. In the classical

approach discussed here, these gyroscopic moments caused by the fan impeller whirling are treated as the external moments. When the Lagrange equation is used to derive the equations of motion of the system, the virtual work of the these moments is considered.

3.2.1 The gyroscopic moments

When the fan impeller has the whirling motion about the spin axis, the rotation of the fan impeller, Ω, and the rocking motion in the xz (or yz) plane together form the gyroscopic moment, as shown in Figure 3-2. This gyroscopic moment follows the right-hand rule and has the magnitude of:

$$T_x = I_a \Omega \dot{\theta}_x \tag{3-17}$$

From Figure 3-2, the motion in the xz plane induces the gyroscopic moment about the x axis. This moment causes a motion in the yz plane, which, in turn, induces the gyroscopic moment about the y axis and so on. Thus, the gyroscopic effect of the rotating fan impeller will cause the motions in the xz and yz planes to become coupled. As a result of this coupling, the rocking motions, which for a non-rotating fan impeller occur independently in the two different planes, are now coupled by a whirling motion about spin axis in the xy plane.

To evaluate the effect of this whirling motion on the system, a simple two-degree-of-freedom disk and rigid massless shaft system is discussed first. Then, it will be expanded to real system shown in Figure 3-1.

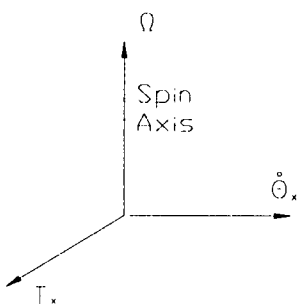

Figure 3-2 The gyroscopic moment

3.2.2 The simple two-degree-of-freedom disk and rigid massless shaft system

As shown in Figure 3-3, the disk and rigid massless shaft system is pivoted at one end of the shaft and the disk is at the other end of the shaft. The motions of the system are restrained by two rocking springs, $K_{\theta x}$ and $K_{\theta y}$, in the xz and yz planes. The coordinates of the motion are θ_x and θ_y.

The velocity components of the mass center of the disk are:

$$\begin{aligned} v_{4x} &= L_4\dot{\theta}_x \\ v_{4y} &= L_4\dot{\theta}_y \end{aligned} \tag{3-18}$$

The kinetic energy of the system is:

$$T = \frac{1}{2}I_4(\dot{\theta}_x^{\,2} + \dot{\theta}_y^{\,2}) + \frac{1}{2}M_4[(L_4\dot{\theta}_x)^2 + (L_4\dot{\theta}_y)^2] \tag{3-19}$$

The potential energy of the system is:

$$V = \frac{1}{2}K_{0x}\theta_x^{\,2} + \frac{1}{2}K_{0y}\theta_y^{\,2} \tag{3-20}$$

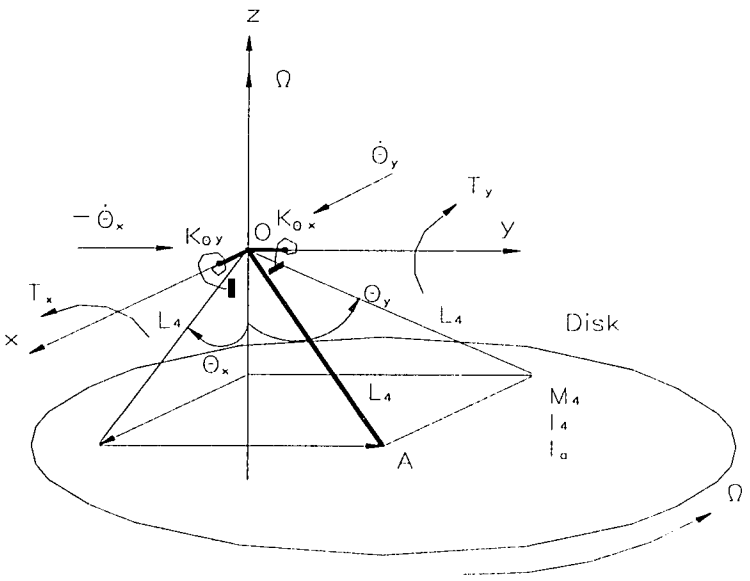

Figure 3-3 The disk and rigid massless system including the gyroscopic effect of the rotating disk - classical approach

The virtual work of the external moments is:

$$\delta W = T_x \delta\theta_y + T_y \delta\theta_x \tag{3-21}$$

According to d'Alembert's principle, the inertial moments can be represented by the static moments with negative sign. Thus, the moments, T_x and T_y, in equation (3-21) are expressed as:

$$\begin{aligned} T_x &= -[I_a \Omega(-\dot{\theta}_x)] = I_a \Omega \dot{\theta}_x \\ T_y &= -I_a \Omega \dot{\theta}_y \end{aligned} \tag{3-22}$$

Thus, the virtual work of the external moments is:

$$\begin{aligned} \delta W &= I_a \Omega \dot{\theta}_x \delta\theta_y - I_a \Omega \dot{\theta}_y \delta\theta_x \\ &= Q_x \delta\theta_x + Q_y \delta\theta_y \\ Q_x &= -I_a \Omega \dot{\theta}_y \\ Q_y &= I_a \Omega \dot{\theta}_x \end{aligned} \tag{3-23}$$

The equations of motion of the system are derived using Lagrange equation as following.

In the θ_x direction:

$$\begin{aligned} \frac{d}{dt}\left(\frac{\partial T}{\partial \dot{\theta}_x}\right) - \frac{\partial T}{\partial \theta_x} + \frac{\partial V}{\partial \theta_x} &= Q_x \\ (I_4 + M_4 L_4^{\,2})\ddot{\theta}_x + I_a \Omega \dot{\theta}_y + K_{\theta x}\theta_x &= 0 \end{aligned} \tag{3-24}$$

In the θ_y direction:

$$\begin{aligned} \frac{d}{dt}\left(\frac{\partial T}{\partial \dot{\theta}_y}\right) - \frac{\partial T}{\partial \theta_y} + \frac{\partial V}{\partial \theta_y} &= Q_y \\ (I_4 + M_4 L_4^{\,2})\ddot{\theta}_y - I_a \Omega \dot{\theta}_x + K_{\theta y}\theta_y &= 0 \end{aligned} \tag{3-25}$$

In the matrix form, equations (3-24) and (3-25) are expressed as:

$$[M]\{\ddot{\Theta}\} + [C]\{\dot{\Theta}\} + [K]\{\Theta\} = \{0\} \tag{3-26}$$

where:

$$[M]=\begin{bmatrix} I_4 + M_4 L_4{}^2 & 0 \\ 0 & I_4 + M_4 L_4{}^2 \end{bmatrix} \tag{3-27}$$

$$[C]=\begin{bmatrix} 0 & I_a\Omega \\ -I_a\Omega & 0 \end{bmatrix} \tag{3-28}$$

$$[K]=\begin{bmatrix} K_{\theta x} & 0 \\ 0 & K_{\theta y} \end{bmatrix} \tag{3-29}$$

$$\{\ddot{\Theta}\}=\begin{Bmatrix} \ddot{\theta}_x \\ \ddot{\theta}_y \end{Bmatrix} \tag{3-30}$$

$$\{\dot{\Theta}\}=\begin{Bmatrix} \dot{\theta}_x \\ \dot{\theta}_y \end{Bmatrix} \tag{3-31}$$

$$\{\Theta\}=\begin{Bmatrix} \theta_x \\ \theta_y \end{Bmatrix} \tag{3-32}$$

As discussion in Section 3.2.1, the gyroscopic moments of the rotating disk couple the motions in the two orthogonal directions into a coupled motion. The coupling term in the equations of motion involves the velocities. This coupling term is skew symmetric, which means that it is of opposite sign in the two equations. Thus, real eigenvalues are assured.

3.2.3 The five-degree-of-freedom fan impeller, motor and motor mount system

When deriving the equations of motion of the fan impeller, motor and motor mount system, as shown in Figures 3-1 and 3-4, the difference with the disk and shaft system is that the kinetic energy of the motor and equivalent system and the potential energy of the equivalent system must be considered. Following the procedures discussed

in Sections 3.1 and 3.2.2, the equations of motion of the fan impeller, motor and motor mount system can be obtained.

The velocity components of the mass centers of the fan impeller and the motor are:

$$\begin{aligned} v_{3x} &= L_3\dot{\theta}_x + \dot{x} \\ v_{3y} &= L_3\dot{\theta}_y + \dot{y} \\ v_{3z} &= \dot{z} \end{aligned} \tag{3-33}$$

$$\begin{aligned} v_{4x} &= L_4\dot{\theta}_x + \dot{x} \\ v_{4y} &= L_4\dot{\theta}_y + \dot{y} \\ v_{4z} &= \dot{z} \end{aligned} \tag{3-34}$$

The kinetic energy of the motor is:

$$T_3 = \frac{1}{2}M_3 v_{3x}^{\ 2} + \frac{1}{2}M_3 v_{3y}^{\ 2} + \frac{1}{2}M_3 v_{3z}^{\ 2} + \frac{1}{2}I_3\dot{\theta}_x^{\ 2} + \frac{1}{2}I_3\dot{\theta}_y^{\ 2} \tag{3-35}$$

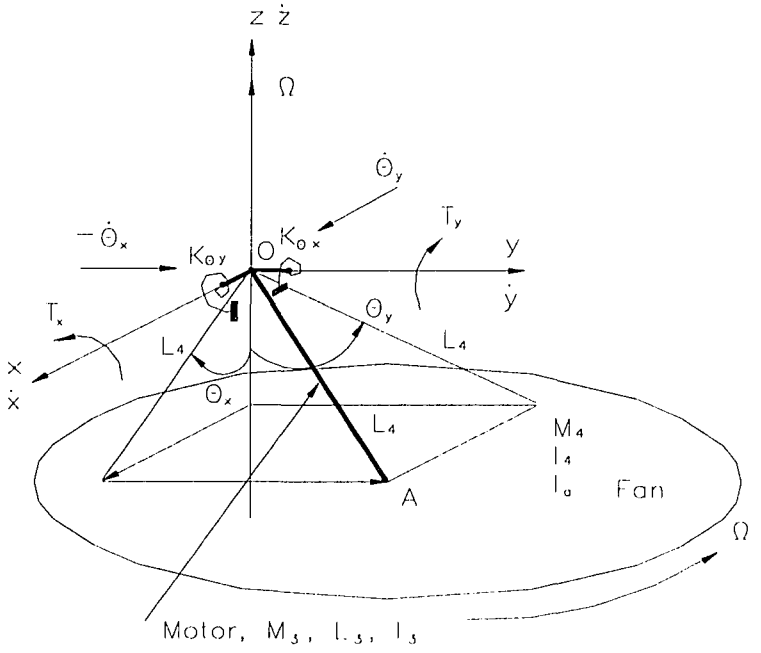

Figure 3-4 The fan impeller, motor and motor mount system including the gyroscopic effect of the rotating fan impeller - classical approach

The kinetic energy of the fan impeller is:

$$T_4 = \frac{1}{2} M_4 v_{4x}^2 + \frac{1}{2} M_4 v_{4y}^2 + \frac{1}{2} M_4 v_{4z}^2 + \frac{1}{2} I_4 \dot{\theta}_x^2 + \frac{1}{2} I_4 \dot{\theta}_y^2 \tag{3-36}$$

The kinetic energy of the motor mount system is:

$$T_e = \frac{1}{2} M_x \dot{x}^2 + \frac{1}{2} M_y \dot{y}^2 + \frac{1}{2} M_z \dot{z}^2 + \frac{1}{2} I_x \dot{\theta}_x^2 + \frac{1}{2} I_y \dot{\theta}_y^2 \tag{3-37}$$

The total kinetic energy of the fan impeller, motor and motor mount system is:

$$T = T_4 + T_3 + T_e \tag{3-38}$$

or,

$$\begin{aligned} T = {} & \frac{1}{2} m_x \dot{x}^2 + \frac{1}{2} m_y \dot{y}^2 + \frac{1}{2} m_z \dot{z}^2 + \frac{1}{2} I_{tx} \dot{\theta}_x^2 \\ & + \frac{1}{2} I_{ty} \dot{\theta}_y^2 + ml(\dot{x}\dot{\theta}_x + \dot{y}\dot{\theta}_x) \end{aligned} \tag{3-39}$$

where:

$$\begin{aligned} I_{tx} &= I_3 + I_4 + M_3 L_3^2 + M_4 L_4^2 + I_x \\ I_{ty} &= I_3 + I_4 + M_3 L_3^2 + M_4 L_4^2 + I_y \\ ml &= M_3 L_3 + M_4 L_4 \\ m_x &= M_3 + M_4 + M_x \\ m_y &= M_3 + M_4 + M_y \\ m_z &= M_3 + M_4 + M_z \end{aligned} \tag{3-40}$$

The potential energy of the fan impeller, motor and motor mount system is:

$$V = \frac{1}{2} K_x x^2 + \frac{1}{2} K_y y^2 + \frac{1}{2} K_z z^2 + \frac{1}{2} K_{\theta x} \theta_x^2 + \frac{1}{2} K_{\theta y} \theta_y^2 \tag{3-41}$$

The virtual work of the external moments is the same as given in equation (3-23):

$$\begin{aligned}\delta W &= I_a \Omega \dot{\theta}_x \delta\theta_y - I_a \Omega \dot{\theta}_y \delta\theta_x \\ &= Q_x \delta\theta_x + Q_y \delta\theta_y \\ Q_x &= -I_a \Omega \dot{\theta}_y \\ Q_y &= I_a \Omega \dot{\theta}_x\end{aligned} \tag{3-42}$$

The equations of motion of the fan impeller, motor and motor mount system are derived using Lagrange equation as following.

In the x direction:

$$\begin{aligned}&\frac{d}{dt}\left(\frac{\partial T}{\partial \dot{x}}\right) - \frac{\partial T}{\partial x} + \frac{\partial V}{\partial x} = 0 \\ &m_x \ddot{x} + ml\ddot{\theta}_x + K_x x = 0\end{aligned} \tag{3-43}$$

In the θ_x direction:

$$\begin{aligned}&\frac{d}{dt}\left(\frac{\partial T}{\partial \dot{\theta}_x}\right) - \frac{\partial T}{\partial \theta_x} + \frac{\partial V}{\partial \theta_x} = Q_x \\ &I_{tx}\ddot{\theta}_x + ml\ddot{x} + I_a \Omega \dot{\theta}_y + K_{\theta x}\theta_x = 0\end{aligned} \tag{3-44}$$

In the y direction:

$$\begin{aligned}&\frac{d}{dt}\left(\frac{\partial T}{\partial \dot{y}}\right) - \frac{\partial T}{\partial y} + \frac{\partial V}{\partial y} = 0 \\ &m_y \ddot{y} + ml\ddot{\theta}_y + K_y y = 0\end{aligned} \tag{3-45}$$

In the θ_y direction:

$$\begin{aligned}&\frac{d}{dt}\left(\frac{\partial T}{\partial \dot{\theta}_y}\right) - \frac{\partial T}{\partial \theta_y} + \frac{\partial V}{\partial \theta_y} = Q_y \\ &I_{ty}\ddot{\theta}_y + ml\ddot{y} - I_a \Omega \dot{\theta}_x + K_{\theta y}\theta_y = 0\end{aligned} \tag{3-46}$$

In the z direction:

$$\frac{d}{dt}\left(\frac{\partial T}{\partial \dot{z}}\right)-\frac{\partial T}{\partial z}+\frac{\partial V}{\partial z}=0$$
$$m_z\ddot{z}+K_z z=0 \tag{3-47}$$

In the matrix form, equations (3-43), (3-44), (3-45), (3-46) and (3-47) are expressed as:

$$[M]\{\ddot{X}\}+[C]\{\dot{X}\}+[K]\{X\}=\{0\} \tag{3-48}$$

where, by substituting the relationships given in equation (3-40):

$$[M]=\begin{bmatrix} M_x+M_3+M_4 & M_3L_3+M_4L_4 & 0 & 0 & 0 \\ M_3L_3+M_4L_4 & I_{tx} & 0 & 0 & 0 \\ 0 & 0 & M_y+M_3+M_4 & M_3L_3+M_4L_4 & 0 \\ 0 & 0 & M_3L_3+M_4L_4 & I_{ty} & 0 \\ 0 & 0 & 0 & 0 & M_z+M_3+M_4 \end{bmatrix} \tag{3-49}$$

$$[C]=\begin{bmatrix} 0 & 0 & 0 & 0 & 0 \\ 0 & 0 & 0 & I_a\Omega & 0 \\ 0 & 0 & 0 & 0 & 0 \\ 0 & -I_a\Omega & 0 & 0 & 0 \\ 0 & 0 & 0 & 0 & 0 \end{bmatrix} \tag{3-50}$$

$$[K]=\begin{bmatrix} K_x & 0 & 0 & 0 & 0 \\ 0 & K_{\theta x} & 0 & 0 & 0 \\ 0 & 0 & K_y & 0 & 0 \\ 0 & 0 & 0 & K_{\theta y} & 0 \\ 0 & 0 & 0 & 0 & K_z \end{bmatrix} \tag{3-51}$$

$$\{\ddot{X}\} = \begin{Bmatrix} \ddot{x} \\ \ddot{\theta}_x \\ \ddot{y} \\ \ddot{\theta}_y \\ \ddot{z} \end{Bmatrix} \tag{3-52}$$

$$\{\dot{X}\} = \begin{Bmatrix} \dot{x} \\ \dot{\theta}_x \\ \dot{y} \\ \dot{\theta}_y \\ \dot{z} \end{Bmatrix} \tag{3-53}$$

$$\{X\} = \begin{Bmatrix} x \\ \theta_x \\ y \\ \theta_y \\ z \end{Bmatrix} \tag{3-54}$$

Equation (3-48) has the identical format with equation (3-26). The gyroscopic effect of the rotating fan impeller couple the motions in the xz and yz planes. The coupling terms in the equations of motion involves the velocities. These are skew symmetric, which means real eigenvalues are assured.

3.3 Analytical models including the gyroscopic effect of rotating fan impeller, model 2 - energy approach

In the classical approach discussed in Section 3.2, the effect of the whirling motion of the rotating fan impeller was considered as external moments. When deriving equations of motion of the system, the virtual work of these external moments was

included in the system equations.

An alternative energy approach is discussed in this section. Instead of considering the virtual work of the external moments, the kinetic energy associated with the whirling motion of the rotating fan impeller is directly used in deriving of the system equations.

3.3.1 The angle relationship

To consider the kinetic energy associated with the whirling motion of the rotating fan impeller, an angle, ψ, is used, which is the angle between the spin axis (z axis) and the rotational axis (OA) of the fan impeller, as shown in Figure 3-5. The relationships between OA, OB, OC and OD are:

$$OC = OA\cos(\psi) = OB\cos(\theta_x) = OD\cos(\theta_y) \tag{3-55}$$

or,

$$OC = r\cos(\psi) = r'\cos(\theta_x) = r''\cos(\theta_y) \tag{3-56}$$

In the problem discussed here, ψ, θ_x and θ_y are assumed to be small angles, which gives:

$$\cos(\psi) \approx \cos(\theta_x) \approx \cos(\theta_y) \approx 1 \tag{3-57}$$

and,

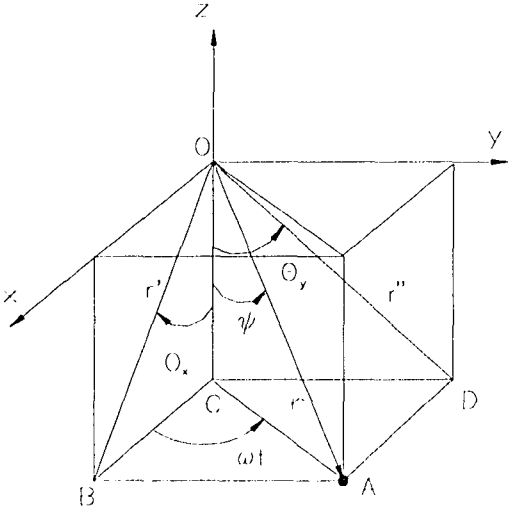

Figure 3-5 The angle relationship between ψ, θ_x and θ_y

$$\begin{aligned} \sin(\psi) &\approx \psi \\ \sin(\theta_x) &\approx \theta_x \\ \sin(\theta_y) &\approx \theta_y \end{aligned} \tag{3-58}$$

Thus, the following relationship between r, r' and r" is obtained:

$$r' = r'' = r \tag{3-59}$$

Also, the relationship between CA, CB and CD is

$$\begin{aligned} CA^2 &= CB^2 + CD^2 \\ (r\sin(\psi))^2 &= (r'\sin(\theta_x))^2 + (r''\sin(\theta_y))^2 \end{aligned} \tag{3-60}$$

or,

$$\sin^2\psi = \sin^2\theta_x + \sin^2\theta_y \tag{3-61}$$

By using equation (3-58), equation (3-61) is reduced to:

$$\psi^2 = \theta_x^2 + \theta_y^2 \tag{3-62}$$

Equation (3-62) gives the non-linear relationship between ψ, θ_x and θ_y. It can be changed and expanded to the following form:

$$\begin{aligned} \psi &= [(\theta_x + \theta_y)^2 - 2\theta_x\theta_y]^{\frac{1}{2}} \\ &= (\theta_x + \theta_y) - \frac{\theta_x\theta_y}{\theta_x + \theta_y} - \cdots\cdots \end{aligned} \tag{3-63}$$

The second term and other higher order terms in equation (3-63) will result in the non-linear vibration problems. Analyzing the changes of ψ, θ_x and θ_y in Figure 3-4 shows that, when $\omega t = 0^0$ and 180^0, $\theta_y = 0.0$ and $\psi = \theta_x$, when $\omega t = 90^0$ and 270^0, $\theta_x = 0.0$ and $\psi = \theta_y$. This means that the second term and other higher order terms in equation (3-63) become zero four times in one whirling cycle. Considering the small angle assumptions, these terms behave as the disturbances superimposed on the main term $(\theta_x + \theta_y)$. To avoid solving non-linear vibrations, these disturbances are neglected and the following linear

relationship between ψ, θ_x and θ_y is assumed:
relationship between ψ, θ_x and θ_y is assumed:

$$\psi = \theta_x + \theta_y \qquad (3\text{-}64)$$

3.3.2 The simple two-degree-of-freedom disk and rigid massless shaft system

Similar to the discussion in Section 3.2, to evaluate the kinetic energy associated with the whirling motion of the fan impeller, a simple two-degree-of-freedom disk and rigid massless shaft system is discussed first. Then, it will be expanded to real system shown in Figure 3-1.

To represent the whirling motion of the rotating disk about the spin axis, the whirling speed, ω, is used as shown in Figure 3-6, in which the whirling speed is in the same direction with the rotating speed. If the system is released from an initial deflection, for example, θ_x in the xz plane, the resulting angular velocity as the system springs back

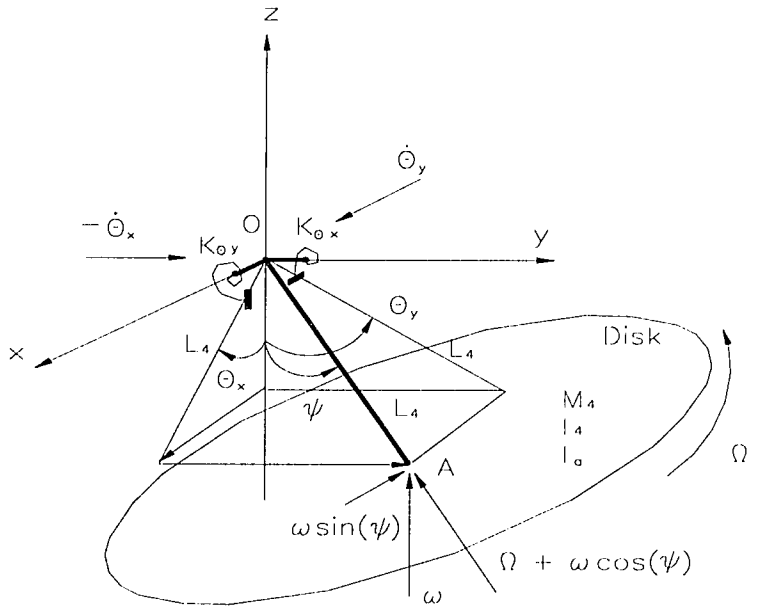

Figure 3-6: The disk and rigid massless system including the gyroscopic effect of the rotating disk - energy approach

induces a gyroscopic moment about the x axis. This moment causes the motion in the yz plane, which, in turn, induces a gyroscopic moment about the y axis and so on. Thus, the whirling motion of the rotating disk is a precession motion. The whirling vector is not parallel to the spin axis. It lies between the spin and rotating axes. Because the angle between spin axis and rotating axis, ψ, is small angle, it is reasonable to assume that the whirling vector, ω, is parallel to the spin axis as shown in Figure 3-5.

To evaluate the kinetic energy associated with the whirling motion of the rotating disk, there are two ways to resolve the whirling vector, ω, and rotating vector, Ω. One way is to resolve them along the rotating axis, which is the OA axis in Figure 3-5. The other is to resolve them along the spin axis, which is z axis in Figure 3-5. In this section, the first way is discussed. The second way will be discussed in the next section.

The translational velocity components of the mass center of the disk associated with the rocking motions in the θ_x and θ_y directions are same as equation (3-18):

$$\begin{aligned} v_{4x} &= L_4\dot{\theta}_x \\ v_{4y} &= L_4\dot{\theta}_y \end{aligned} \tag{3-65}$$

The kinetic energy of the system associated with the rocking motions in the θ_x and θ_y directions is:

$$T_r = \frac{1}{2} I_4(\dot{\theta}_x^{\,2} + \dot{\theta}_y^{\,2}) + \frac{1}{2} M_4[(L_4\dot{\theta}_x)^2 + (L_4\dot{\theta}_y)^2] \tag{3-66}$$

The translational velocity of the mass center of the disk associated with whirling motion is:

$$v_\omega = L_4 \sin\psi\omega \tag{3-67}$$

The rotational velocities parallel and perpendicular to the rotation axis are:

$$\begin{aligned} &\Omega + \omega\cos\psi \\ &\omega\sin\psi \end{aligned} \tag{3-68}$$

The kinetic energy of the system associated with the whirling motions of the

rotating disk is:

$$T_{\omega} = \frac{1}{2} M_4 (L_4 \sin\psi\omega)^2 + \frac{1}{2} I_4 (\omega \sin\psi)^2 + \frac{1}{2} I_a (\Omega + \omega \cos\psi)^2 \tag{3-69}$$

By using the relationships given in equations (3-61), (3-62) and (3-64), T_{ω} can be expressed as:

$$T_{\omega} = \frac{1}{2}(M_4 L_4^{\,2} + I_4)\omega^2(\theta_x^{\,2} + \theta_y^{\,2}) + \frac{1}{2} I_a [\Omega + \omega \cos(\theta_x + \theta_y)]^2 \tag{3-70}$$

The total kinetic energy of the system is:

$$\begin{aligned} T &= T_r + T_{\omega} \\ &= \frac{1}{2}(M_4 L_4^{\,2} + I_4)(\dot{\theta}_x^{\,2} + \dot{\theta}_y^{\,2}) + \frac{1}{2}(M_4 L_4^{\,2} + I_4)\omega^2(\theta_x^{\,2} + \theta_y^{\,2}) \\ &\quad + \frac{1}{2} I_a [\Omega + \omega \cos(\theta_x + \theta_y)]^2 \end{aligned} \tag{3-71}$$

The potential energy of the system is:

$$V = \frac{1}{2} K_{\theta x} \theta_x^{\,2} + \frac{1}{2} K_{\theta y} \theta_y^{\,2} \tag{3-72}$$

There is no external moments in this energy approach. Thus, the virtual work of the system is equal to zero:

$$\delta W = 0 \tag{3-73}$$

The equations of motion of the system are derived using Lagrange equation as following.

In the θ_x direction:

$$\begin{aligned} \frac{d}{dt}\left(\frac{\partial T}{\partial \dot{\theta}_x}\right) - \frac{\partial T}{\partial \theta_x} + \frac{\partial V}{\partial \theta_x} &= 0 \\ (I_4 + M_4 L_4^{\,2})\ddot{\theta}_x + [I_a \Omega\omega + (I_a - I_4 - M_4 L_4^{\,2})\omega^2 + K_{\theta x}]\theta_x & \\ + (I_a \Omega\omega + I_a \omega^2)\theta_y &= 0 \end{aligned} \tag{3-74}$$

In the θ_y direction:

$$\frac{d}{dt}\left(\frac{\partial T}{\partial \dot{\theta}_y}\right) - \frac{\partial T}{\partial \theta_y} + \frac{\partial V}{\partial \theta_y} = 0$$

$$(I_4 + M_4 L_4^2)\ddot{\theta}_y + [I_a \Omega\omega + (I_a - I_4 - M_4 L_4^2)\omega^2 + K_{\theta y}]\theta_y + (I_a \Omega\omega + I_a \omega^2)\theta_x = 0 \tag{3-75}$$

In the matrix form, equations (3-74) and (3-75) are expressed as:

$$[M]\{\ddot{\Theta}\} + [K]\{\Theta\} = \{0\} \tag{3-76}$$

where:

$$[M] = \begin{bmatrix} I_4 + M_4 L_4^2 & 0 \\ 0 & I_4 + M_4 L_4^2 \end{bmatrix} \tag{3-77}$$

$$[K] = \begin{bmatrix} I_a \Omega\omega + (I_a - I_4 - M_4 L_4^2)\omega^2 + K_{\theta x} & (I_a \Omega\omega + I_a \omega^2) \\ (I_a \Omega\omega + I_a \omega^2) & I_a \Omega\omega + (I_a - I_4 - M_4 L_4^2)\omega^2 + K_{\theta y} \end{bmatrix} \tag{3-78}$$

$$\{\ddot{\Theta}\} = \begin{Bmatrix} \ddot{\theta}_x \\ \ddot{\theta}_y \end{Bmatrix} \tag{3-79}$$

$$\{\Theta\} = \begin{Bmatrix} \theta_x \\ \theta_y \end{Bmatrix} \tag{3-80}$$

In this approach, since the kinetic energy associated with the whirling motion of the rotating disk was considered independently, the gyroscopic effect of the rotating disk was incorporated in the stiffness matrix [K]. Equation (7-78) shows the gyroscopic effect of the rotating disk both changes the effective stiffness of the system and presents coupling terms in the stiffness matrix. The mass matrix is the same as the classical approach.

Examining equation (7-78) shows that, when the rotating speed, Ω, goes to zero, stiffness matrix [K] does not go back to the non-rotating case automatically. Considering the nature of the whirling motion of the rotating disk, it is physically caused by the disk

rotation. When there is no rotation, $\Omega = 0$, there is no whirling motion, $\omega = 0$. Thus, mathematically, the condition that $\Omega = 0$, $\omega = 0$ can be assigned to equation (7-78). This condition assure that equation (7-78) goes back to the non-rotating case when the rotating speed, Ω, goes to zero.

For the case that the whirling speed, ω, is in the opposite direction with rotating speed, Ω, simply replace ω with $-\omega$ in the equation (3-78).

3.3.3 The five-degree-of-freedom fan impeller, motor and motor mount system

As was discussed in Section 3.2.3, when deriving the equations of motion of the fan impeller, motor and motor mount system, the kinetic energy of the motor and equivalent system and the potential energy of the equivalent system must be considered. Following the same procedures used in Sections 3.2.3, the equations of motion of the fan impeller, motor and motor mount system, as shown in Figures 3-1 and 3-6 can be obtained.

The translational velocity components of the mass centers of the fan impeller and the motor associated with the rocking motions in the xz and yz plane and the translational motion in the x, y and z directions are:

$$\begin{aligned} v_{3x} &= L_3\dot{\theta}_x + \dot{x} \\ v_{3y} &= L_3\dot{\theta}_y + \dot{y} \\ v_{3z} &= \dot{z} \end{aligned} \tag{3-81}$$

$$\begin{aligned} v_{4x} &= L_4\dot{\theta}_x + \dot{x} \\ v_{4y} &= L_4\dot{\theta}_y + \dot{y} \\ v_{4z} &= \dot{z} \end{aligned} \tag{3-82}$$

The kinetic energy of the motor associated with these motions is:

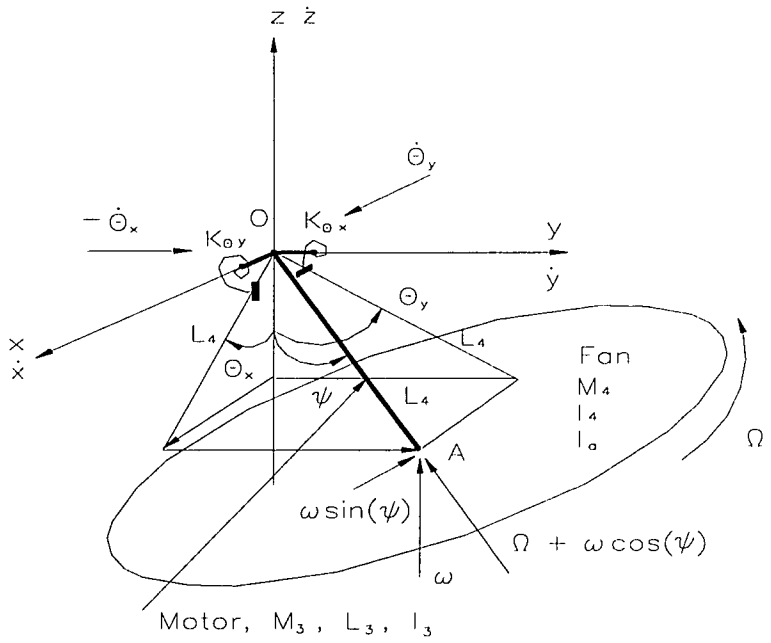

Figure 3-7: The fan impeller, motor and motor mount system including the gyroscopic effect of the rotating fan impeller - energy approach

$$T_3 = \frac{1}{2} M_3 v_{3x}^2 + \frac{1}{2} M_3 v_{3y}^2 + \frac{1}{2} M_3 v_{3z}^2 + \frac{1}{2} I_3 \dot{\theta}_x^2 + \frac{1}{2} I_3 \dot{\theta}_y^2 \tag{3-83}$$

The kinetic energy of the fan impeller associated with these motions is:

$$T_4 = \frac{1}{2} M_4 v_{4x}^2 + \frac{1}{2} M_4 v_{4y}^2 + \frac{1}{2} M_4 v_{4z}^2 + \frac{1}{2} I_4 \dot{\theta}_x^2 + \frac{1}{2} I_4 \dot{\theta}_y^2 \tag{3-84}$$

The kinetic energy of the motor mount system associated with these motions is:

$$T_e = \frac{1}{2} M_x \dot{x}^2 + \frac{1}{2} M_y \dot{y}^2 + \frac{1}{2} M_z \dot{z}^2 + \frac{1}{2} I_x \dot{\theta}_x^2 + \frac{1}{2} I_y \dot{\theta}_y^2 \tag{3-85}$$

The translational velocities of the mass centers of the fan impeller and the motor associated with whirling motion are:

$$\begin{aligned} v_{\omega 3} &= L_3 \sin\psi\omega \\ v_{\omega 4} &= L_4 \sin\psi\omega \end{aligned} \tag{3-86}$$

The rotational velocities parallel and perpendicular to the rotation axis are same with equation (3-68):

$$\begin{matrix} \Omega + \omega\cos\psi \\ \omega\sin\psi \end{matrix} \tag{3-87}$$

The kinetic energy of the system associated with the whirling motions of the rotating fan impeller is:

$$\begin{aligned} T_\omega &= \frac{1}{2} M_3 (L_3 \sin\psi\omega)^2 + \frac{1}{2} M_4 (L_4 \sin\psi\omega)^2 + \\ &\frac{1}{2} I_3 (\omega \sin\psi)^2 + \frac{1}{2} I_4 (\omega \sin\psi)^2 + \frac{1}{2} I_x (\omega \sin\theta_x)^2 \\ &+ \frac{1}{2} I_y (\omega \sin\theta_y)^2 + \frac{1}{2} I_a (\Omega + \omega\cos\psi)^2 \end{aligned} \tag{3-88}$$

By using the relationships given in equations (3-61), (3-62) and (3-64), T_ω can be expressed as:

$$T_\omega = \frac{1}{2} I_{tx} \omega^2 \theta_x^{\,2} + \frac{1}{2} I_{ty} \omega^2 \theta_y^{\,2} + \frac{1}{2} I_a [\Omega + \omega\cos(\theta_x + \theta_y)]^2 \tag{3-89}$$

where:

$$\begin{aligned} I_{tx} &= I_3 + I_4 + M_3 L_3^{\,2} + M_4 L_4^{\,2} + I_x \\ I_{ty} &= I_3 + I_4 + M_3 L_3^{\,2} + M_4 L_4^{\,2} + I_y \end{aligned} \tag{3-90}$$

The total kinetic energy of the fan impeller, motor and motor mount system is:

$$\begin{aligned} T &= T_3 + T_4 + T_e + T_\omega \\ &= \frac{1}{2} m_x \dot{x}^2 + \frac{1}{2} m_y \dot{y}^2 + \frac{1}{2} m_z \dot{z}^2 + \frac{1}{2} I_{tx} \dot{\theta}_x^{\,2} + \frac{1}{2} I_{ty} \dot{\theta}_y^{\,2} \\ &+ \frac{1}{2} I_{tx} \omega^2 \theta_x^{\,2} + \frac{1}{2} I_{ty} \omega^2 \theta_y^{\,2} + \frac{1}{2} I_a [\Omega + \omega\cos(\theta_x + \theta_y)]^2 \end{aligned} \tag{3-91}$$

where:

$$
\begin{aligned}
ml &= M_3 L_3 + M_4 L_4 \\
m_x &= M_3 + M_4 + M_x \\
m_y &= M_3 + M_4 + M_y \\
m_z &= M_3 + M_4 + M_z
\end{aligned}
\tag{3-92}
$$

The potential energy of the fan impeller, motor and motor mount system is:

$$
V = \frac{1}{2} K_x x^2 + \frac{1}{2} K_y y^2 + \frac{1}{2} K_z z^2 + \frac{1}{2} K_{\theta x} \theta_x^{\,2} + \frac{1}{2} K_{\theta y} \theta_y^{\,2} \tag{3-93}
$$

The virtual work of the system is zero:

$$
\delta W = 0 \tag{3-94}
$$

The equations of motion of the fan impeller, motor and motor mount system are derived using Lagrange equation as following.

In the x direction:

$$
\begin{aligned}
&\frac{d}{dt}\left(\frac{\partial T}{\partial \dot{x}}\right) - \frac{\partial T}{\partial x} + \frac{\partial V}{\partial x} = 0 \\
&m_x \ddot{x} + ml\ddot{\theta}_x + K_x x = 0
\end{aligned}
\tag{3-95}
$$

In the θ_x direction:

$$
\begin{aligned}
&\frac{d}{dt}\left(\frac{\partial T}{\partial \dot{\theta}_x}\right) - \frac{\partial T}{\partial \theta_x} + \frac{\partial V}{\partial \theta_x} = 0 \\
&I_{tx}\ddot{\theta}_x + ml\ddot{x} + [I_a \Omega\omega + (I_a - I_{tx})\omega^2 + K_{\theta x}]\theta_x \\
&\quad + (I_a \Omega\omega + I_a \omega^2)\theta_y = 0
\end{aligned}
\tag{3-96}
$$

In the y direction:

$$
\begin{aligned}
&\frac{d}{dt}\left(\frac{\partial T}{\partial \dot{y}}\right) - \frac{\partial T}{\partial y} + \frac{\partial V}{\partial y} = 0 \\
&m_y \ddot{y} + ml\ddot{\theta}_y + K_y y = 0
\end{aligned}
\tag{3-97}
$$

In the θ_y direction:

$$\frac{d}{dt}\left(\frac{\partial T}{\partial \dot{\theta}_y}\right)-\frac{\partial T}{\partial \theta_y}+\frac{\partial V}{\partial \theta_y}=0$$

$$I_{ty}\ddot{\theta}_y+ml\ddot{y}+[I_a\Omega\omega+(I_a-I_{ty})\omega^2+K_{\theta y}]\theta_y \qquad (3\text{-}98)$$

$$+(I_a\Omega\omega+I_a\omega^2)\theta_x=0$$

In the z direction:

$$\frac{d}{dt}\left(\frac{\partial T}{\partial \dot{z}}\right)-\frac{\partial T}{\partial z}+\frac{\partial V}{\partial z}=0 \qquad (3\text{-}99)$$

$$m_z\ddot{z}+K_z z=0$$

In the matrix form, equations (3-95) through (3-99) are expressed as:

$$[M]\{\ddot{X}\}+[K]\{X\}=\{0\} \qquad (3\text{-}100)$$

where, by substituting the relationships given in equations (3-90) and (3-92):

$$[M]=\begin{bmatrix} M_x+M_3+M_4 & M_3L_3+M_4L_4 & 0 & 0 & 0 \\ M_3L_3+M_4L_4 & I_{tx} & 0 & 0 & 0 \\ 0 & 0 & M_y+M_3+M_4 & M_3L_3+M_4L_4 & 0 \\ 0 & 0 & M_3L_3+M_4L_4 & I_{ty} & 0 \\ 0 & 0 & 0 & 0 & M_z+M_3+M_4 \end{bmatrix} \qquad (3\text{-}101)$$

$$[K]=\begin{bmatrix} K_x & 0 & 0 & 0 & 0 \\ 0 & I_a\Omega\omega+(I_a-I_{tx})\omega^2+K_{\theta x} & 0 & I_a\Omega\omega+I_a\omega^2 & 0 \\ 0 & 0 & K_y & 0 & 0 \\ 0 & I_a\Omega\omega+I_a\omega^2 & 0 & I_a\Omega\omega+(I_a-I_{ty})\omega^2+K_{\theta y} & 0 \\ 0 & 0 & 0 & 0 & K_z \end{bmatrix} \qquad (3\text{-}102)$$

$$\{\ddot{X}\} = \begin{Bmatrix} \ddot{x} \\ \ddot{\theta}_x \\ \ddot{y} \\ \ddot{\theta}_y \\ \ddot{z} \end{Bmatrix} \tag{3-103}$$

$$\{X\} = \begin{Bmatrix} x \\ \theta_x \\ y \\ \theta_y \\ z \end{Bmatrix} \tag{3-104}$$

Equation (102) has the identical format with equation (3-78). Thus, all discussions in Section 3.3.2 are applicable to equation (102).

3.4 Analytical models including the gyroscopic effect of rotating fan impeller, model 3 - energy approach

To evaluate the kinetic energy associated with the whirling motion of the rotating disk, there are two ways to resolve the whirling vector, ω, and rotating vector, Ω. One way is to resolve them along the rotating axis, which was discussed in Section 3.3. The other is to resolve them along the spin axis, which is discussed in this section.

As shown in Figure 3-8, when resolving the whirling motion and rotating motion of the disk along the spin axis, comparing with Figure 3-7, the rotational velocities parallel and perpendicular to the spin axis become:

$$\begin{matrix} \omega + \Omega\cos\psi \\ \Omega\sin\psi \end{matrix} \tag{105}$$

For the simple two-degree-of-freedom disk and massless rigid shaft system, the

stiffness matrix in equation (3-78) becomes:

$$[K]=\begin{bmatrix} I_a\Omega\omega+(I_a-I_4-M_4L_4{}^2)\Omega^2+K_{\theta x} & I_a\Omega\omega+I_a\Omega^2 \\ I_a\Omega\omega+I_a\Omega^2 & I_a\Omega\omega+(I_a-I_4-M_4L_4{}^2)\Omega^2+K_{\theta y} \end{bmatrix} \quad (106)$$

For the five-degree-of-freedom fan impeller, motor and motor mount system, the stiffness matrix in equation (3-102) becomes:

$$[K]=\begin{bmatrix} K_x & 0 & 0 & 0 & 0 \\ 0 & I_a\Omega\omega+(I_a-I_{tx})\Omega^2+K_{\theta x} & 0 & I_a\Omega\omega+I_a\Omega^2 & 0 \\ 0 & 0 & K_y & 0 & 0 \\ 0 & I_a\Omega\omega+I_a\Omega^2 & 0 & I_a\Omega\omega+(I_a-I_{ty})\Omega^2+K_{\theta y} & 0 \\ 0 & 0 & 0 & 0 & K_z \end{bmatrix} \quad (3\text{-}107)$$

3.5 Discussion

When including the gyroscopic effect of the rotating fan impeller in the equations

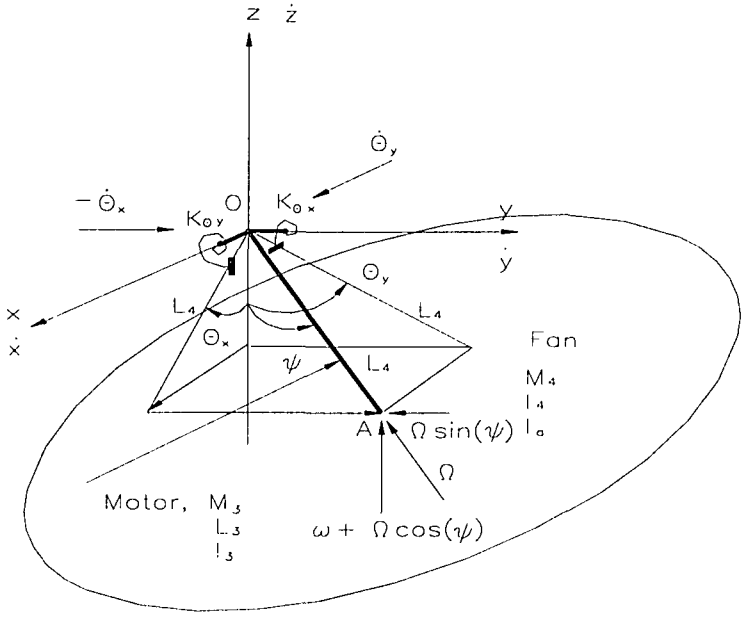

Figure 3-8: The fan impeller, motor and motor mount disk system including the gyroscopic effect of rotating fan impeller - energy approach

of motion, the mass matrix is not changed. In the classic approach, an additional damping matrix is added to the equations of motion. In the energy approaches, extra terms are added to the stiffness matrix. All these terms represents the modal coupling between two rocking motions and between two swaying motions.

The studies before show that the gyroscopic effect of the rotating fan impeller will cause the two non-rotating modes in the xz and yz planes, which are the two rocking modes, $f_{\theta x}$ and $f_{\theta y}$, and the two swaying modes, f_x and f_y in this case, to separate as rotational speed is increased. One mode will decrease in frequency, which is visualized as the whirling speed of the fan impeller, ω, is in the opposite direction as the shaft rotation, Ω. The other mode will increase in frequency, which is visualized as the whirling speed of the fan impeller, ω, is in the same direction as the shaft rotation, Ω. The modes shifting caused by the opposite direction whirling are called backward modes, which are f_θ - BW for the rocking mode and f_{xy} - BW for the swaying mode in this case. The modes shifting caused by the same direction whirling are called forward modes, which are f_θ - FW for the rocking mode and f_{xy} - FW for the swaying mode in this case.

As pointed by Den Hartog in his book [9], the forward mode can be excited by the fan impeller unbalance and it is a resonance phenomenon. The vibration amplitude at this forward mode is proportional to the amount of the fan impeller unbalance. In other word, the centrifugal force of the fan impeller unbalance will do work and input energy into the system to increase the vibration of the system. However, the backward mode is hardly excited by the fan impeller unbalance. Studies in NASA and Lockheed Aircraft [10] show that the backward mode is important only when the aeroelastic stability is considered. The rotating tests in this project proved that the backward mode did exist in the investigated air-conditioning units, but the vibration amplitude at this mode was fairly small. It did not cause vibration problems.

In this work, the equations of motion given in equation (3-26), (3-48), (3-76),

(3-100), (3-106) and (3-107) were solved by using Matlab software. Appendix C gives the Matlab files for different models.

CHAPTER 4

TECHNIQUES TO ESTIMATE

ANALYTICAL MODEL PARAMETERS

In this Chapter, information from Chapters 2 and 3 was used to estimate the parameters, M_x, M_y, M_z, I_x, I_y, K_x, K_y, K_z, $K_{\theta x}$ and $K_{\theta y}$ in the analytical model. All other parameters used in the calculation were measured. Table 2 in Chapter 2 presented these measured parameters for test unit #1 and test unit #2.

Depending on different test setups used for different test units, three parameter estimation techniques were developed. First one was the one-degree-of-freedom method, which was used to identify parameters in the z direction for the both units and to identify the rocking parameters in the xz and yz planes for test unit #1. The second one was the one-degree-of-freedom method plus the static stiffness measurement in the x and y directions, which was used to identify the parameters in the x and y directions for test unit #1. The third one was the two-degree-of-freedom method, which was used to identify the parameters in the x and y directions and in the xz and yz planes for test unit #2.

4.1 One-degree-of-freedom method

The one-degree-of-freedom method was used to identify parameters in the z

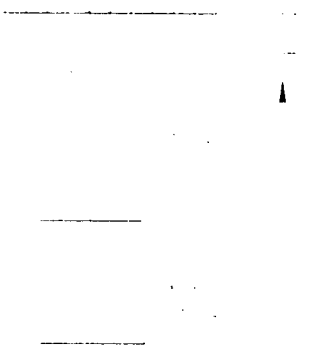

Figure 4-1: The one-degree-of-freedom model

direction for both units and to identify the rocking parameters in the xz and yz planes for test unit #1.

First, consider an one-degree-of-freedom system in the z direction, as shown in Figure 4-1. The resonance frequency of this system is expressed as:

$$f_{z1} = \frac{1}{2\pi}\sqrt{\frac{K_z}{M_z}} \tag{4-1}$$

The frequency, f_{z1}, was measured from the **frame only test** for test units #1 and test unit #2 (as addressed in Section 2.4).

Next, consider the same one-degree-of-freedom system with an added mass, M_a, as shown in Figure 4-2. The only change in the system is the change of mass, which becomes M_a+M_z. The new resonance frequency of the system is:

$$f_{z2} = \frac{1}{2\pi}\sqrt{\frac{K_z}{M_z + M_a}} \tag{4-2}$$

Where, the frequency, f_{z2}, was measured from the **motor and circular disk test** for test unit #1 and **motor and fan test** for test unit #2 (as addressed in Section 2.4).

In equations (4-1) and (4-2), there are only two unknowns: K_z and M_z. These

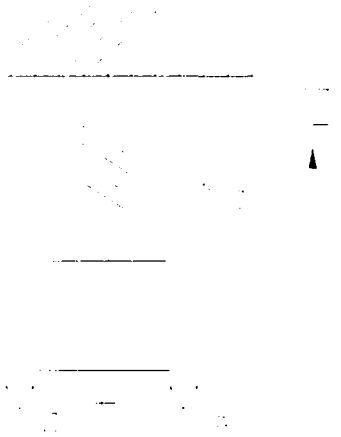

Figure 4-2: The one-degree-of-freedom model with added mass

values are obtained by:

$$M_z = \frac{M_a}{(\frac{f_{z1}}{f_{z2}})^2 - 1} \tag{4-3}$$

$$K_z = (2\pi f_{z1})^2 M_z \tag{4-4}$$

Equations (4-3) and (4-4) were used to identify the appropriate parameters in the z direction for both test unit #1 and test unit #2. The added mass, M_a, was equal to the sum of the mass of the motor and the circular disk/fan impeller, $M_a = M_3 + M_4$.

The same procedures were also used to identify the parameters in the xz and yz planes for test unit #1. Unfortunately, the motions in the x and q_χ directions, for example, were coupled. From an engineering point view, for the purpose of identifying the necessary parameters, the coupling effect between the motions in the x and q_χ directions was neglected. Thus, the motion in the θ_χ direction was modeled as an one-degree-of-freedom system and $K_{\theta\chi}$ and I_χ were calculated using the following equations:

$$I_\chi = \frac{I_{add}}{(\frac{f_{\theta x1}}{f_{\theta x2}})^2 - 1} \tag{4-5}$$

$$K_{\theta x} = (2\pi f_{\theta x1})^2 I_{add} \quad (4\text{-}6)$$

Where, the frequency $f_{\theta x1}$ in equations (4-5) and (4-6) was measured from the **frame only test** and $f_{\theta x2}$ in equation (4-5) was measured from the **motor and circular disk test**. The I_{add} in equation (4-5) was the added mass moment of inertia, which was equal to the sum of mass moment of inertia of motor and the circular disk, $I_{add} = I_3 + I_4 + M_3L_3^2 + M_4L_4^2$.

Similarly, equations (4-5) and (4-6) were used to identify the parameters in the yz plane too. The only difference was that $f_{\theta x1}$ and $f_{\theta x2}$ were replaced by $f_{\theta y1}$ and $f_{\theta y2}$ and they were measured from the **frame only test** and **motor and circular disk test**, respectively.

The errors caused by this simplification for two rocking modes in the xz and yz planes of test unit #1 were less than 7%.

4.2 One-degree-of-freedom method plus static stiffness measurement

Because there were difficulties in identifying the swaying modes in the test unit #1, the one-degree-of-freedom method plus the static stiffness measurement technique was developed to identify the parameters in the x and y directions.

Since the stiffness was measured, the effective mass is the only unknown in equation (4-1) and can be calculated directly. This applies to the swaying modes in the x and y directions.

The static deflection in the x direction, D_x, was measured by rigidly mounting the whole unit on an inertia base. A Dial Indicator mounted on one side of the unit was used to measure the static deflection, D_x, associated with a force, F_x, applied to the other side of the unit, as shown in Figure 4-3. The static stiffness was calculated by:

$$K_x = \frac{F_x}{D_x} \quad (4\text{-}7)$$

After obtaining K_x, the effective mass M_x was calculated by:

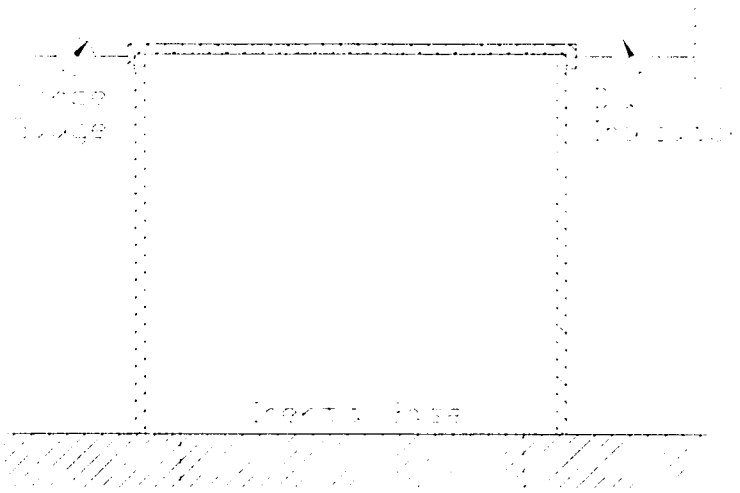

Figure 4-3: The schematic of static stiffness measurement

$$M_x = \frac{K_x}{(2\pi f_n)^2} \tag{4-8}$$

Similarly, the static deflection, D_y, and applied force, F_y, were obtained by using the same setup shown in Figure 4-3. K_y and M_y were calculated using equation (4-7) and (4-8), respectively. Appendix B gives the static stiffness data of test unit #1 on case.

4.3 Two-degree-of-freedom method.

Figures 4-4 and 4-5 are two dimensional model in the xz plane for one mass test and motor and fan test. Because that the motion in the z direction was uncoupled from motions in other two directions, the parameters in the z direction was identified using the one-degree-of-freedom method discussed in Section 4.1. The parameters in the x and y directions and in the xz and yz planes were identified using two-degree-of-freedom method discussed below for test unit #2.

4.3.1 The one mass test.

Figure 4-4 shows the two dimensional model in the xz plane for one mass test

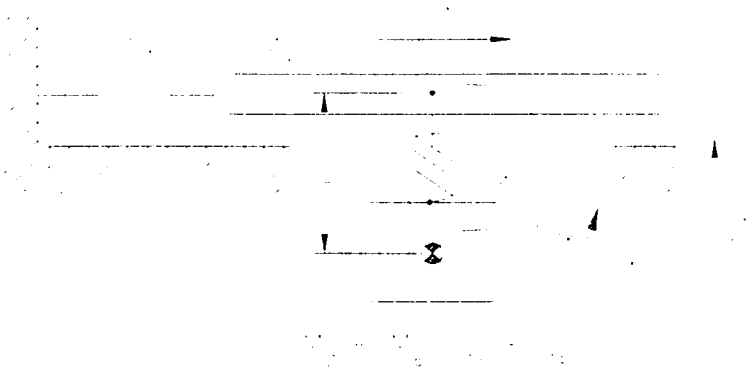

Figure 4-4: The two dimensional model for one mass test setup

setup. The equations of motions in the x and the θ_1 directions for this test setup are:

$$\begin{bmatrix} M_1 + M_b & M_b L_b \\ M_b L_b & M_b L_b^2 + I_b + I_1 \end{bmatrix} \begin{Bmatrix} \ddot{x} \\ \ddot{\theta}_1 \end{Bmatrix} + \begin{bmatrix} K_1 & 0 \\ 0 & K_{\theta_1} \end{bmatrix} \begin{Bmatrix} x \\ \theta_1 \end{Bmatrix} = \begin{Bmatrix} 0 \\ 0 \end{Bmatrix} \tag{4-9}$$

Assuming that motions in the x and θ_1 direction are harmonic, the following relationships are obtained:

$$\begin{aligned} x &= Ae^{i\omega t} \\ \theta_1 &= Be^{i\omega t + \varphi} \end{aligned} \tag{4-10}$$

$$\begin{aligned} \ddot{x} &= -\omega^2 x \\ \ddot{\theta}_1 &= -\omega^2 \theta_1 \end{aligned} \tag{4-11}$$

Substituting the relationships in equation (4-11) into equation (4-9), the eigenvalue equation of the two-degree-of-freedom system are obtained by setting following determinant to zero:

$$\begin{vmatrix} K_1 - \omega^2 (M_1 + M_b) & -M_b L_b \omega^2 \\ -M_b L_b \omega^2 & K_{\theta_1} - \omega^2 (I_1 + I_b + M_b L_b^2) \end{vmatrix} = 0 \tag{4-12}$$

After expansion, equation (4-12) is expanded as:

$$a_1 \omega^4 - b_1 \omega^2 + c_1 = 0 \tag{4-13}$$

the values of the coefficients are:

$$
\begin{aligned}
a_1 &= (M_1 + M_b)(I_1 + I_b + M_b L_b^2) - (M_b L_b)^2 \\
b_1 &= K_{\theta 1}(M_1 + M_b) + K_1(I_1 + I_b + M_b L_b^2) \\
c_1 &= K_1 K_{\theta 1}
\end{aligned}
\tag{4-14}
$$

Equation (4-13) is a quadratic equation of variable ω^2. There are two roots for this equation. They are $\omega_{x1}^2 = (2\pi f_{x1})^2$ and $\omega_{\theta x1}^2 = (2\pi f_{\theta x1})^2$, which correspond to the swaying mode and the rocking mode of the system shown in Figure 4-4, and are expressed as:

$$
\omega_{x1}^2 = \frac{b_1 + \sqrt{b_1^2 - 4a_1c_1}}{2a_1} \tag{4-15}
$$

$$
\omega_{\theta x1}^2 = \frac{b_1 - \sqrt{b_1^2 - 4a_1c_1}}{2a_1} \tag{4-16}
$$

where $\omega_{x1} = 2\pi f_{x1}$ and $\omega_{\theta x1} = 2\pi f_{\theta x1}$. The f_{x1} and $f_{\theta x1}$ were measured from the one mass test.

In equations (4-15) and (4-16), there are four unknowns, M_1, I_1, K_1 and $K_{\theta x}$. Thus another two equations Are needed to solve these unknowns. This Is done by running the motor and fan test.

4.3.2 The motor and fan test

The two dimensional model in the xz plane for motor and fan test setup is shown in Figure 4-5. The equations of motion in the x and the θ_1 directions for this test setup are expressed as:

$$
\begin{bmatrix} M_1 + M_3 + M_4 & M_3L_3 + M_4L_4 \\ M_3L_3 + M_4L_4 & M_3L_3^2 + M_4L_4^2 + I_3 + I_4 + I_1 \end{bmatrix} \begin{Bmatrix} \ddot{x} \\ \ddot{\theta}_1 \end{Bmatrix} + \begin{bmatrix} K_1 & 0 \\ 0 & K_{\theta 1} \end{bmatrix} \begin{Bmatrix} x \\ \theta_1 \end{Bmatrix} = \begin{Bmatrix} 0 \\ 0 \end{Bmatrix} \tag{4-17}
$$

The quadratic eigenvalue equation for this system is same as equation (4-9) except that the coefficients are different. For the condition of the determinant to be zero, the quadratic eigenvalue equation becomes:

$$
a_2\omega^4 - b_2\omega^2 + c_2 = 0 \tag{4-18}
$$

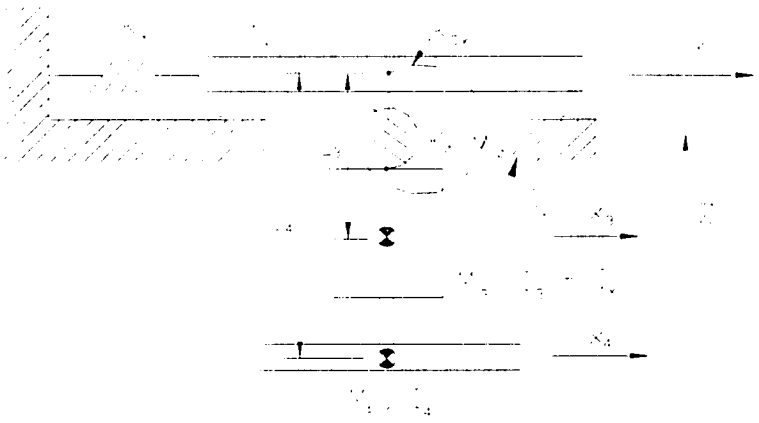

Figure 4-5: The two dimensional model of motor and fan test setup

the values of the coefficients are:

$$\begin{aligned} a_2 &= (M_1 + M_3 + M_4)(M_3L_3^2 + M_4L_4^2 + I_3 + I_4 + I_1) - (M_3L_3 + M_4L_4)^2 \\ b_2 &= K_{\theta x}(M_1 + M_3 + M_4) + K_1(M_3L_3^2 + M_4L_4^2 + I_3 + I_4 + I_1) \\ c_2 &= K_1 K_{\theta x} \end{aligned} \tag{4-19}$$

The two roots of equation (4-18) are $\omega_{x2}^2 = (2\pi f_{x2})^2$ and $\omega_{\theta x2}^2 = (2\pi f_{\theta x2})^2$, which correspond to the swaying mode and the rocking mode of the system shown in Figure 4-5, and are expressed as:

$$\omega_{x2}^2 = \frac{b_2 + \sqrt{b_2^2 - 4a_2c_2}}{2a_2} \tag{4-20}$$

$$\omega_{\theta x2}^2 = \frac{b_2 - \sqrt{b_2^2 - 4a_2c_2}}{2a_2} \tag{4-21}$$

where $\omega_{x2} = 2\pi f_{x2}$ and $\omega_{\theta x2} = 2\pi f_{\theta x2}$. The f_{x2} and $f_{\theta x2}$ were measured from the motor and fan test.

In equations (4-15), (4-16), (4-20) and (4-21), there are four unknowns and four measured frequencies: f_{x1}, $f_{\theta x1}$, f_{x2} and $f_{\theta x2}$. By solving the four equations simultaneously, the four unknowns, M_1, I_1, K_1 and $K_{\theta x}$, were obtained. In the same way, the parameters in

the yz plane were identified.

4.4 The Results

Table 3 gives the parameters identified using one-degree-freedom method and one-degree-freedom method plus static stiffness measurement for test unit #1 on case.

Table 4 gives the parameters identified using the one-degree-of-freedom method and the two-degree-of-freedom method for test unit #2 on case.

Table 3: The parameters for test unit #3 on the case identified using one-degree-of-freedom method plus static stiffness measurement

Mass (Kg)	M_x	M_y	M_z
	29.50	23.90	2.03
Mass Moment of Inertia ($Kg\text{-}m^2$)	I_x	I_y	
	0.00927	0.00858	
Translational Stiffness (N/m)	K_x	K_y	K_z
	442,000.00	494,000.00	84,000.00
Rocking Stiffness (N-m)	$K_{\theta x}$	$K_{\theta y}$	
	623.00	668.00	

Table 4: The parameters for test unit #2 on the case identified using one-degree-of -freedom method and two-degree-of-freedom method

Mass (Kg)	M_x	M_y	M_z
	22.10	22.90	2.60
Mass Moment of Inertia ($Kg\text{-}m^2$)	I_x	I_y	
	0.0117	0.00566	
Translational Stiffness (N/m)	K_x	K_y	K_z
	45,000.00	46,000.00	33,000.00
Rocking Stiffness (N-m)	$K_{\theta x}$	$K_{\theta y}$	
	610.00	539.00	

CHAPTER 5

FOUR-LEG FRAME

As discussed in Chapters 2 and 4, there were difficulties in identifying the swaying modes in the x and y directions for test unit #1. Thus, a four-leg frame was used to simulate the shell of this test unit. This frame was used to eliminate the unwanted vibration modes of the side panels of the unit and to make the installation of the vibration sensors simpler.

5.1 Design of four-leg frame

The four-leg frame, which had stiffness in both the x and y directions proportional to the corresponding stiffness of test unit #1, is schematically shown in Figure 5-1. The measurement points shown in the figure were the same points that were used to make the mobility measurements on the test unit #1, as shown in Figure 2-1. The four-leg frame was attached to an inertia base. The four horizontal bottom beams in the four-leg frame were used to make the stiffness in x and y directions uniform and to provide a way to attach the whole frame to the inertia base. The legs and bottom beams were made from 25.4 mm x 25.4 mm square tubing with a wall thickness of 1.651 mm.

Relative to the swaying modes in the x and y directions, the effect of the frame of the unit was visualized as four free-end cantilever beams. A small tip at the end of each

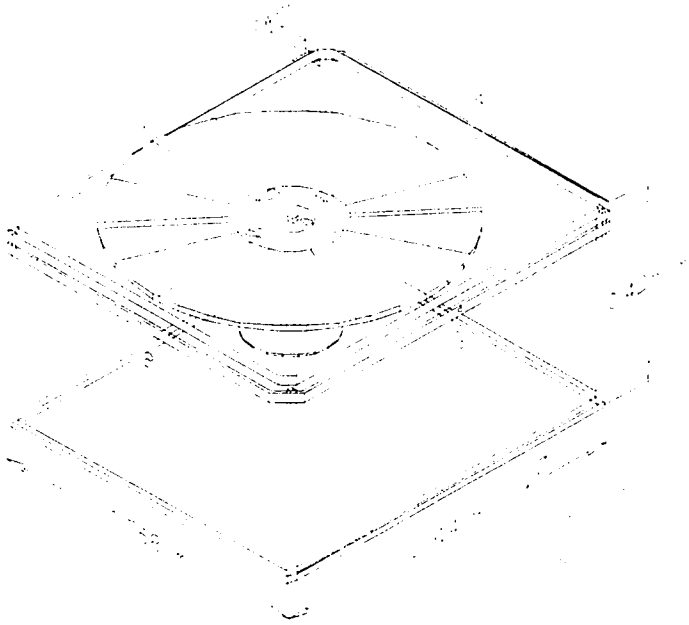

Figure 5-1: The schematic of four-leg frame and measurement points

leg was used to simulate the free-end (Figure 5-2). The top of the unit was attached to the four-legs at the four tips. This allowed the four-legs to work together as a free-end cantilever beam. The horizontal bottom beams were welded to the legs.

The boundary conditions of the top at the four-leg frame were analyzed. To more closely simulate the boundary conditions of the top of test unit #1, one angle frame was

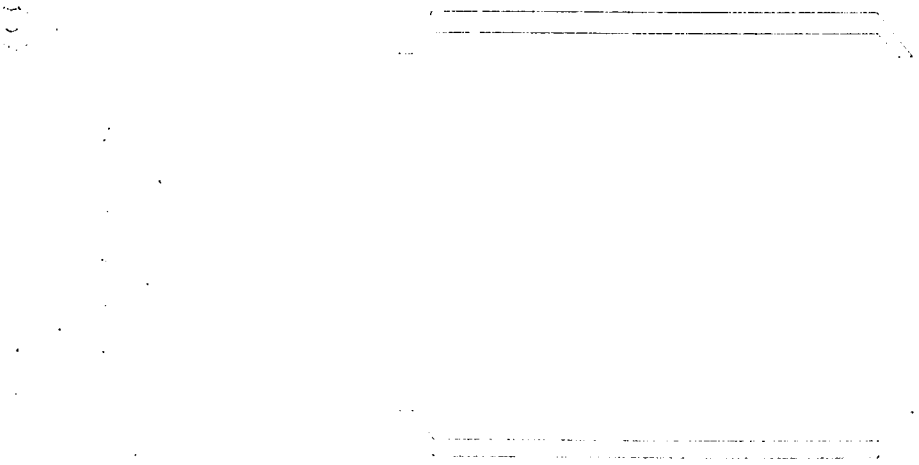

Figure 5-2: The leg and bottom beams

Figure 5-3: The angle frame for stiffening top

used to stiffen the top of the unit (Figure 5-3). The top of the unit was attached to the angle frame with bolts. The total mass of the top and angle frame was 16.38Kg.

5.2 Modifications of analytical model parameters

Because the structure and boundary conditions were changed when the top was supported on four-leg frame, the parameters used in the analytical model were changed correspondingly. These parameter changes were discussed in this section.

5.2.1 The modified stiffness and mass in the x and y directions

The effective stiffness, K_x and K_y, for the four-leg frame in both the x and y directions were measured as described in Section 4.2. The results of the static stiffness measurement in both the x and y directions for the four-leg frame are summarized in Appendix C.

The effective masses in both the x and y directions of the unit that was supported by the four-leg frame consisted of two parts:

(1) The total mass of the top and angle frame, which was 16.38Kg; and

(2) The effective mass from the four-legs.

Recalling the discussion about the equations of motion of the frame only test in Chapter 4, the motions in all directions were uncoupled from each other. In another words, the motion in any direction could be modeled as an one-degree-of-freedom system. Thus, the easiest way to obtain the effective masses, M_x and M_y, in both the x and y directions is to calculate them using following equations:

$$M_x = \frac{K_x}{(2\pi f_{x1})^2} \tag{5-1}$$

Table 5: The parameters for test unit #1 on four-leg frame

Mass (Kg)	M_x	M_y	M_z
	18.10	17.60	2.03
Mass Moment of Inertia ($Kg\text{-}m^2$)	I_x	I_y	
	0.00927	0.00858	
Translational Stiffness (N/m)	K_x	K_y	K_{eqz}
	303,000.00	313,000.00	70,000.00
Rocking Stiffness (N-m)	$K_{eq\theta x}$	$K_{eq\theta y}$	
	546.00	601.00	

$$M_x = \frac{K_x}{(2\pi f_{x1})^2} \tag{5-2}$$

where, the K_x, K_y, f_{x1} and f_{y1} were experimentally measured as described in Chapters 2 and 4.

Table 3 in Chapter 4 presented the parameters that were identified for the test unit #1 on case. Table 5 lists the parameters that were obtained with the top of test unit #1 supported on the four-leg frame.

5.2.2 The modified stiffness in the xz and yz planes and in the z direction

An angle frame was used to stiffen the top of the test unit #1 when it was mounted on the four-leg frame (Figure 5-3). However, the stiffness values of the test unit #1 mounted on the four-leg frame were less than the corresponding values that were measured when test unit #1 was fully assembled because the boundary conditions of the top of test unit #1 were different when it was mounted on four-leg frame.

When the top was fully assembled, it was visualized as a beam with two simply-supported ends, as shown in Figure 5-4. The equivalent model for the first vibration mode of the beam, which corresponds to the translational mode of the top in the z

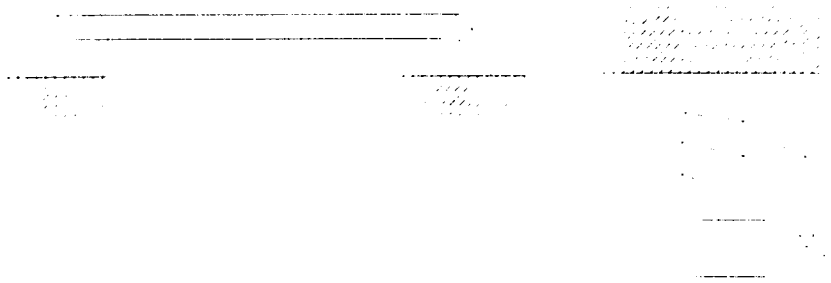

Figure 5-4: The simply supported beam and equivalent model for its first vibration mode

direction, was also shown in Figure 5-4.

When the four-leg frame was used to support the top of the test unit #1, the top became joined to the legs at four corners and supported by resilient supports at four points. This configuration was visualized as a beam that was supported by two springs at its ends, as shown in Figure 5-5. The equivalent model for this system's first vibration mode, i.e. the translational mode in the z direction, contained two springs in series. One spring was the effective spring of the beam, with stiffness K_z, which was identified before. The other spring was the sum of two supporting springs, which was K_z'. The new equivalent stiffness for the translational mode in z direction was designated K_{eqz} and obtained by:

$$\frac{1}{K_{eqz}} = \frac{1}{K_z} + \frac{1}{K'_z} \tag{5-3}$$

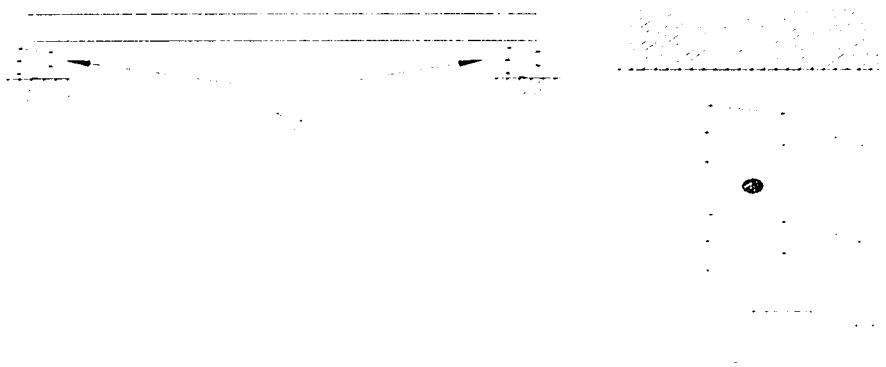

Figure 5-5: The spring supported beam and equivalent model for its first vibration mode

By assuming that the effective mass, M_z, did not change with the changes of boundary conditions, the value of K_{eqz} were directly calculated by:

$$K_{eqz} = (2\pi f_{z1})^2 M_z \tag{5-4}$$

where, the f_{z1} was experimentally measured as described in Chapter 2.

Similarly, by assuming that the effective mass moment of inertia, I_x and I_y, in the xz and yz planes did not change with the change of the boundary conditions, the new equivalent rocking stiffness, $K_{eq\theta x}$ and $K_{eq\theta y}$, in the xz and yz planes were calculated by:

$$K_{eq\theta x} = (2\pi f_{\theta x1})^2 I_x \tag{5-5}$$

$$K_{eq\theta y} = (2\pi f_{\theta y1})^2 I_y \tag{5-6}$$

where, the $f_{\theta x1}$ and $f_{\theta y1}$ were experimentally measured as described in Chapter 2.

Parameters for the top supported on the four-leg frame were given in Table 5. All other parameters used in the calculation were given in Table 2 in Chapter 2.

CHAPTER 6

EXPERIMENTS

Chapters 2, 3 and 4 discussed the test procedures used to identify the modes of interest, the analytical models used to predict these modes, and the identifications of the parameters used in these models. In this Chapter, the summaries of the results of both the non-rotating tests and the rotating tests and the results calculated from the analytical models are presented for test unit #1 both on the four-leg frame and the case and for test unit #2 on the case.

6.1 Non-rotating tests

The test procedures discussed in Chapter 2 were used in the non-rotating tests for identifying the modes of interest. The analytical model developed in Section 3.1 with fan impeller not rotating and the parameters identified in Section 4.4 were used to calculated these modes.

Because that motions in the xz and yz planes are uncoupled from each other for non-rotating case, the parameter changes in one plane will not affect the calculated results in the other plane. To identify which frequency in the results corresponds to, for example, the rocking mode in the xz plane, first, set all parameters in the yz plane to zero. Then the corresponding one-degree-of-freedom (ODF) resonance frequency of the rocking mode is

calculated by using equation (4-1). Since the swaying mode and the rocking mode in xz plane are the only modes left and they are separated very well, the frequency in the results which is closer to the ODF frequency is the rocking frequency in the xz plane. Using same approach, the rocking mode in the yz plane can be identified. The translational mode in the z direction is uncoupled from other mode. It can be calculated using equation (4-1).

6.1.1 Test unit #1 on the four-leg frame

Table 6 gives the measured and the calculated results for different test setups of test unit #1 on the four-leg frame. The calculated resonance frequencies agreed very well with the corresponding measured resonance frequencies. The swaying modes in both the x and y directions were exactly identified.

6.1.2 Test unit #1 on the case

Table 7 gives the measured results and the calculated results for different test setups of test unit #1 on the case. The analytical model yielded fairly good results for all of the modes except for some of the swaying mode in the y direction. The reason for this was that the swaying and rocking modes in xz plane and yz plane were coupled to each other. When the one-degree-of-freedom method was used to identify parameters, this coupling effect was neglected.

6.1.3 Test unit #2 on case

Table 8 gives the measured and calculated results for different test setups of test unit #2 on the case. The analytical model yielded very good results because the two-degree-of-freedom method was used in identifying the parameters.

Table 6: The non-rotating test results of test unit #1 on four-leg frame

Frequencies(Hz)		f_x	f_y	f_z	$f_{\theta x}$	$f_{\theta y}$
Frame only test	Measured	20.60	21.30	29.60	38.60	42.10
1/4 HP motor and circular disk	Calculated	19.60	20.20	13.70	11.50	12.10
	Measured	19.80	20.10	13.90	12.00	12.90
1/4 HP motor and No.60799501 fan impeller	Calculated	19.60	20.20	13.80	11.70	12.20
	Measured	20.00	20.50	14.00	12.30	13.10
1/3 HP motor and No.60843301 fan impeller	Calculated	19.30	19.90	12.80	10.40	10.90
	Measured	19.50	20.00	13.50	10.90	11.40

Table 7: The non-rotating test results of test unit #1 on case

Frequencies(Hz)		f_x	f_y	f_z	$f_{\theta x}$	$f_{\theta y}$
Frame only test	Measured	19.50	22.90	32.40	41.30	44.40
1/4 HP motor and circular disk	Calculated	19.10	22.00	15.00	12.40	13.00
	Measured	18.10	17.80	15.00	13.80	14.10
1/4 HP motor and No.60799501 fan impeller	Calculated	19.10	22.00	15.10	12.50	13.10
	Measured	18.90	18.30	15.40	12.90	14.40
1/3 HP motor and No.60843301 fan impeller	Calculated	18.90	21.70	14.00	11.10	11.60
	Measured	18.90	22.00	14.60	11.40	12.00

Table 8: The non-rotating test results of test unit #2 on case

Frequencies(Hz)		f_x	f_y	f_z	$f_{\theta x}$	$f_{\theta y}$
Frame only test	Measured	7.00	7.00	18.00	N/A	N/A
One mass test	Measured	6.60	6.60	11.30	30.90	36.60
No.LA01RA025 fan impeller	Calculated	6.40	6.40	10.10	16.40	16.30
	Measured	6.40	6.40	10.10	16.40	16.30
No. 203020-A fan impeller	Calculated	6.40	6.40	10.10	16.40	16.20
	Measured	7.00	7.00	10.30	16.30	16.10
No. 203020-C fan impeller	Calculated	6.40	6.40	10.10	16.40	16.20
	Measured	7.30	7.30	10.30	16.30	16.50
No. 203020-E fan impeller	Calculated	6.40	6.40	10.10	16.40	16.20
	Measured	7.30	7.30	10.40	16.90	16.90

6.2 Rotating Tests

To experimentally verify the forward and backward mode shifting and the resonance speeds corresponding to the gyroscopic effect of rotating fan impeller/disk, three types of rotating tests were conducted. The first type was rotating mobility tests, in which the motor and fan impeller/disk were rotating and which was used to verify the shifting of the forward and backward modes. The second type was peak hold spectrum, which measured the maximum vibration amplitudes at each frequency at selected points on the units while the motor speed was slowly varied. The third type was coast down test, which was completed by running the motor and fan impeller at a specific speed then

cutting off the power. The last two rotating tests were used to verify the system resonance speeds corresponding to the gyroscopic effect of the rotating fan impeller.

The forward and backward modes, which were caused by rotating fan impeller/ disk, occurred simultaneously. Both the forward and backward modes were measured in the experiments. The translational mode in the z direction was uncoupled from any other motion. It was not affected by the gyroscopic effect.

6.2.1 The rotating mobility test

The test setup for the rotating mobility test was identical with the **motor and fan** or **motor and circular disk** test setup. For the rotating mobility tests, the motor and fan impeller or circular disk were operated at a specified speed. The mobility as a function of frequency was measured.

To measure the forward and backward modes at any motor speed simultaneously, the impact force must be applied and accelerometer must be fixed at previously selected points. All the discussions in Chapter 2 about the mobility measurements and the points shown in Figures 2-12 and 2-13 are applicable to the rotating mobility measurements. As discussed in Section 3.5, the forward modes will be excited by the fan impeller unbalance and it is a resonance phenomenon. Thus, the forward modes are much more of interest and more important in this project. The backward modes will not be excited by the unbalance. But they will be excited by aerodynamic forces acting on the rotating fan impeller. In the peak hold spectrum test and the coast down test discussed later, the aerodynamically excited backward modes were measured. The vibration amplitudes at these backward modes were small because the motor speeds in the test units were low. The backward mode should not cause vibration problems in the investigated air-conditioning units.

Figures 6-1 and 6-2 give the rotating mobility measurements of test unit #1 on four leg frame with 1/4 HP motor and No. 60799501 fan impeller at speed 1000 RPM.

Figure 6-1 is the rotating mobility for the forward and backward rocking modes. Figure 6-2 is the rotating mobility for the forward and backward swaying modes.

The motor speed was varied using a variable frequency power supply. Thus, the forward and backward modes at the different rotation speeds were obtained. The measured forward and backward modes were compared with the predicted forward and backward modes by the models developed in Chapter 3.

Model 1 was developed by using the classical approach, in which the gyroscopic effect of the rotating fan impeller was treated as the additional external moments and included in the system equation by considering the virtual work of the moments. The equations of motion of the fan impeller, motor and motor mount system for the model 1 were given by equations (3-48) through (3-54).

Model 2 was developed by using the energy approach, in which the gyroscopic effect of the rotating fan impeller was treated as the additional kinetic energy. The whirling speed of the fan impeller, ω, was resolved into two components, which are parallel and perpendicular to the rotational axis. The equations of motion of fan impeller, motor and motor mount system for the model 2 were given by equations (3-100) through (3-104).

Model 3 was developed by using the same approach with model 2. In this model, the rotational speed of the fan impeller, Ω, was resolved into two components, which are parallel and perpendicular to the spin axis. The equations of motion of fan impeller, motor and motor mount system for the model 3 were same as model 2 except that the stiffness matrix given in equation (3-102) was replaced by equation (3-107).

6.2.1.1 The rotating mobility measurements of test unit #1 on the four-leg frame

Two group test data are discussed here. One group data is the rotating mobility measurements of the unit with 1/4 HP motor and circular disk. The results from this test

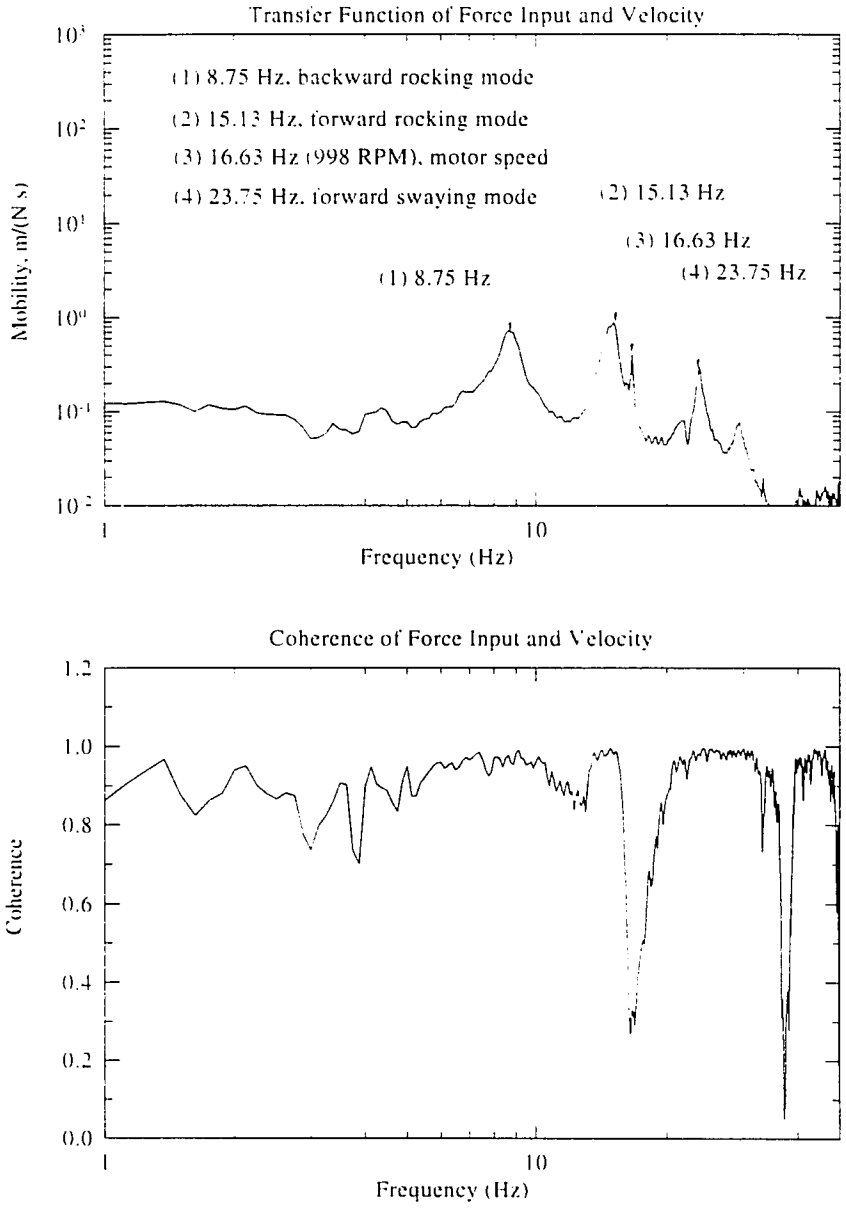

Figure 6-1: The rotating mobility measurement for both the forward and backward rocking modes of test unit #1 on four leg frame with 1/4 HP motor and No. 60799501 fan impeller, the motor speed is 1000 RPM.

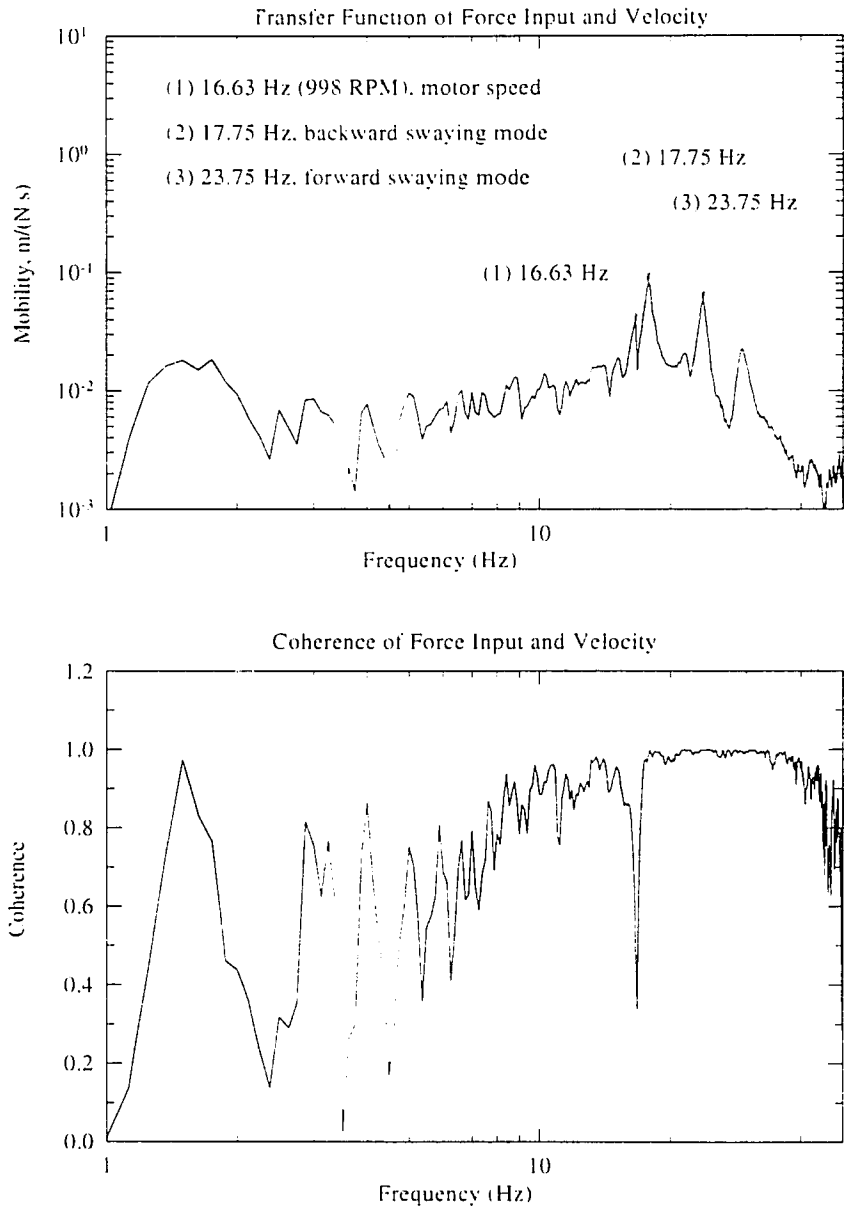

Figure 6-2: The rotating mobility measurement for both the forward and backward swaying modes of test unit #1 on four leg frame with 1/4 HP motor and No. 60799501 fan impeller, the motor speed is 1000 RPM.

setup are used to validate the analytical models. The other group data is the rotating mobility measurements of the unit with 1/4 HP motor and 60799501 fan impeller.

Figure 6-3 gives the measured forward and backward rocking modes and the calculated ones from models 1, 2 and 3 for test unit #1 supported on four leg frame with 1/4 HP motor and circular disk. For the forward rocking mode, model 1 and model 2 have the same accuracies. The average and standard deviations of two models are very close. The problem for model 2 is that this model does not converge to the non-rotating modes as the rotating speed is decreased to zero. This is because the assumed whirling vector, ω, does not fully represent the wobbling motion of the fan impeller at low motor speeds. At higher speeds, model 2 gives equally good predictions about the forward rocking mode as model 1 does, especially around the resonance speed. It is very important in this project to obtain good predictions of the resonance speeds of the system. For the backward rocking mode, model 1 gives better predictions than model 2. Because the backward rocking mode will not be excited by the fan impeller unbalance, it is not important in this work. For model 3, it gives acceptable predictions for forward rocking mode. But it does not give good predictions for the backward rocking mode.

Figure 6-4 gives the measured forward and backward swaying modes and the calculated ones from models 1, 2 and 3 for test unit #1 supported on four leg frame with 1/4 HP motor and circular disk. For the forward swaying mode, model 2 gives the best predictions. The average and standard deviations of model 2 is much better than model 1 and model 3. For the backward swaying mode, model 1, 2 and 3 have almost same accuracies.

Figure 6-5 is the measured and calculated translational mode in the z direction for test unit #1 supported on four leg frame with 1/4 HP motor and circular disk. Because this mode is uncoupled from all other modes and is not affected by the gyroscopic effect of the rotating fan impeller, all models give the same prediction. The measured rotating mobility data verified this.

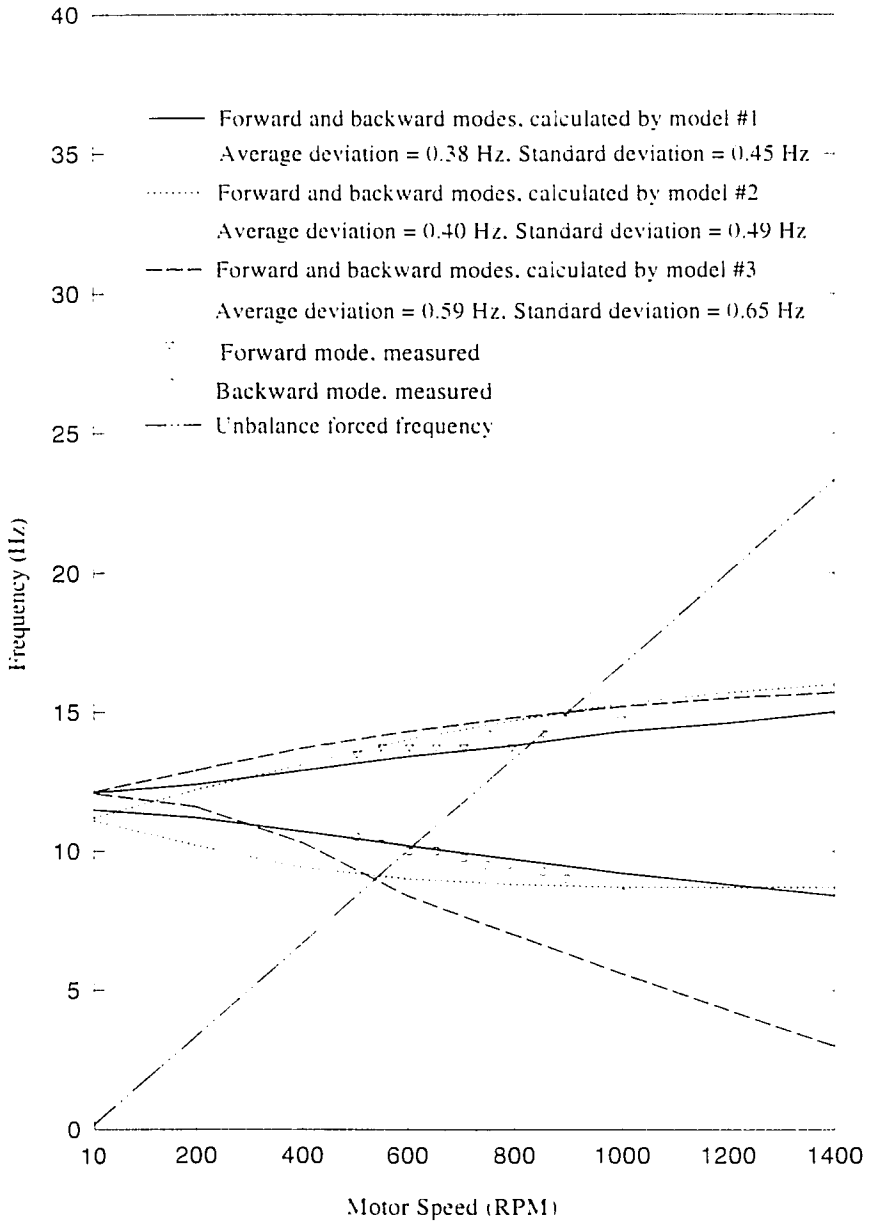

Figure 6-3: The forward and backward rocking modes of test unit #1 on four leg frame with 1/4 HP motor and circular disk, the given average and standard deviations are for the forward rocking mode.

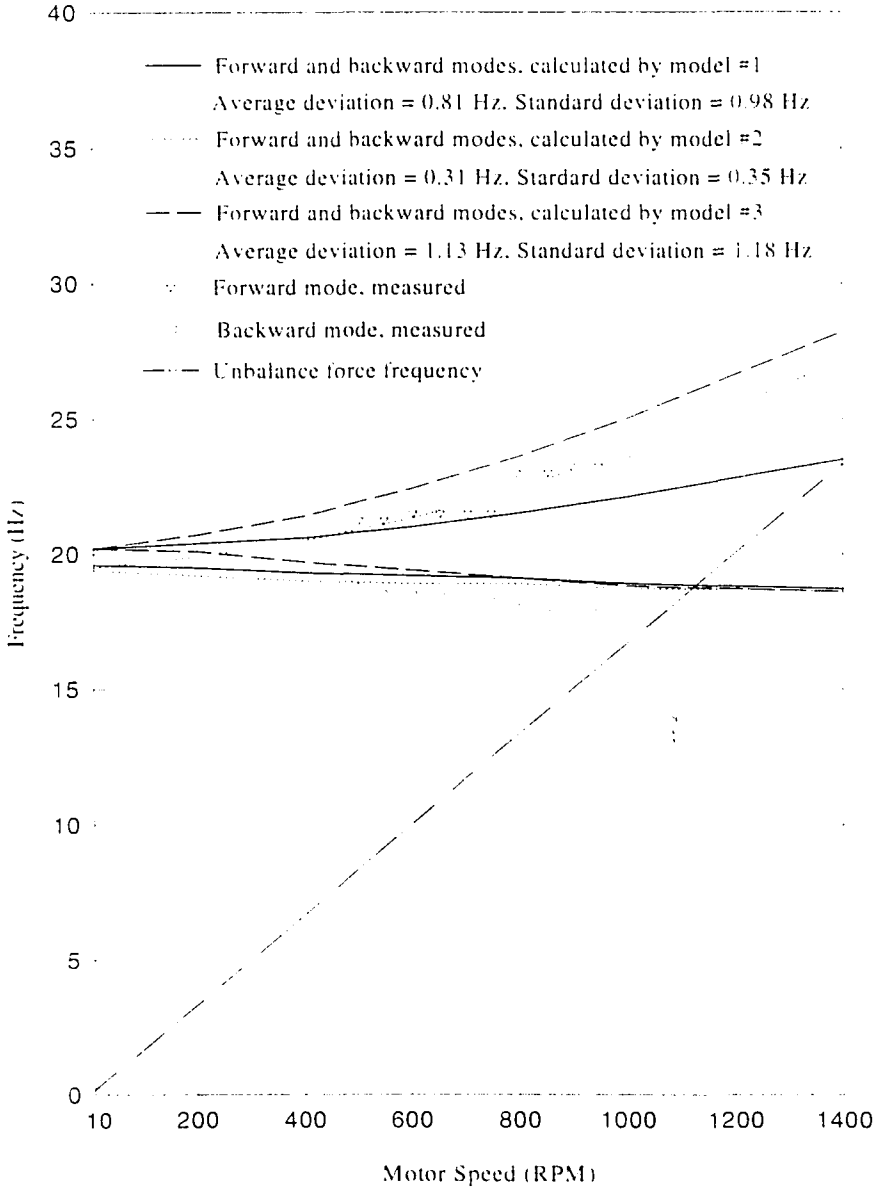

Figure 6-4: The forward and backward swaying modes of test unit #1 on four leg frame with 1/4 HP motor and circular disk, the given average and standard deviations are for the forward swaying mode.

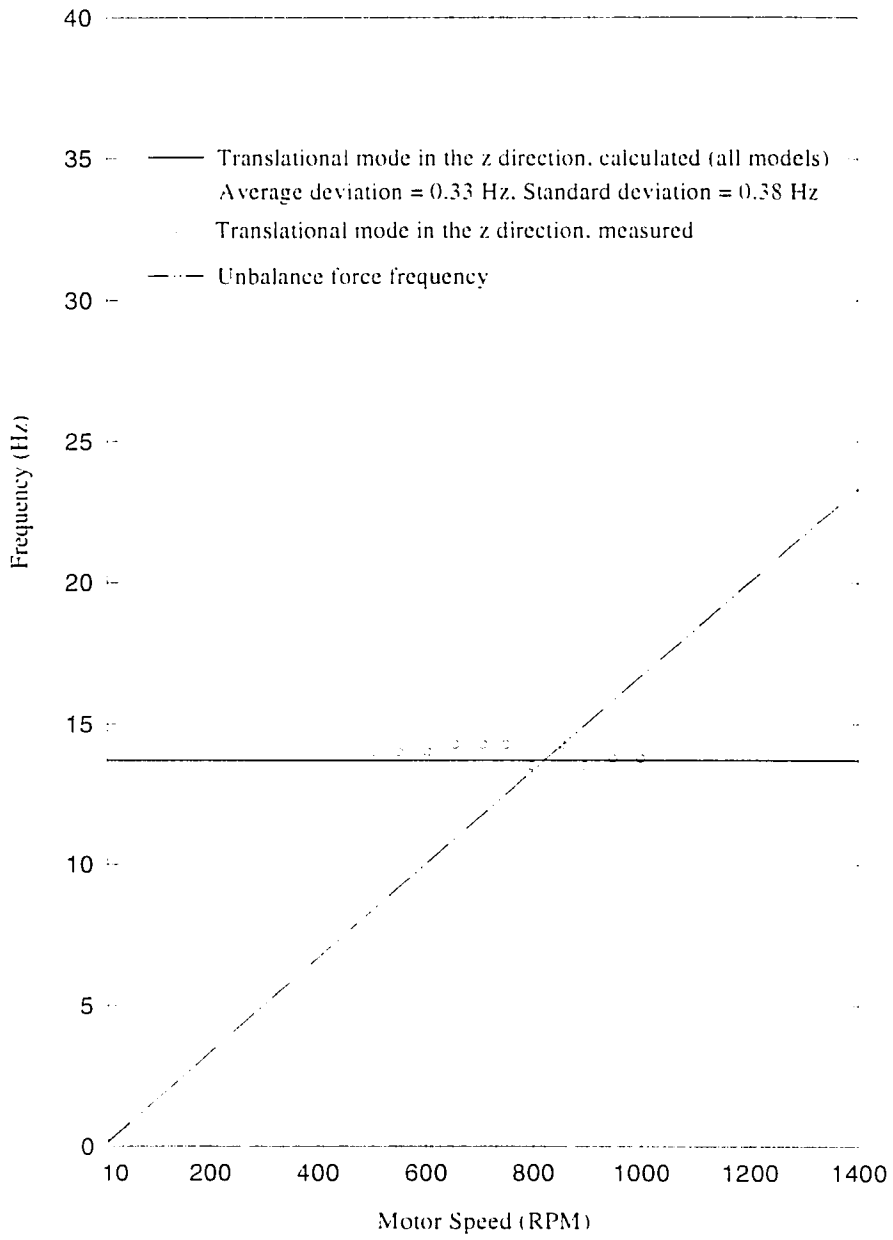

Figure 6-5: The translation mode in the z direction of test unit #1 on four leg frame with 1/4 HP motor and circular disk.

From an overall point view, both model 1 and model 2 are the valid models which can be used to predict the mode shifting corresponding to the gyroscopic effect of the rotating fan impeller. In the following discussions, only the data from model 1 and model 2 are presented.

Figure 6-6 gives the measured forward and backward rocking modes and the calculated ones from models 1 and 2 for test unit #1 supported on the four leg frame with 1/4 HP motor and No. 60799501 fan impeller. In this case, model 2 gives better prediction for the forward rocking mode than model 1 does. For the backward rocking mode, model 1 gives better predictions than model 2.

Figure 6-7 gives the measured forward and backward swaying modes and the calculated ones from models 1 and 2 for test unit #1 supported on the four leg frame with 1/4 HP motor and No. 60799501 fan impeller. Again, model 2 gives better predictions for the forward swaying mode than model 1 does. For the backward swaying mode, the two models give almost same accuracies.

Figure 6-8 is the measured and calculated translational mode in the z direction for test unit #1 supported on the four leg frame with 1/4 HP motor and No. 60799501 fan impeller. This mode is uncoupled from all other modes and is not affected by the gyroscopic effect of the rotating fan impeller, the two models give same predictions.

6.2.1.2 The rotating mobility measurements of test unit #1 on the case

Figure 6-9 gives the measured forward and backward rocking modes and calculated ones from models 1 and 2 for test unit #1 supported on case with 1/4 HP motor and No. 60799501 fan impeller. Model 2 still gives better prediction for the forward rocking mode than model 1 does. For the backward rocking mode, model 1 gives better prediction than model 2.

Figure 6-10 gives the measured forward and backward swaying modes and

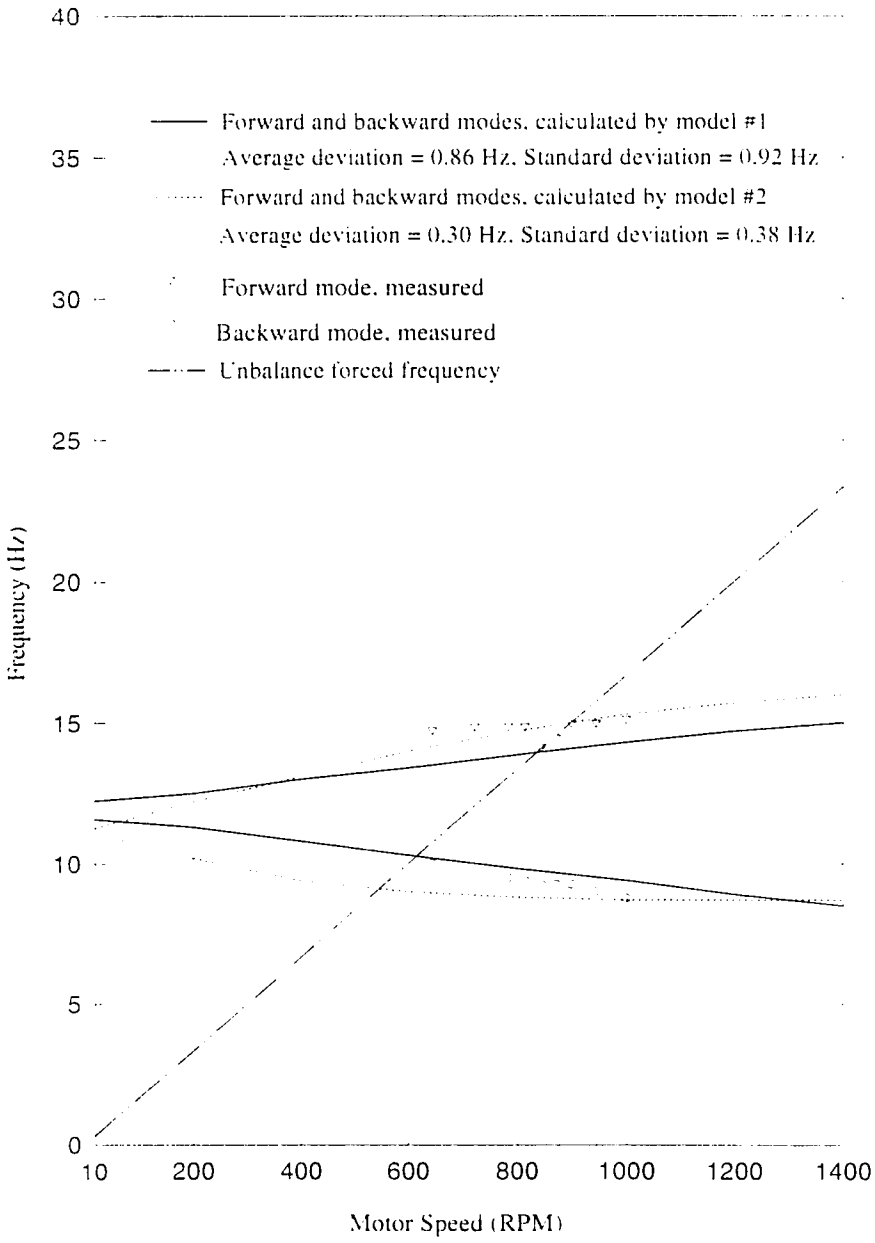

Figure 6-6: The forward and backward rocking modes of test unit #1 on four leg frame with 1/4 HP motor and No. 60799501 fan impeller, the given average and standard deviations are for the forward rocking mode.

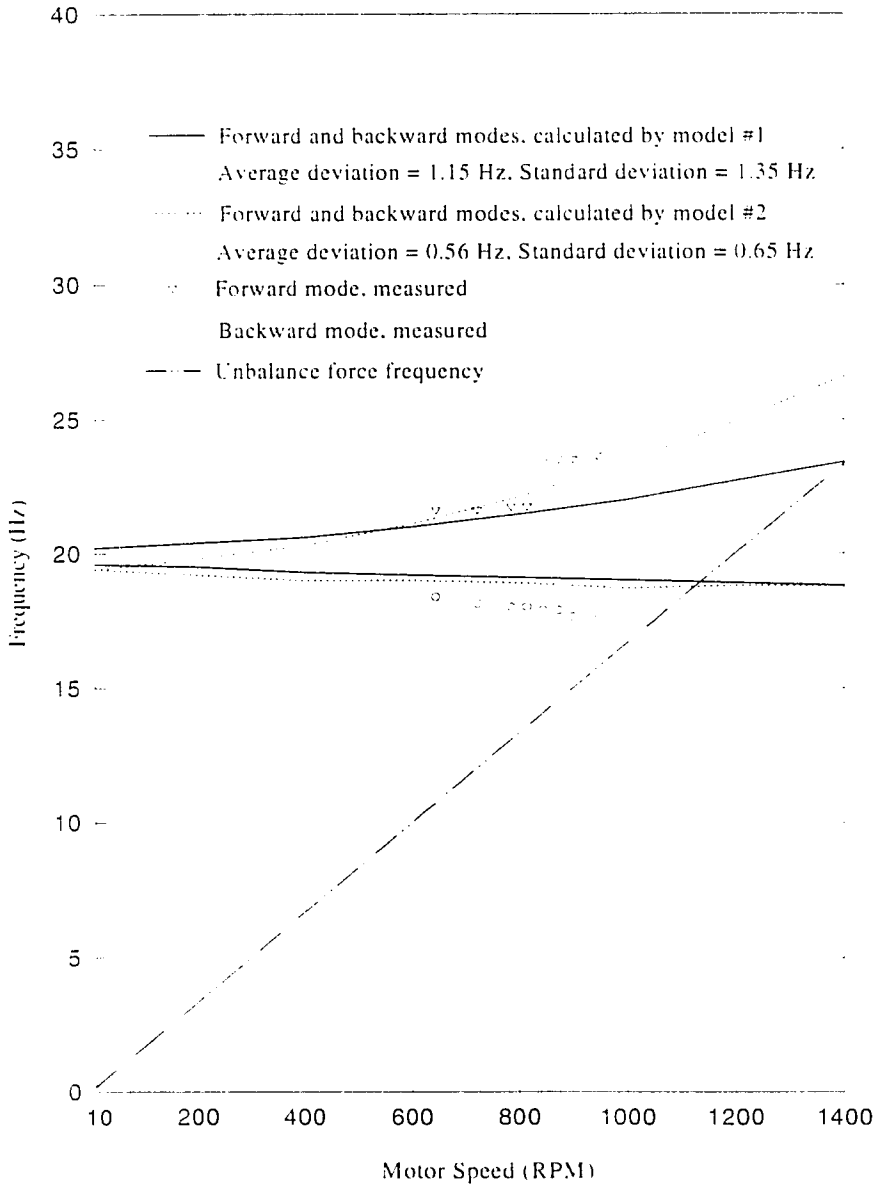

Figure 6-7: The forward and backward swaying modes of test unit #1 on four leg frame with 1/4 HP motor and No. 60799501 fan impeller, the given average and standard deviations are for the forward swaying mode.

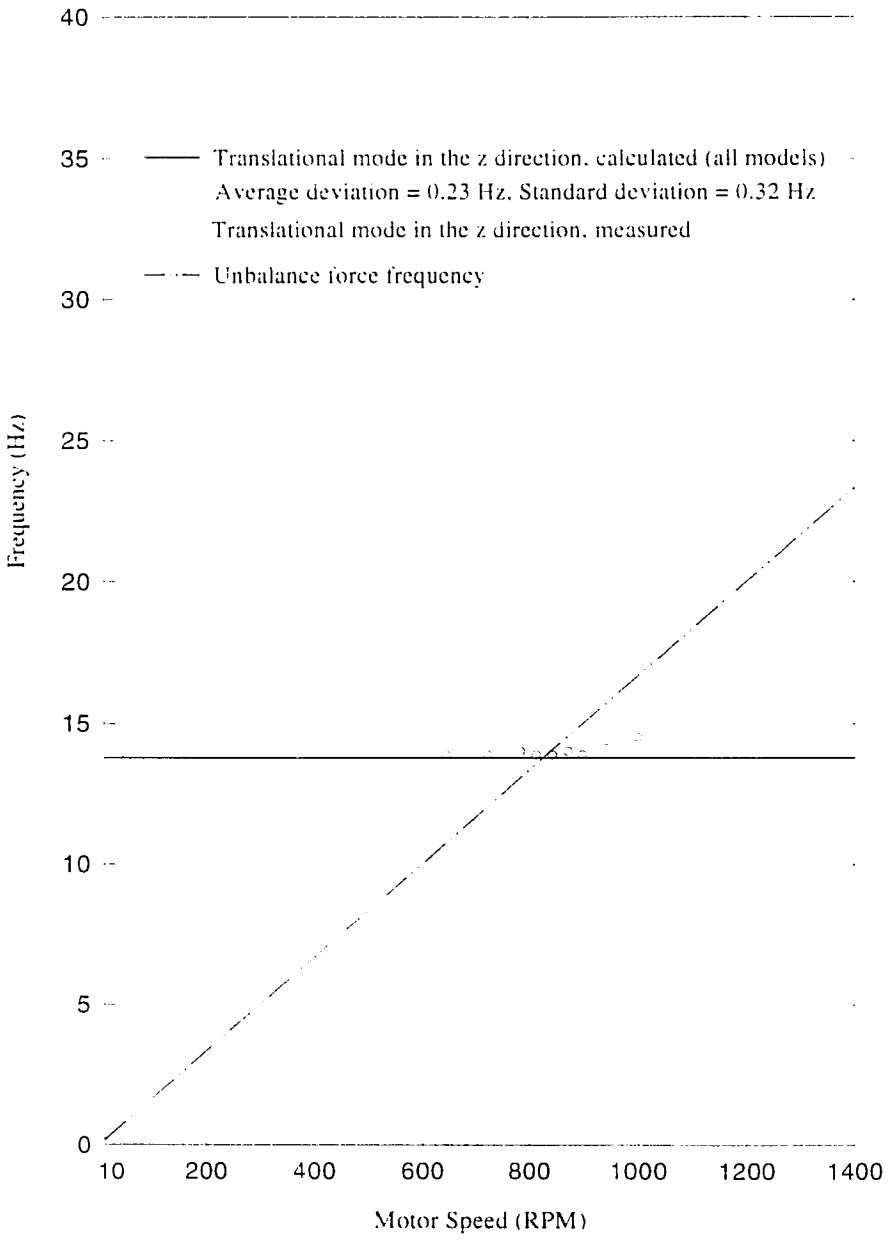

Figure 6-8: The translation mode in the z direction of test unit #1 on four leg frame with 1/4 HP motor and No. 60799501 fan impeller.

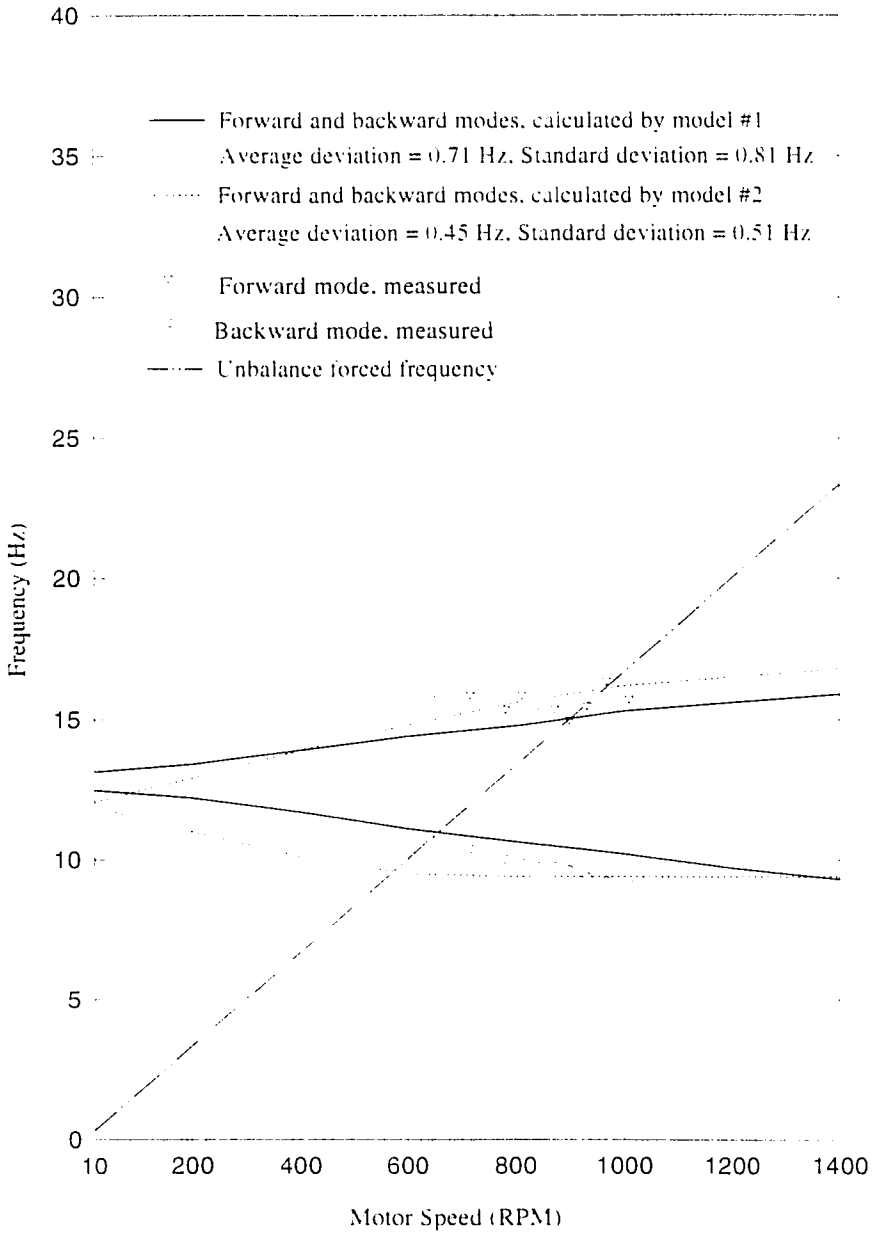

Figure 6-9: The forward and backward rocking modes of test unit #1 on case with 1/4 HP motor and No. 60799501 fan impeller, the given average and standard deviations are for the forward rocking mode.

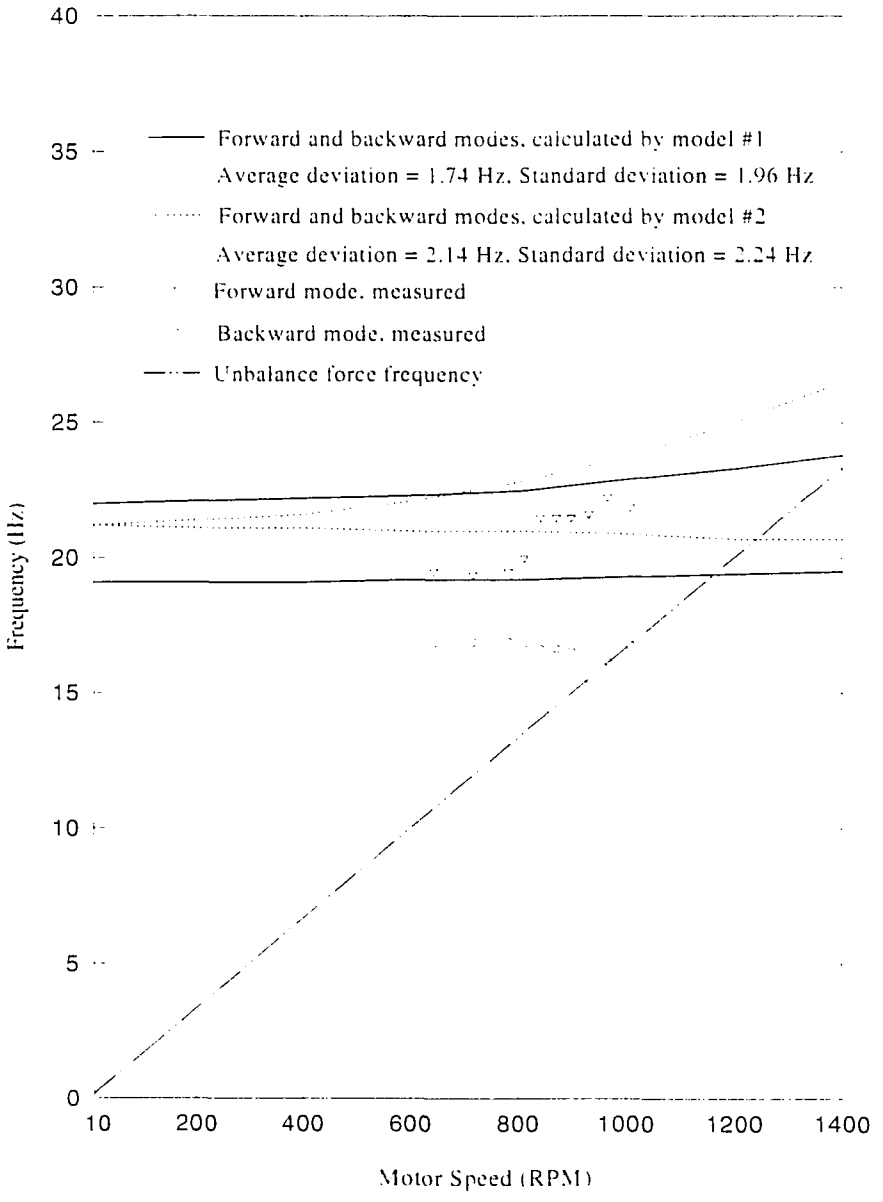

Figure 6-10: The forward and backward swaying modes of test unit #1 on case with 1/4 HP motor and No. 60799501 fan impeller, the given average and standard deviations are for the forward swaying mode.

calculated ones from models 1 and 2 for test unit #1 supported on case with 1/4 HP motor and No. 60799501 fan impeller. In the non-rotating tests, there were difficulties in identifying the swaying modes, and the parameters used for this test setup gave larger errors for the swaying modes. These errors in the non-rotating tests were transferred to the rotating tests. Thus, both models do not give acceptable predictions both for the forward and backward swaying modes.

Examining the measured rotating mobility data for forward and backward swaying modes shows that the predictive curves from analytical models have the same trend with respect to the measured data. These curves appear to be shifted from their correct positions. This was compensated for by adjusting the stiffness, K_y, in the y direction to shift the swaying mode curves down. This did not significantly change the predictive curves for the rocking modes.

Figure 6-11 gives the corrected forward and backward swaying modes from models 1 and 2 by adjusting the stiffness, K_y, in the y direction from its original number of 494,000.0 N/m to 320,000.0 N/m. Both models give acceptable predictions for the forward swaying mode. For the backward swaying mode, predictions are not very good. But it is not important.

Figure 6-12 gives the forward and backward rocking modes after adjusting the stiffness in the y direction. Both models give acceptable prediction for both the forward and backward rocking modes.

Figure 6-13 is the measured and calculated translational mode in the z direction for test unit #1 supported on case with 1/4 HP motor and No. 60799501 fan impeller. This mode is uncoupled from all other modes and is not affected by the gyroscopic effect of the rotating fan impeller, two models give same predictions.

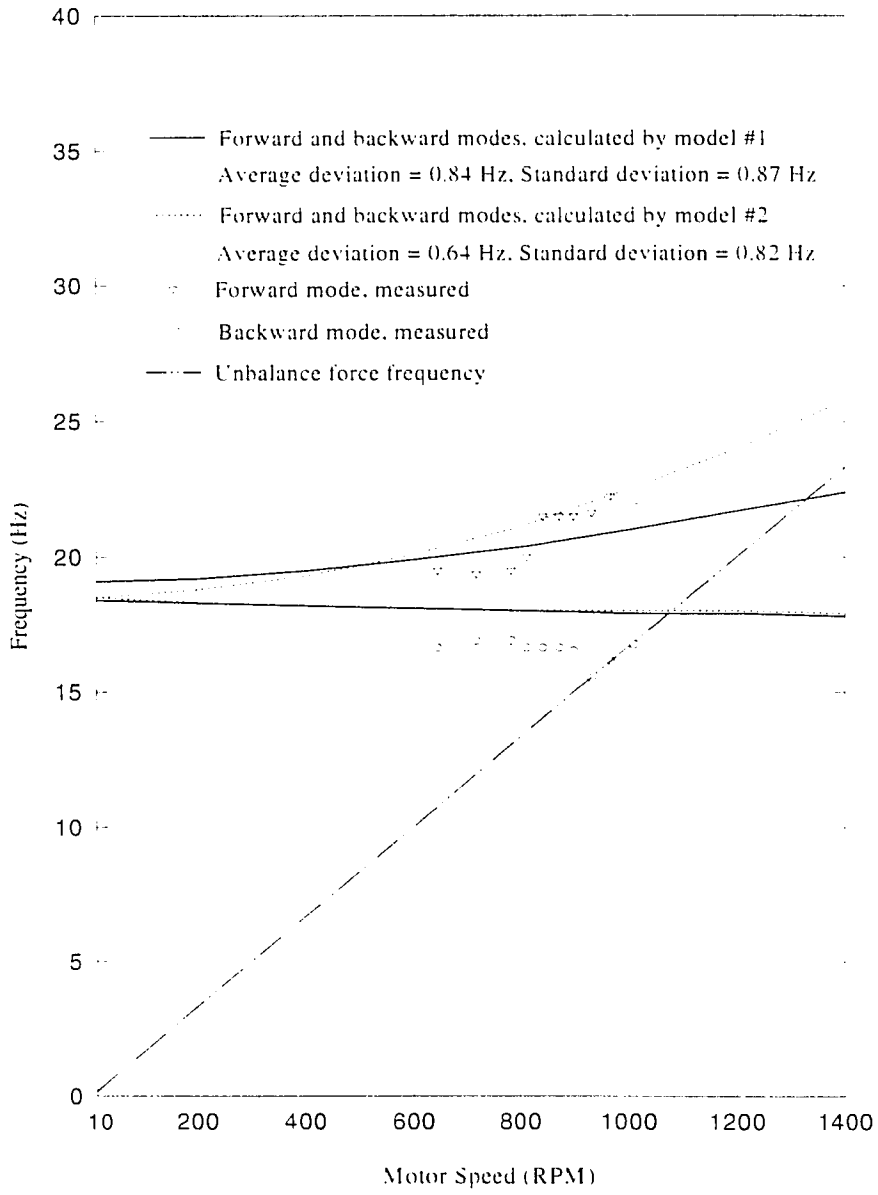

Figure 6-11: The forward and backward swaying modes of test unit #1 on case with 1/4 HP motor and No. 60799501 fan impeller with modified stiffness in y direction, the given average and standard deviations are for the forward swaying mode.

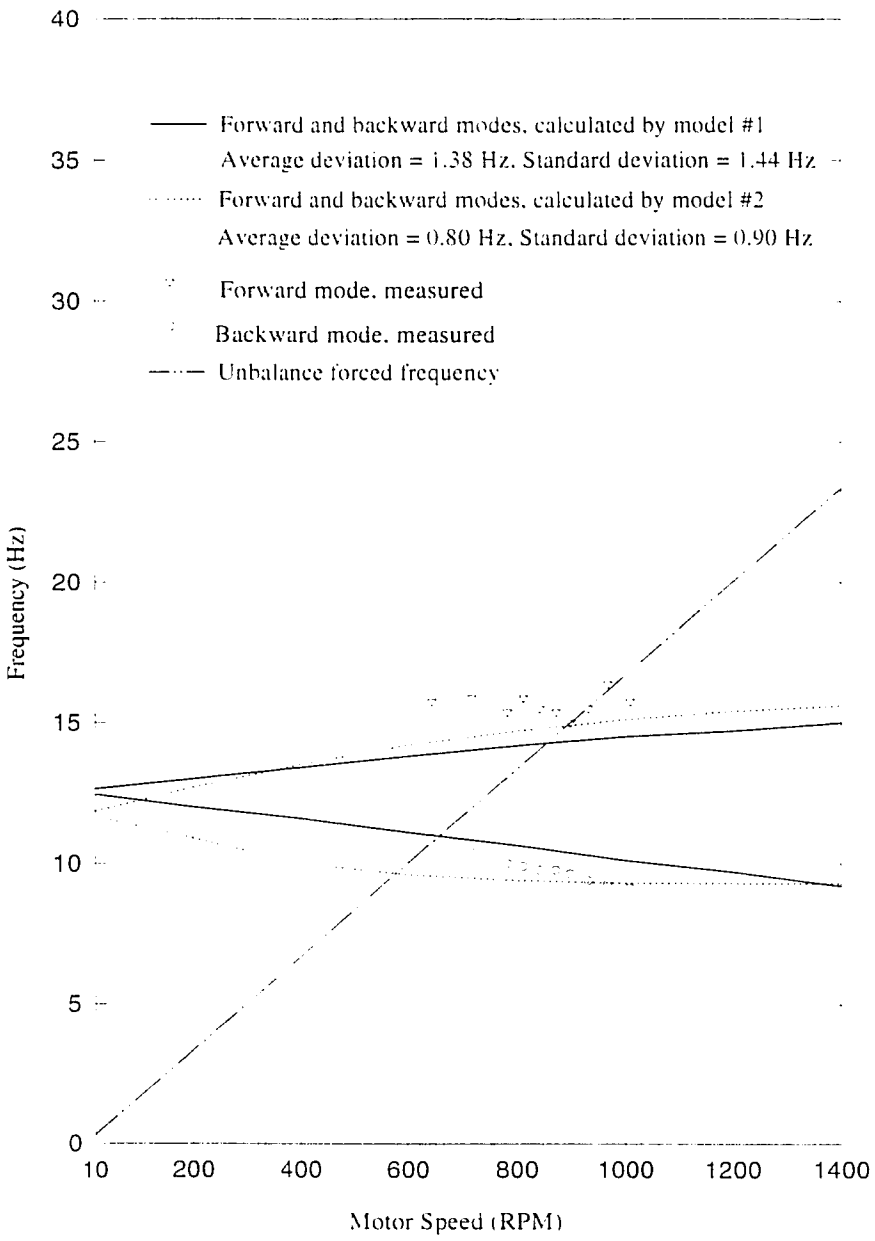

Figure 6-12: The forward and backward rocking modes of test unit #1 on case with 1/4 HP motor and No. 60799501 fan impeller with modified stiffness in y direction, the given average and standard deviations are for the forward rocking mode.

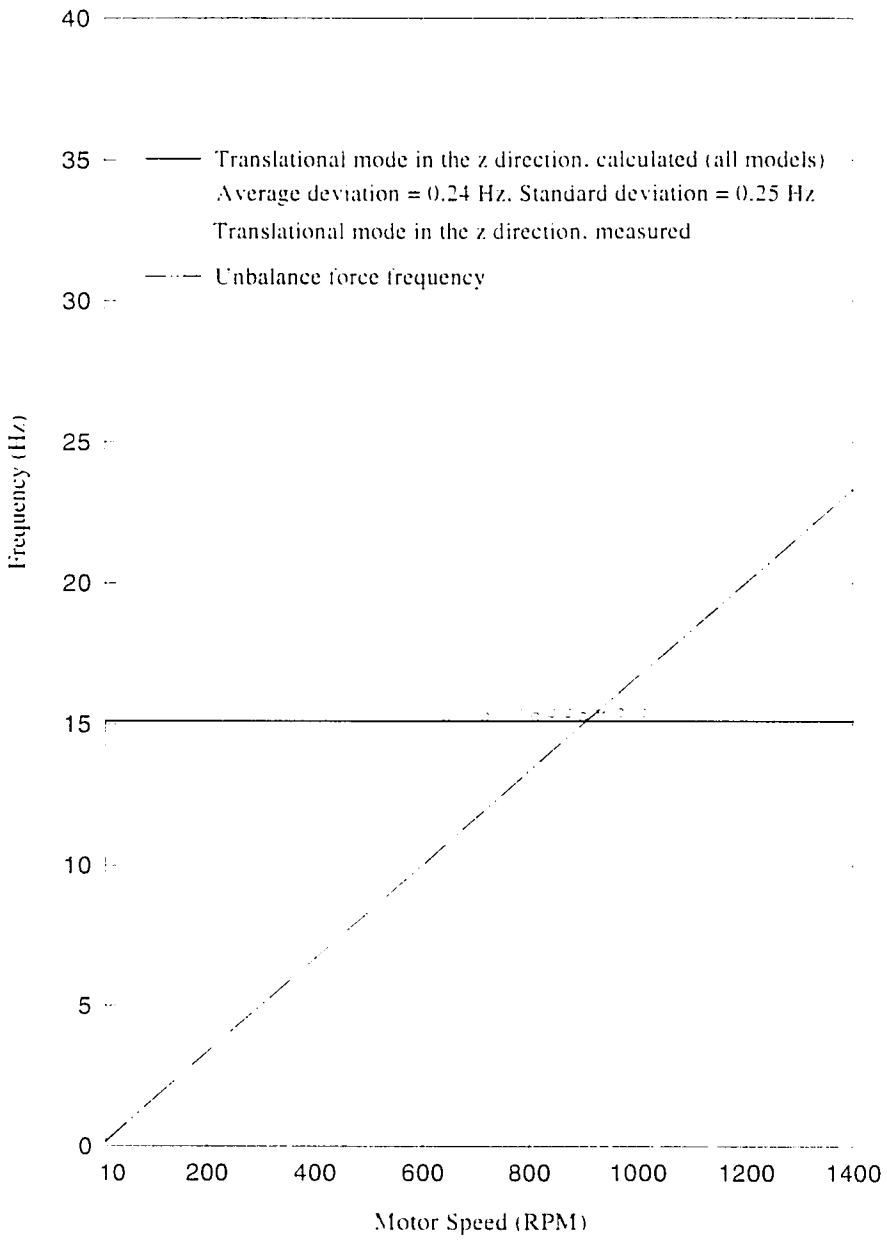

Figure 6-13: The translation mode in the z direction of test unit #1 on case with 1/4 HP motor and No. 60799501 fan impeller.

6.2.1.3 The rotating mobility measurements of test unit #2 on the case

Figure 6-14 gives the measured forward and backward rocking modes and calculated ones from models 1 and 2 for test unit #2 supported on case with No. 203020-A fan impeller. Model 1 gives better predictions for both the forward rocking mode and backward mode than model 2. The non-converge problem at low speed of model 2 affects results significantly in this case.

Figure 6-15 gives the measured forward and backward swaying modes and calculated ones from models 1 and 2 for test unit #2 supported on case with No 203020-A fan impeller. Both models give the same predictions. The gyroscopic effect of the rotating fan impeller does not affect the swaying modes in test unit #2. The measured rotating mobility data proved this.

Figure 6-16 is the measured and calculated translational mode in the z direction for test unit #2 supported on case with No. 203020-A fan impeller. This mode is uncoupled from all other modes and is not affected by the gyroscopic effect of the rotating fan impeller, two models give same predictions.

6.2.2 The peak hold test

The peak hold tests were used to verify the system resonance speeds corresponding to the gyroscopic effect of the rotating fan impeller. In peak hold tests, the maximum vibration amplitudes were measured while varying motor speed by using the peak-hold-averaging mode in the WavePak card. By using the peak-hold-averaging function, the largest amplitudes at any spectrum line were retained to form the "Peak Hold" spectrum. In these measurements, the accelerometer was attached at the location where the rocking mode mobility measurements were made. The vibration velocity amplitudes excited by fan impeller unbalance were measured. The same variable frequency power supply was used to manually scan the speed range of interest. Thus, the

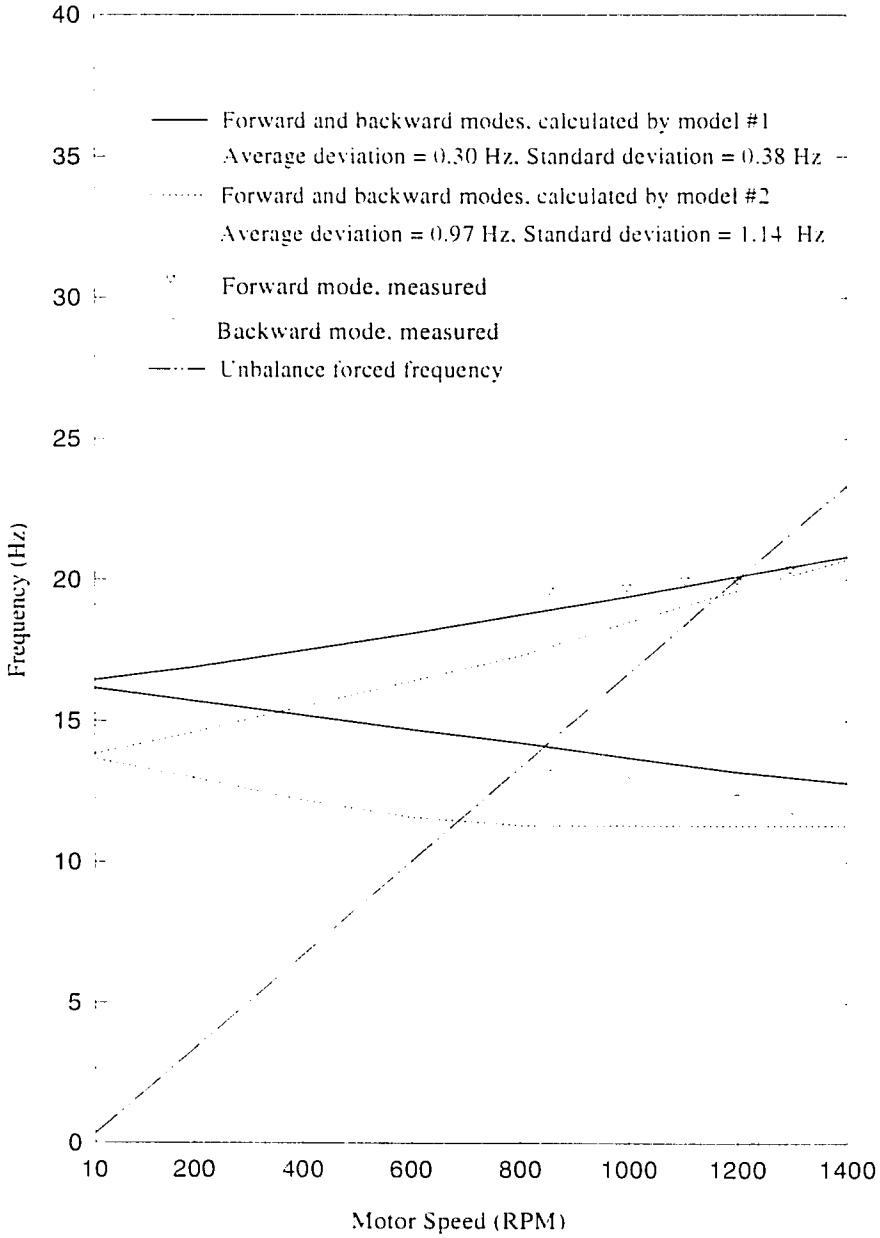

Figure 6-14: The forward and backward rocking modes of test unit #2 on case with No. 203020-A fan impeller, the given average and standard deviations are for the forward rocking mode.

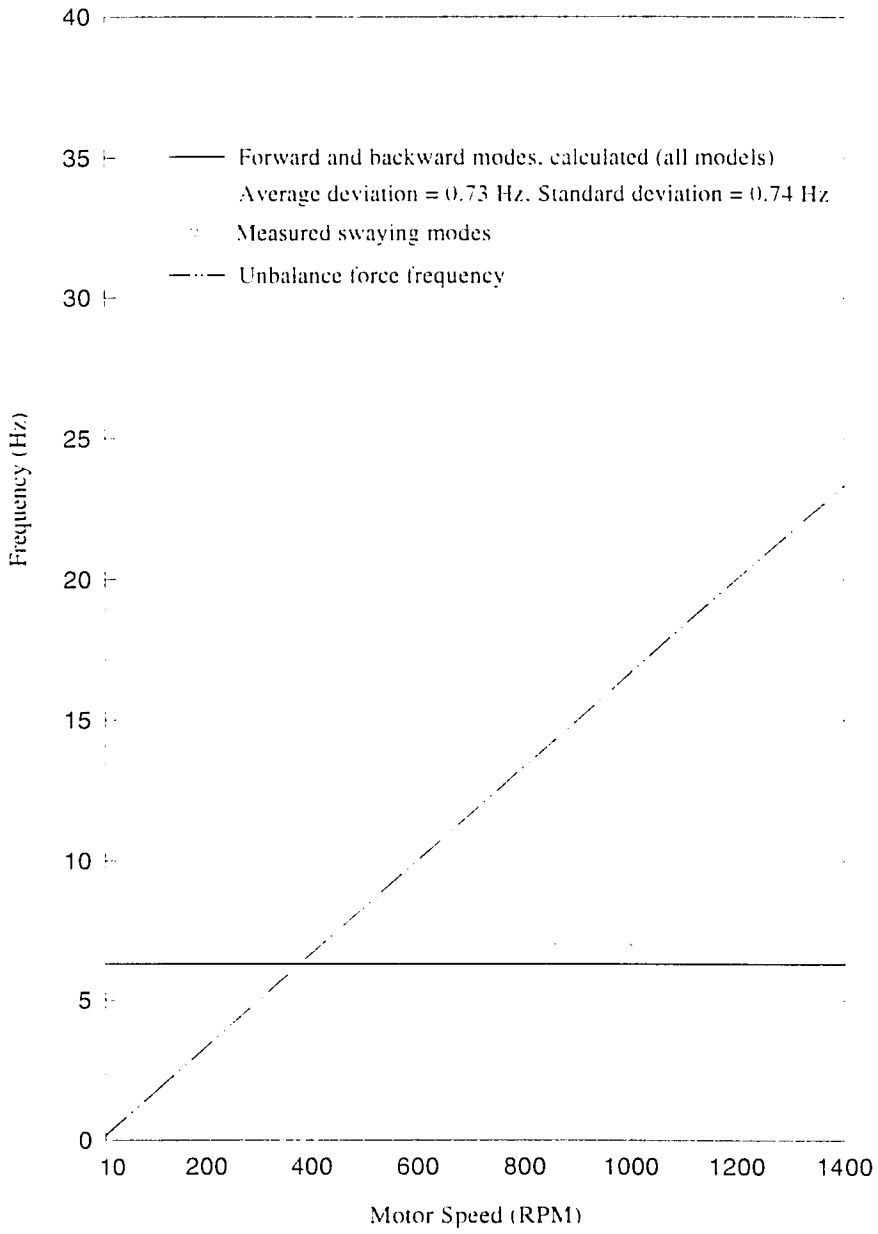

Figure 6-15: The forward and backward swaying modes of test unit #2 on case with No. 203020-A fan impeller, the given average and standard deviations are for both the forward and backward swaying mode.

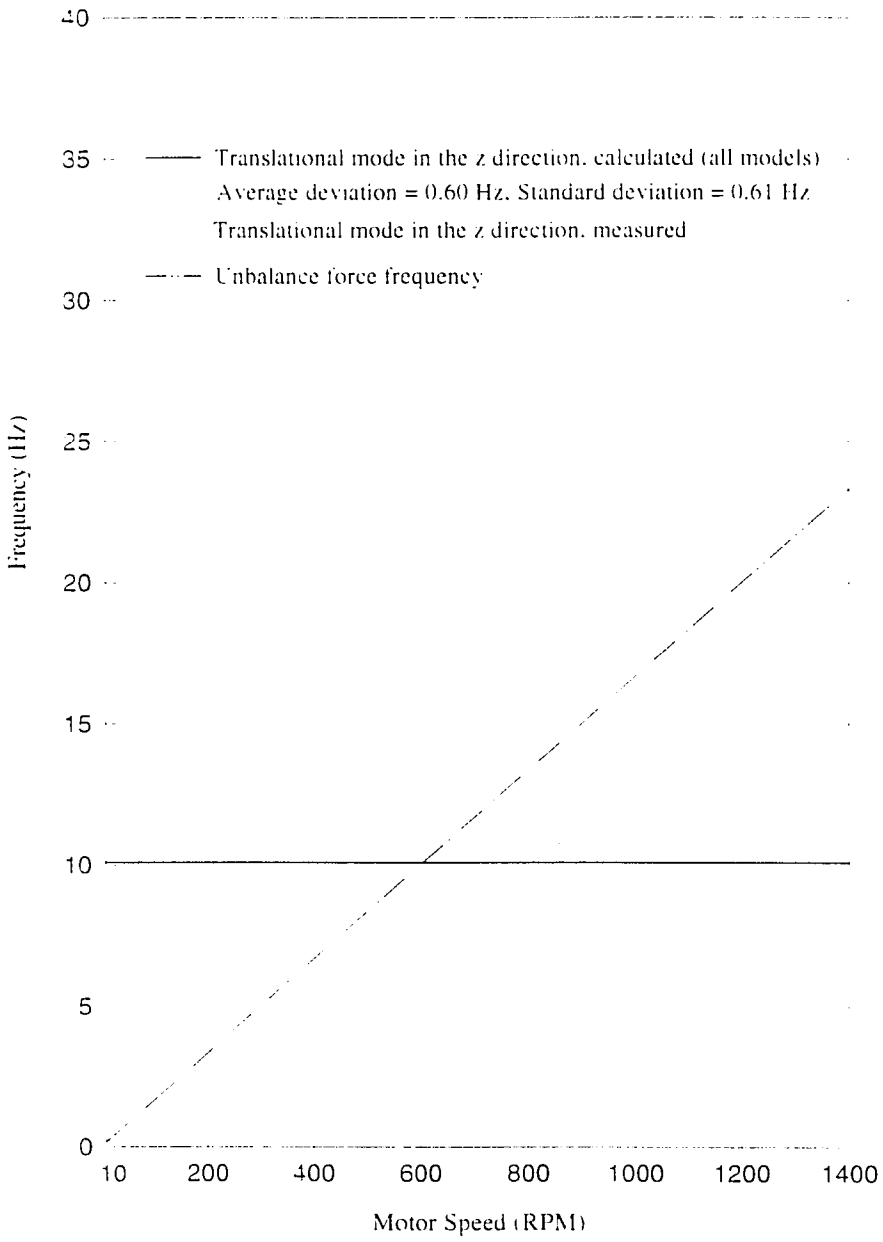

Figure 6-16: The translation mode in the z direction of test unit #2 on case with No. 203020-A fan impeller.

resonance speeds, at which the shifted forward or backward modes because of the gyroscopic effect of the rotating fan impeller coincided with the rotation speeds, were located.

In the peak hold spectrum measurements, to obtain the resonance speeds corresponding to both the forward and backward rocking modes at same measurement, the motor needed to be run from the lowest speed, which was typically 30-40% lower than the motor normal speed, to the highest speed, which was typically 20-30% higher than the motor normal speed. The lowest and highest speeds were decided by the predicted the resonance speed at the forward rocking mode and the resonance speed at the backward rocking mode by the analytical models. The lowest speed for peak hold spectrum measurement should be 50 - 100 RPM lower than the predicted resonance speed at the backward rocking mode. The highest speed for peak hold spectrum measurement should be 50 - 100 RPM higher than the predicted resonance speed at the forward rocking mode.

The variable frequency power supply used in this work has an internal oscillator, which has the frequency range from 45 Hz to 75 Hz. The upper limit of the frequency range of this internal oscillator satisfies all the highest motor speeds needed in this work. But the lower limit of the frequency range of the internal oscillator does not satisfy the lowest motor speeds needed in this work. To obtain the lowest speeds needed in the tests, the external signal input in the variable frequency power supply was used. The sine wave signal from a function generator was used as signal input of the power supply, which acts as a power amplifier now. By changing the signal frequency of the function generator, any motor speed can be obtained. Starting from the needed lowest motor speed, the signal frequency of the function generator was slowly increased to little higher than 45 Hz. At this moment, it was necessary to switch back to the internal oscillator of the power supply. By using internal oscillator of the power supply, the supply voltage were adjusted automatically. But, in the external signal input mode, the supply voltage must be adjusted

manually by adjusting the signal amplitude of the function generator. To safely switch from external signal input mode back to internal oscillator mode, the power was cut off first. Then, the switch button, which is used to control the working mode of power supply, was quickly switched back to the internal oscillator mode and power was turn on again. Because the spectrum measurement was at peak-hold-averaging mode, the switching procedure did not affect the measurement results.

The FFT spectrum at lowest and highest speed were taken in the tests, which were used to accurately locate the starting and ending speeds in the peak hold spectrum measurement.

The forward and backward swaying modes in all test units in this work were far away from the normal motor speeds. They were either much higher than the normal motor speed, which is the case for test unit #1, or much lower than the normal motor speed, which is the case for test unit #2. Thus, they did not cause the vibration problems in the investigated air-conditioning units. They were not measurable in the test conditions in this work.

To predict the resonance speeds corresponding to both forward and backward rocking and swaying modes by the analytical models, simply set the rotating speed, Ω, of the motor equal to the whirling speed, ω, of the fan impeller in the models. For model 1, $\Omega = \omega$ will give all the resonance speeds corresponding to both the forward and backward rocking and swaying modes simultaneously. For model 2, because of the way the problem was setup, $\Omega = \omega$ will give only the resonance speeds corresponding to the forward rocking and swaying modes. By setting $\Omega = -\omega$, the resonance speeds corresponding to the backward rocking and swaying modes will be obtained.

6.2.2.1 Test unit #1 on the four-leg frame

Table 9 summaries the resonance speeds measured from peak hold tests and predicted by the analytical models for test unit #1 on the four-leg frame.

Table 9: The resonance speeds of test unit #1 on the four-leg frame

Resonances(RPM)		f_ϕ - BW	f_θ - FW	f_z	f_{xy} - BW	f_{xy} - FW
1/4 HP motor and circular disk	Model 1	612.0	834.0	824.0	1134.0	1416.0
	Model 2	534.0	900.0	824.0	1116.0	2022.0
	Peak-Hold	605.0	861.0	821.0	1078.0	N/A
	Coast Down	612.0	857.0	811.0	N/A	N/A
1/4 HP motor and No.60799501 fan impeller	Model 1	618.0	840.0	827.0	1134.0	1404.0
	Model 2	540.0	900.0	827.0	1122.0	1848.0
	Peak-Hold	616.0	884.0	824.0	N/A	N/A
1/3 HP motor and No.60843301 fan impeller	Model 1	582.0	762.0	767.0	1122.0	1350.0
	Model 2	504.0	780.0	767.0	1098.0	1404.0
	Peak-Hold	570.0	748.0	811.0	N/A	N/A

Figure 6-17 gives the peak hold spectrum measurement of test unit #1 with 1/4 HP motor and No. 60799501 fan impeller on the four-leg frame. Three resonance speeds were measured. The resonance speed at 616 RPM corresponds to the backward rocking mode, which was excited by aerodynamic force of the fan impeller. The resonance speed at 824 RPM corresponds to the translational mode in the z direction. The resonance speed at 884 RPM corresponds to the forward rocking mode, which was excited by the fan impeller unbalance. Figures 6-18 and 6-19 give the FFT spectrum at the specific speeds for locating the starting and ending speeds in the peak hold spectrum measurement.

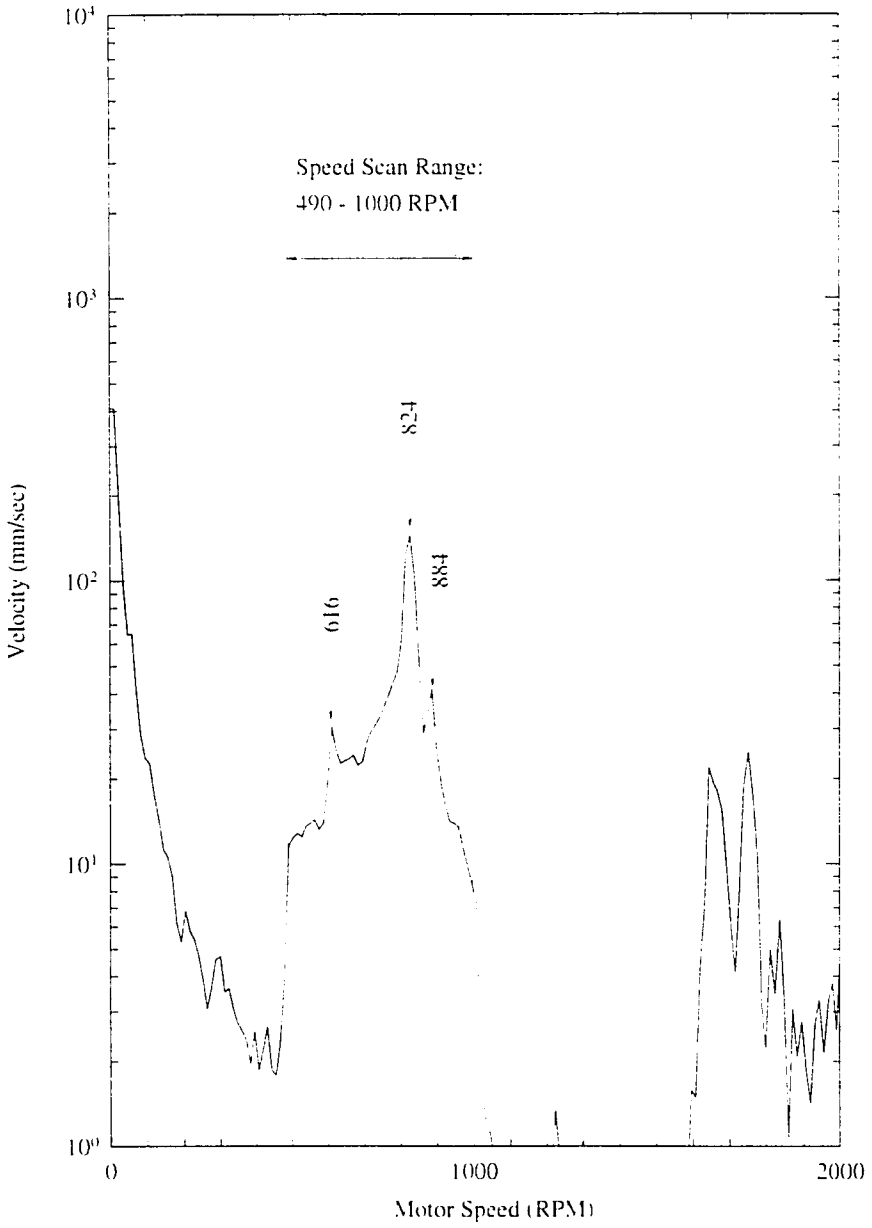

Figure 6-17: The peak hold spectrum for test unit #1 on four-leg frame with 1/4 HP motor and No. 60795501 fan impeller, speed scan range: 490 - 1000 RPM

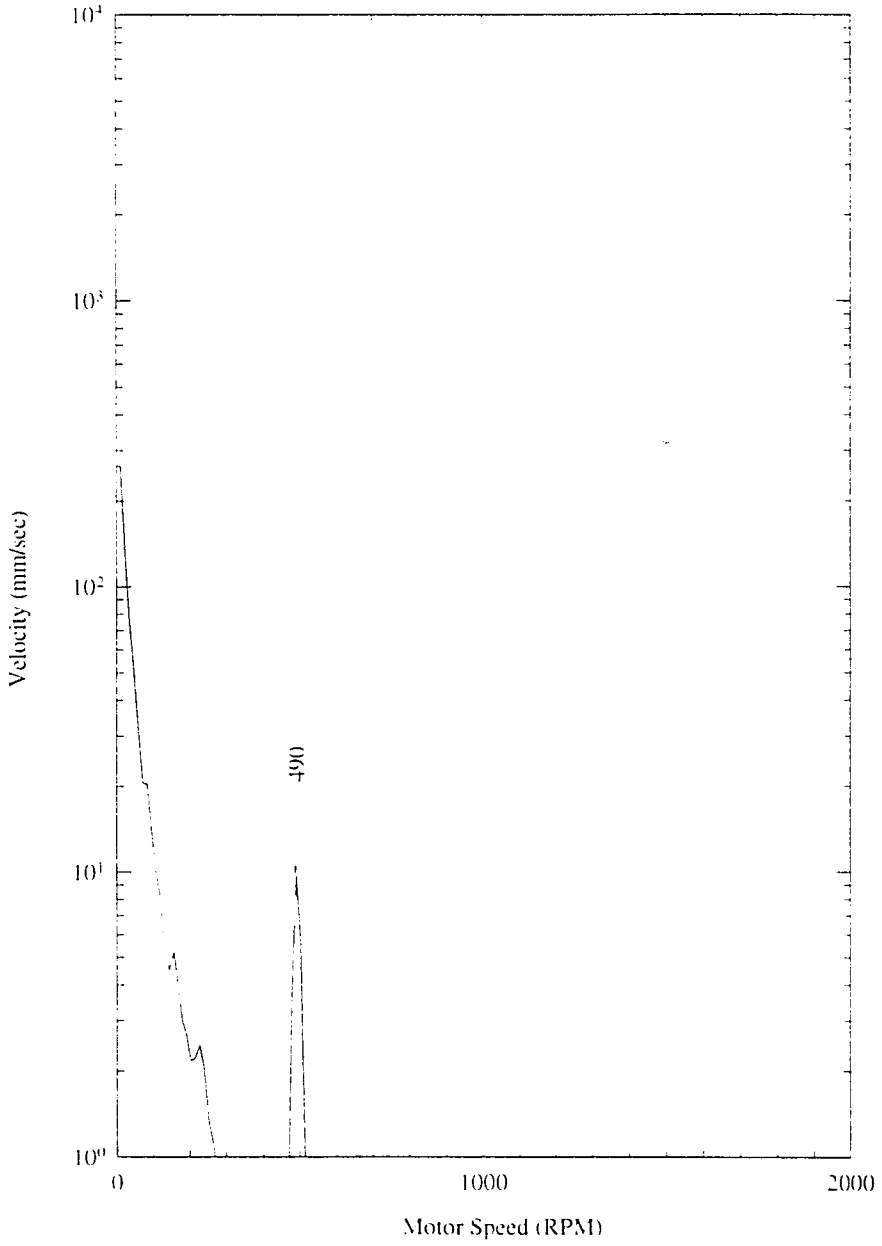

Figure 6-18: The FFT spectrum for test unit #1 on four-leg frame with 1/4 HP motor and No. 60795501 fan impeller at speed of 490 RPM

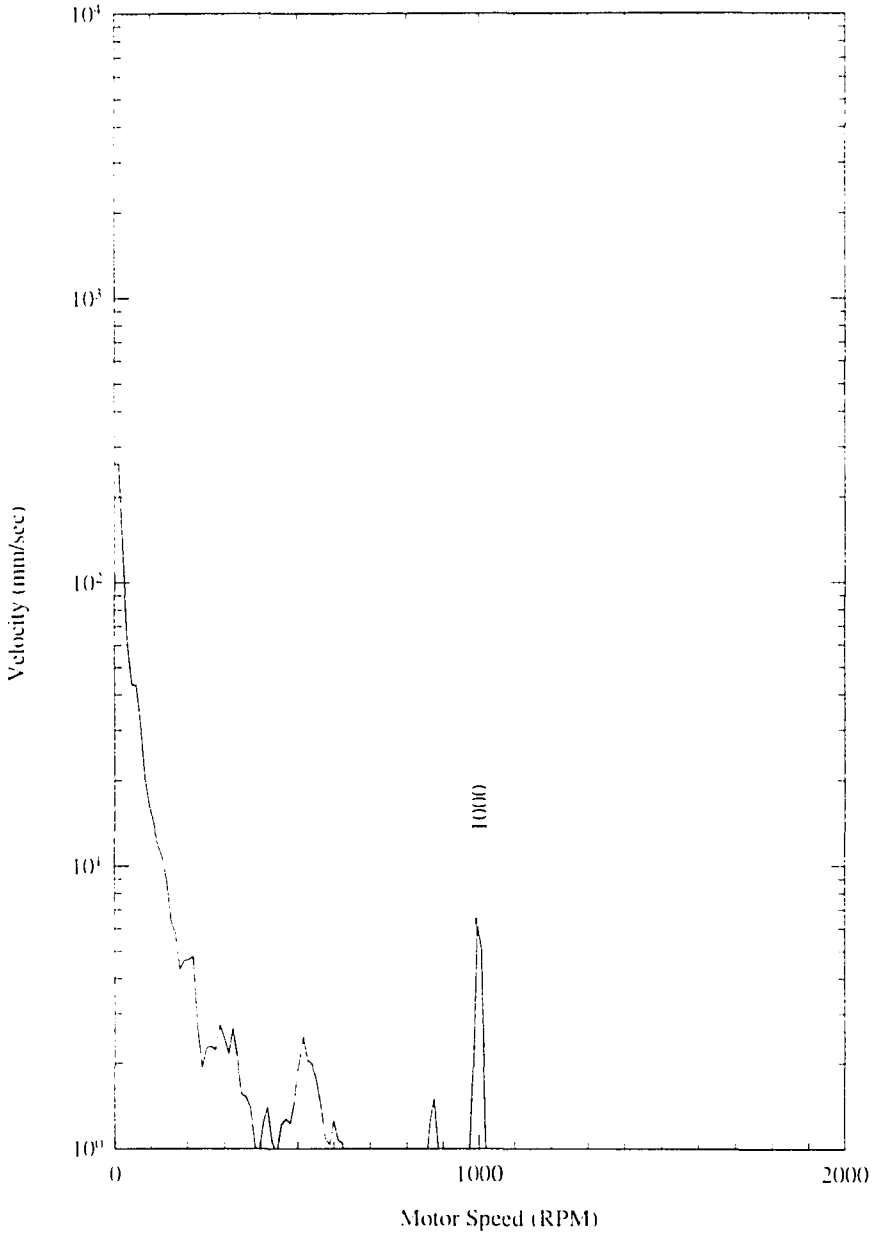

Figure 6-19: The FFT spectrum for test unit #1 on four-leg frame with 1/4 HP motor and No. 60795501 fan impeller at speed of 1000 RPM

6.2.2.2 Test unit #1 on the case

Table 10 summaries the resonance speeds measured from peak hold tests and predicted by the analytical models for test unit #1 the case.

Figure 6-20 gives the peak hold spectrum measurement of test unit #1 with 1/4 HP motor and No. 60799501 fan impeller on the case. Four resonance speeds were measured. The resonance speed at 634 RPM corresponds to the backward rocking mode, which was excited by aerodynamic force of the fan impeller. The resonance speed at 776 RPM is an unknown system resonance. The resonance speed at 934 RPM corresponds to the translational mode in the z direction. The resonance speed at 956 RPM corresponds to the forward rocking mode, which was excited by the fan impeller unbalance. Figures 6-21 and 6-22 give the FFT spectrum at the specific speeds for locating the starting and ending

Table 10: The resonance speeds of test unit #1 on the case

Resonances(RPM)		f_θ - BW	f_θ - FW	f_z	f_{xy} - BW	f_{xy} - FW
1/4 HP motor and circular disk	Model 1	654.0	900.0	901.0	1164.0	1446.0
	Model 2	564.0	966.0	901.0	1242.0	1938.0
	Peak-Hold	641.0	940.0	891.0	N/A	N/A
1/4 HP motor and No.60799501 fan impeller	Model 1	660.0	906.0	904.0	1164.0	1434.0
	Model 2	570.0	966.0	904.0	1242.0	1800.0
	Peak-Hold	634.0	956.0	934.0	N/A	N/A
1/3 HP motor and No.60843301 fan impeller	Model 1	624.0	828.0	838.0	1146.0	1392.0
	Model 2	528.0	846.0	838.0	1224.0	1428.0
	Peak-Hold	589.0	772.0	N/A	N/A	N/A

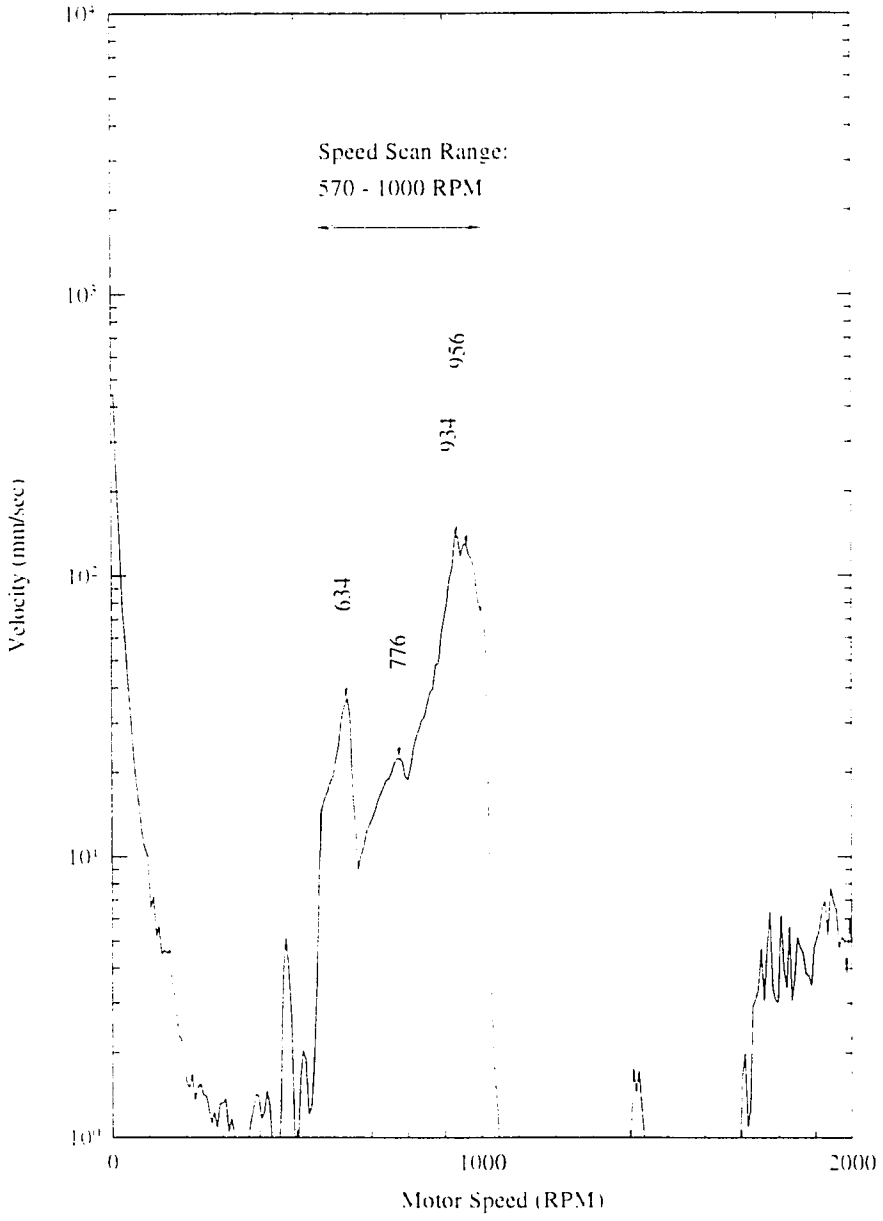

Figure 6-20: The peak hold spectrum for test unit #1 on case with 1/4 HP motor and No. 60795501 fan impeller, speed scan range: 570 - 1000 RPM

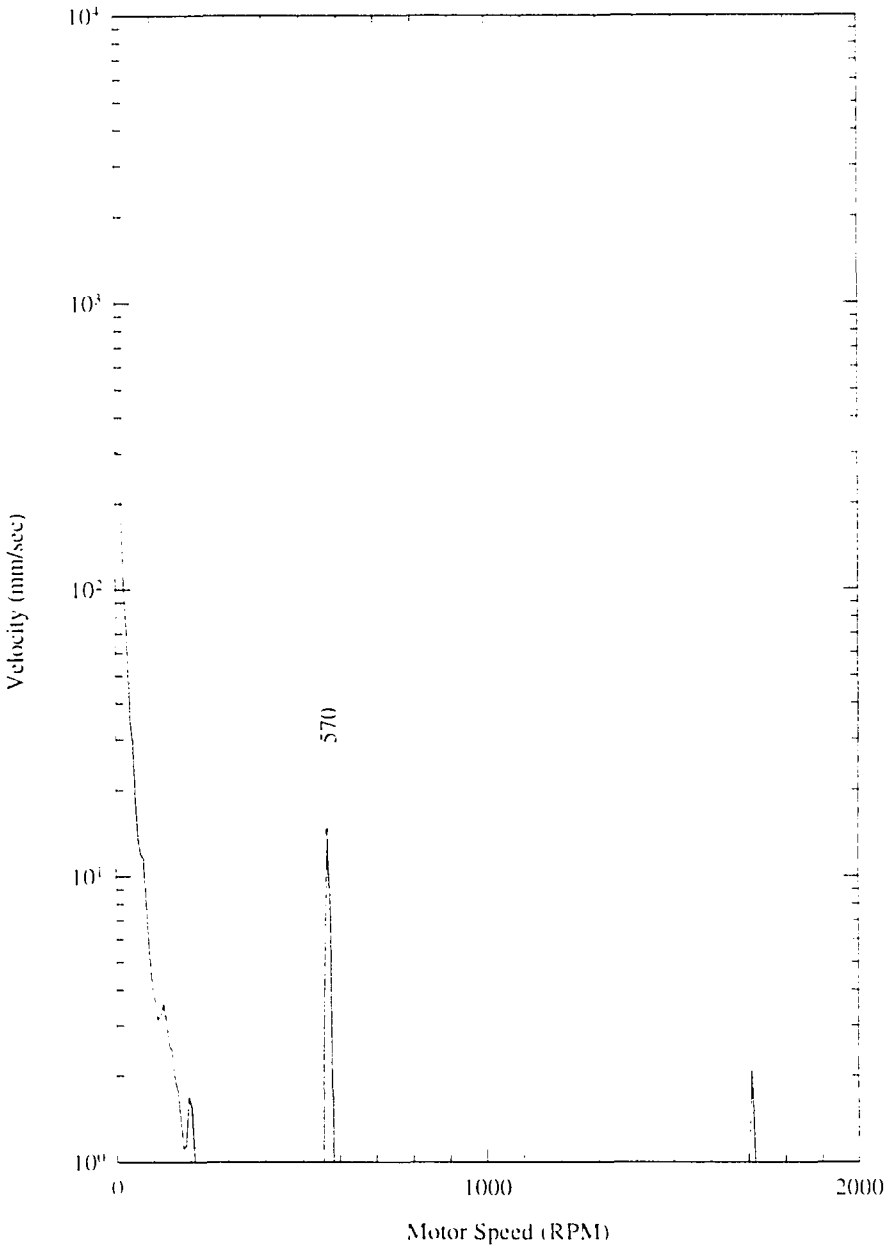

Figure 6-21: The FFT spectrum for test unit #1 on case with 1/4 HP motor and No. 60795501 fan impeller at speed of 570 RPM

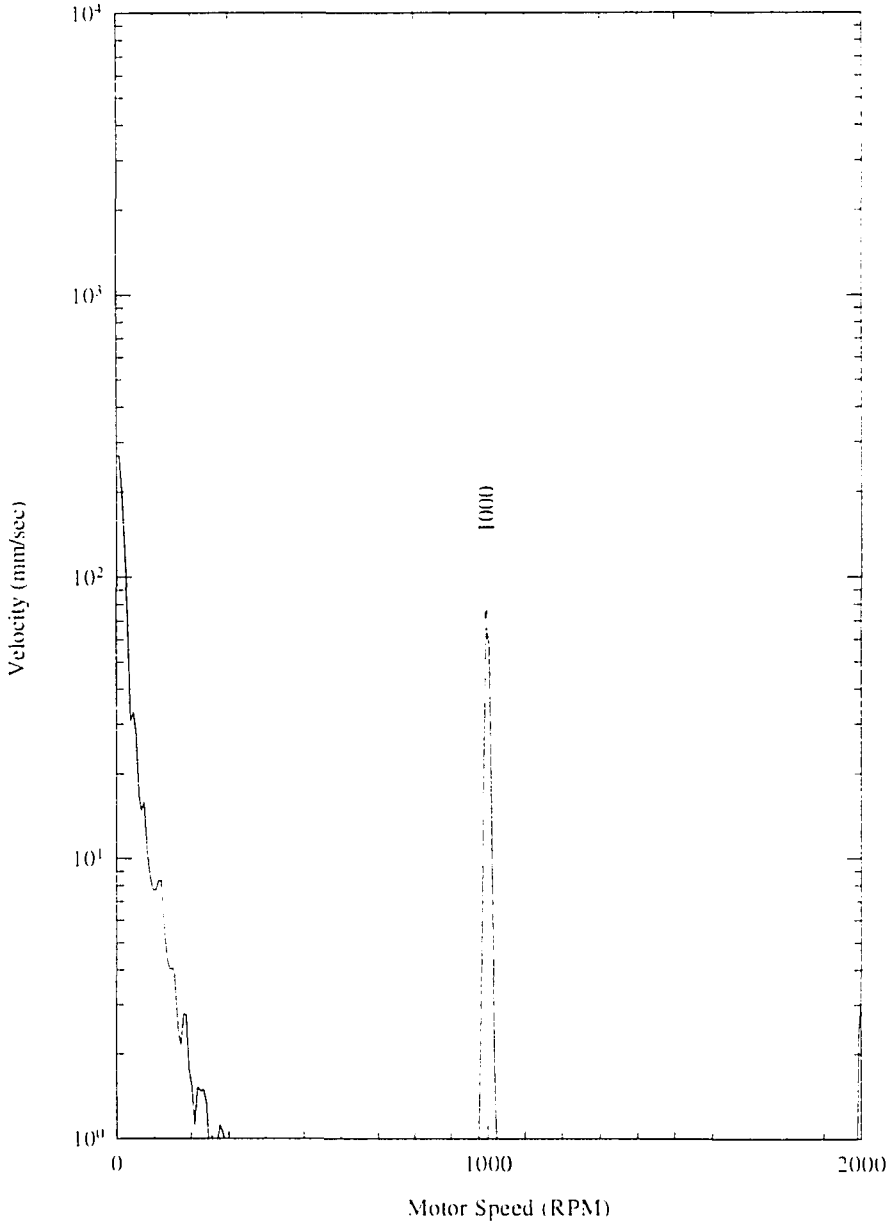

Figure 6-22: The FFT spectrum for test unit #1 on case with 1/4 HP motor and No. 60795501 fan impeller at speed of 1000 RPM

speeds in the peak hold spectrum measurement.

6.3.3 Test unit #2 on the case

Table 11 summaries the resonance speeds measured from peak hold tests and predicted by the analytical models for test unit #2 on case.

Figure 6-23 gives the peak hold spectrum of test unit #2 with No. 203020-A fan impeller on the case. The peak at 1105 RPM corresponds to the normal working speed of

Table 11: The resonance speeds of test unit #2 on the case

Resonances(RPM)		f_θ - BW	f_θ - FW	f_z	f_{xy} - BW	f_{xy} - FW
No.LA01RA025A fan impeller	Model 1	846.0	1212.0	608.0	378.0	378.0
	Model 2	678.0	1158.0	608.0	378.0	378.0
	Peak-Hold	823.0	1237.0	N/A	N/A	N/A
No. 203020-A fan impeller	Model 1	840.0	1206.0	608.0	378.0	378.0
	Model 2	678.0	1158.0	608.0	378.0	378.0
	Peak-Hold	804.0	1208.0	N/A	N/A	N/A
No. 203020-C fan impeller	Model 1	846.0	1212.0	608.0	378.0	378.0
	Model 2	678.0	1158.0	608.0	378.0	378.0
	Peak-Hold	825.0	1236.0	N/A	N/A	N/A
No. 203020-E fan impeller	Model 1	846.0	1212.0	608.0	378.0	378.0
	Model 2	678.0	1158.0	608.0	378.0	378.0
	Peak-Hold	803.0	1222.0	N/A	N/A	N/A

the motor. Two resonance speeds were measured in this case. The resonance speed at 804 RPM corresponds to the backward rocking mode, which was excited by aerodynamic force of the fan impeller. The resonance speed at 1208 RPM corresponds to the forward rocking mode, which was excited by the fan impeller unbalance. Figures 6-24 and 6-25 give the FFT spectrum at the specific speeds for locating the starting and ending speeds in the peak hold spectrum measurement.

In the peak hold tests of test unit #2, the fan impellers with different projected width and different unbalance were used to study the effect of these parameters on the vibrations of the unit. As long as the fan impeller had same values of the mass moment of inertia both about their rotating axis and about one of its diameter, the resonance speeds at forward and backward rocking modes did not change with the projected width and the unbalance, as shown in Figures 6-26(a) and 6-27(a). But these two parameters did affect the vibration amplitudes of the unit, as shown in Figures 6-26(b) and 6-27(b).

6.2.3 The coast down test

The other type of rotating test was conducted in this work to verify the resonance speeds corresponding to the forward and backward rocking modes, which was coast down test. The coast down tests were conducted by running the motor at a specific speed, which was decided similarly to the highest speed in the peak hold test. Then the power was cut off. The time waveforms of the speed signal of the rotating circular disk/fan impeller from a photo sensor and the acceleration signal from an accelerometer were recorded from the moment of power being cut off until the circular disk/fan impeller and motor stopped rotating. Any resonance speeds, which occur during the coast down, will be recorded in the vibration signals.

To ensure that signal recording was started at the moment of power being cut off, a simple external trigger signal generator was used in the test. Figure 6-28 shows the principle layout of the external trigger signal generator. It consists of a normally closed

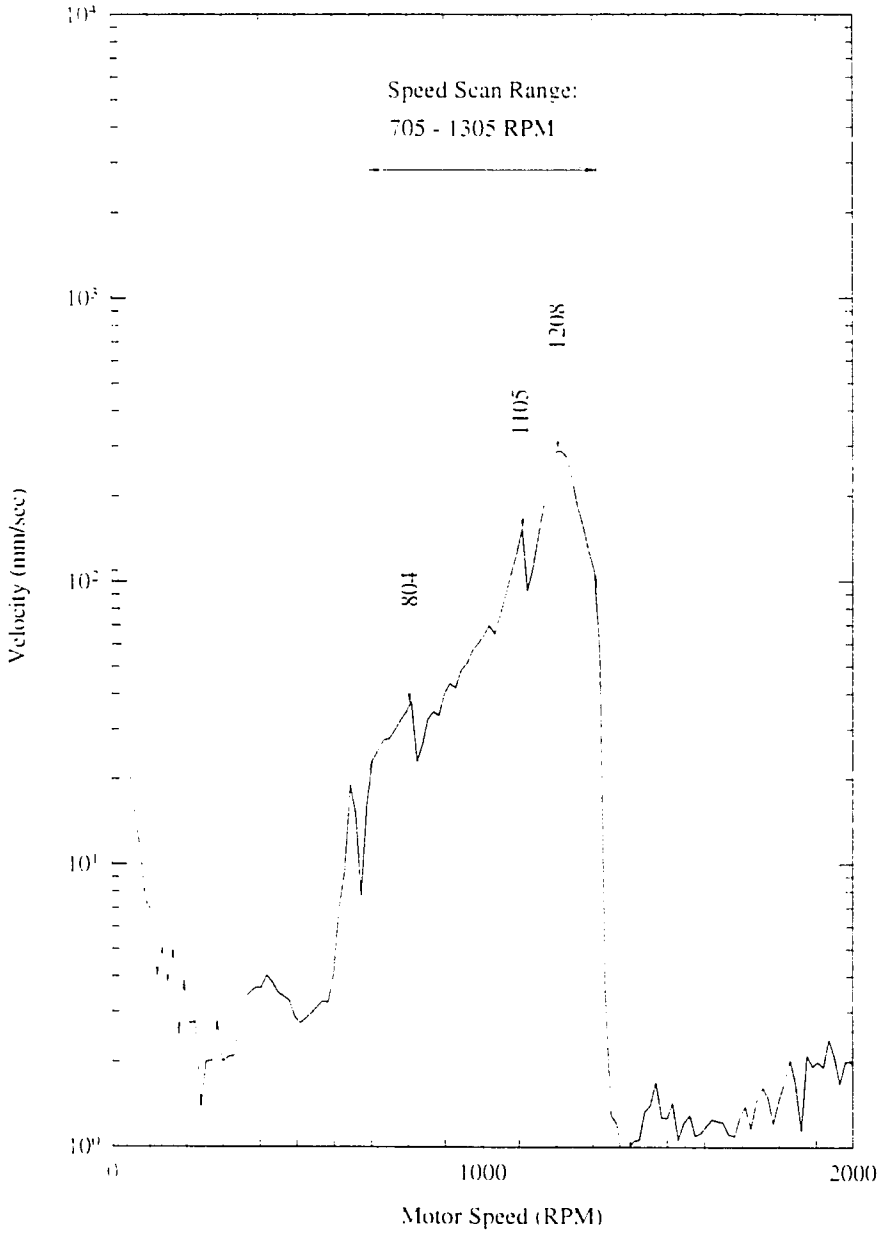

Figure 6-23: The peak hold spectrum for test unit #2 on case with No. 203020-A fan impeller, speed scan range: 705 - 1305 RPM

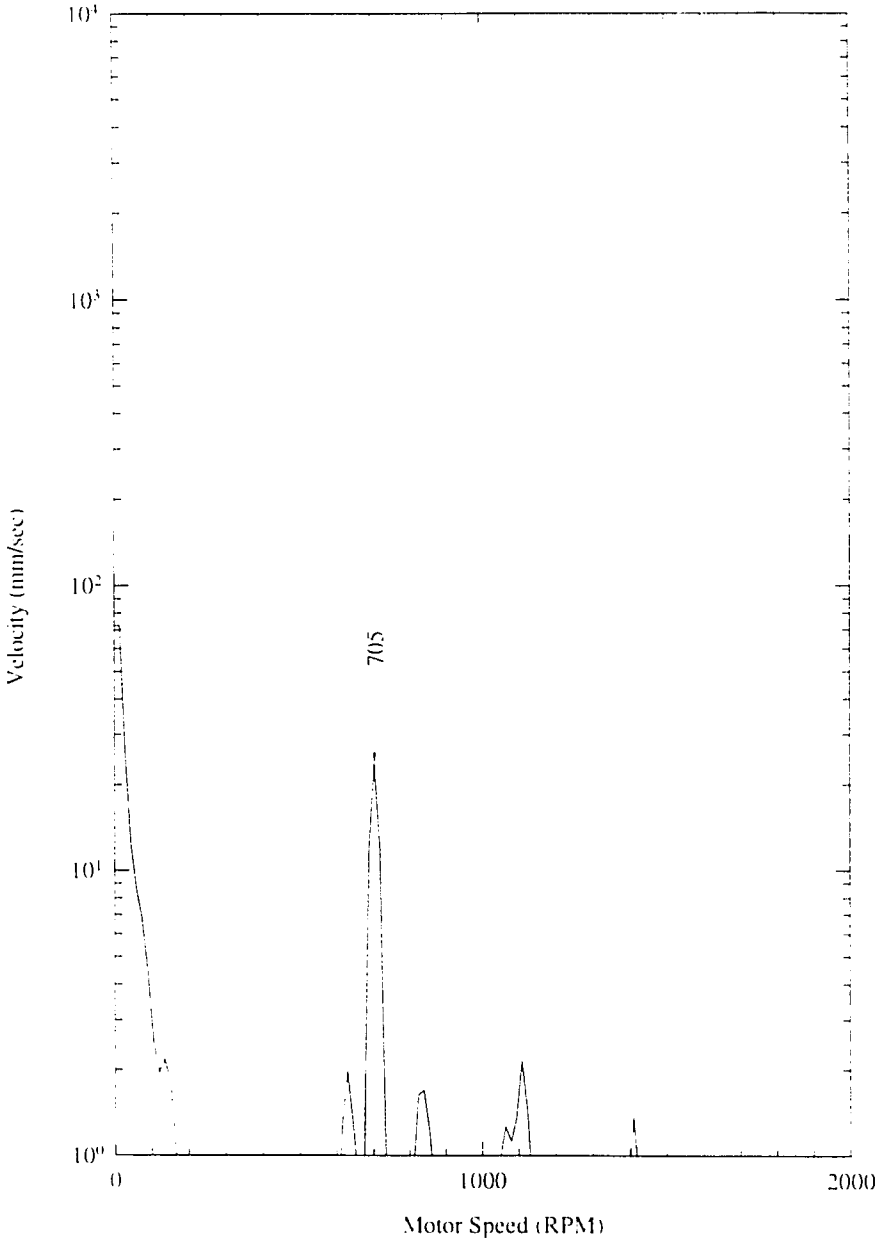

Figure 6-24: The FFT spectrum for test unit #2 on case with No. 203020-A fan impeller at speed of 705 RPM

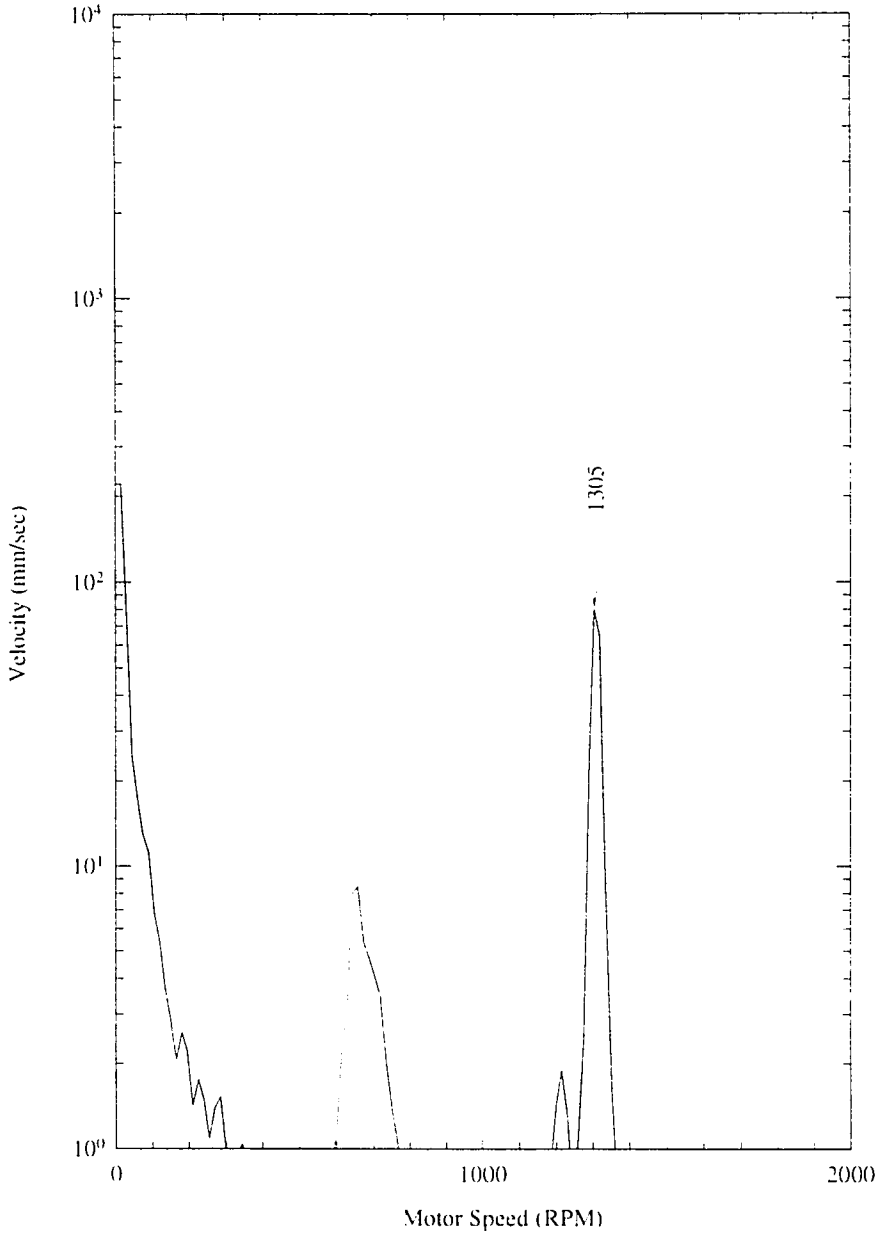

Figure 6-25: The FFT spectrum for test unit #2 on case with No. 203020-A fan impeller at speed of 1305 RPM

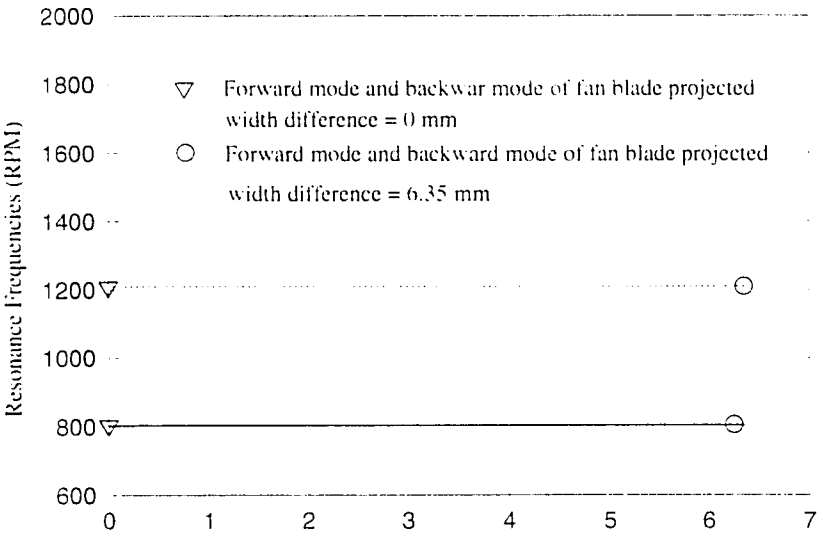

(a) Fan Blade Projected Width Difference (mm)

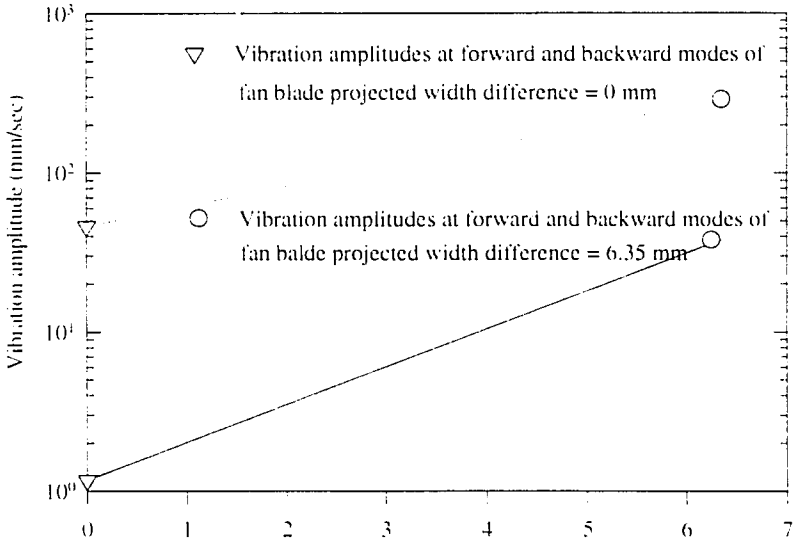

(b) Fan Blade Projected Width Difference (mm)

Figure 6-26: The effect of fan blade projected width on the forward and backward modes and vibration amplitudes (both fan impellers with 0.0 g-mm unbalance)

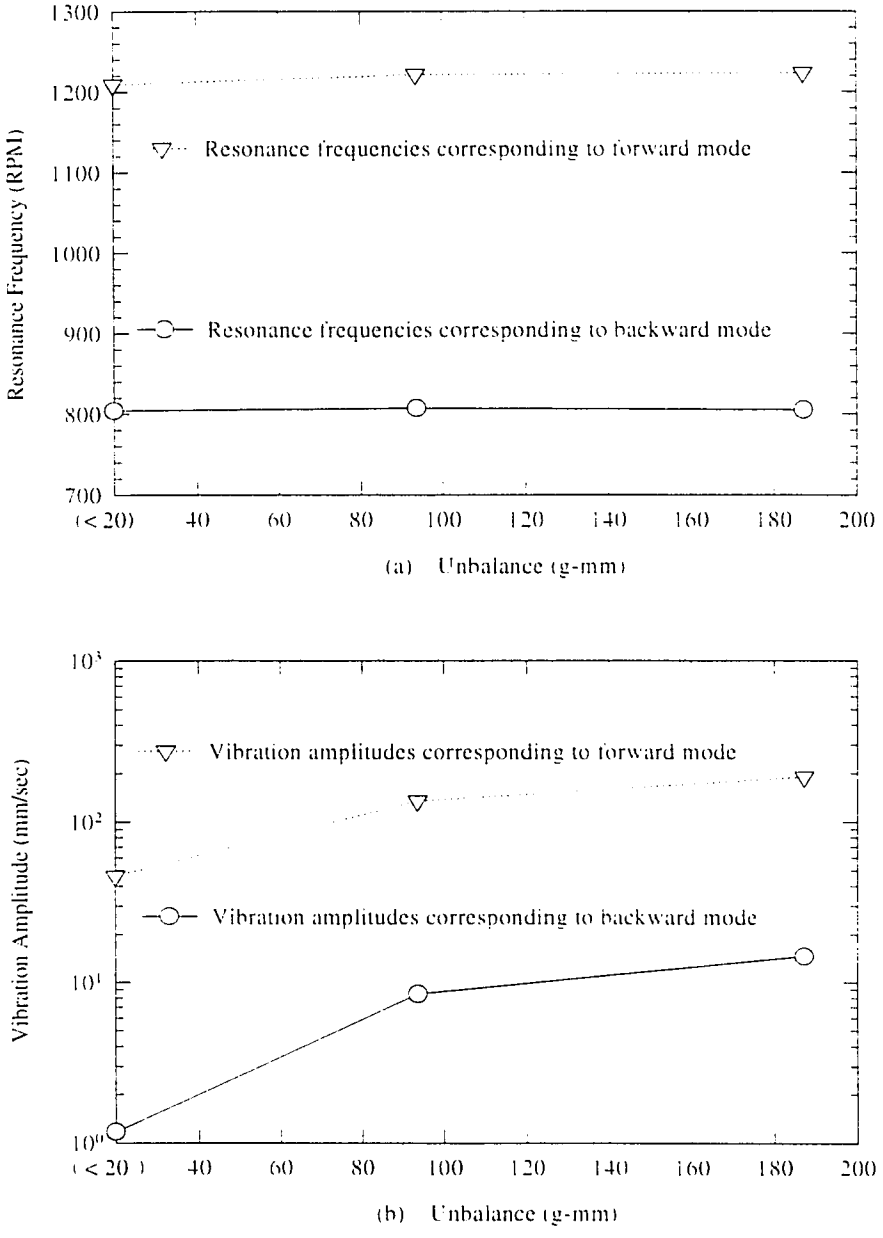

Figure 6-27: The effect of fan impeller unbalance on forward and backward modes and vibration amplitudes (all the fan impeller with same projected width)

Figure 6-28: The principle layout of the external trigger signal generator

contact relay and trigger signal circuit. The relay is connected to the motor power. When the motor power is on, the relay opened and the voltage output by the trigger signal circuit is low (zero). When the motor power is cut off, the relay returns to the normal closed contact and the voltage output by the trigger signal circuit is high (3 Volts). Thus, at the moment of power being cut off, there is a low to high signal output by trigger signal circuit. This low to high signal triggers the start of signal recording.

The coast down test was only done for test unit #1 supported on the four leg frame.

Figure 6-29 to Figure 6-31 are the coast down test of test unit #1 on four leg frame with 1/4 HP motor and circular disk. The cutting off speed was 1060 RPM and the recording time was 20 seconds. Figure 6-29 shows the entire coast down records. It was clearly seen that there were two resonances that occurred during the coast down. One was around 10 second. Another was around 13 second. Figure 6-30 shows the zoom display of the coast down test between 9 to 11 seconds. The period of the acceleration signal was analyzed. The period of the resonance which occurred during that period was equal to 0.07 second, which corresponded to 857 RPM and was caused by the forward rocking mode. Figure 6-31 shows the zoom display of the coast down test between 12 to 14 seconds. The period of the resonance which occurred during this period was 0.074 second, which corresponded to 811 RPM and was caused by the translational mode in the

z direction.

Figures 6-32 and 6-33 are the coast down test of same test setup with cutting off speed of 750 RPM and recording time of 18 seconds. One resonance occurred. The period of the resonance was 0.098 second, which corresponded to 612 RPM and was caused by the backward rocking mode, as shown in Figure 6-33.

Figure 6-34 is the coast down test of test unit #1 on four leg frame with 1/4 HP motor and No. 60799501 fan impeller. The cutting off speed was 1010 RPM and the recording time was 4 seconds. There were some resonances that occurred during the coast down. Because of the effect of the aerodynamic force of the fan impeller, the coast down of the fan impeller was much faster than that of a circular disk. In general, the coast down tests with the fan impellers would not provide much useful information.

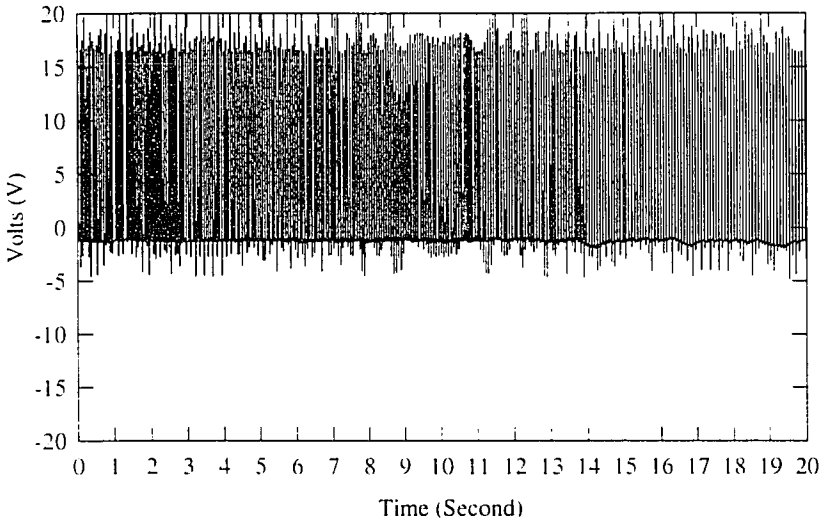

(a) Photocell signal (three pulse per revolution)

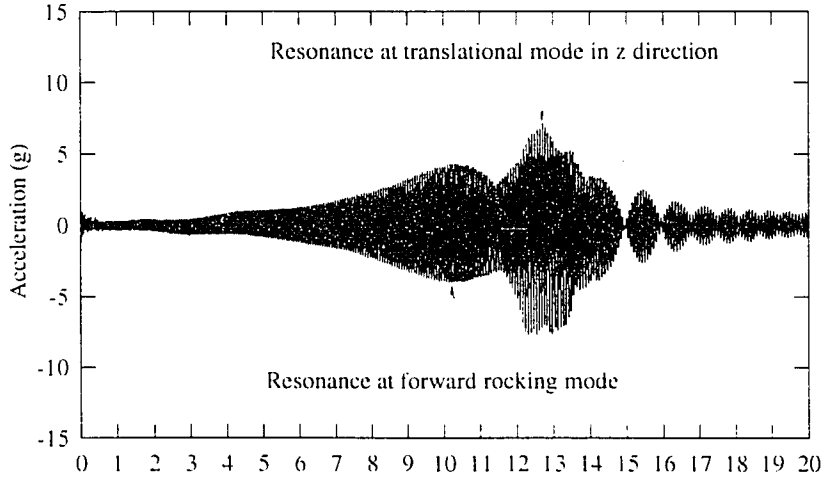

(b) Accelerometer signal

Figure 6-29: The coast down test of test unit #1 on four-leg frame with 1/4 HP motor and circular disk, cutting off at 1060 RPM, 20 second record

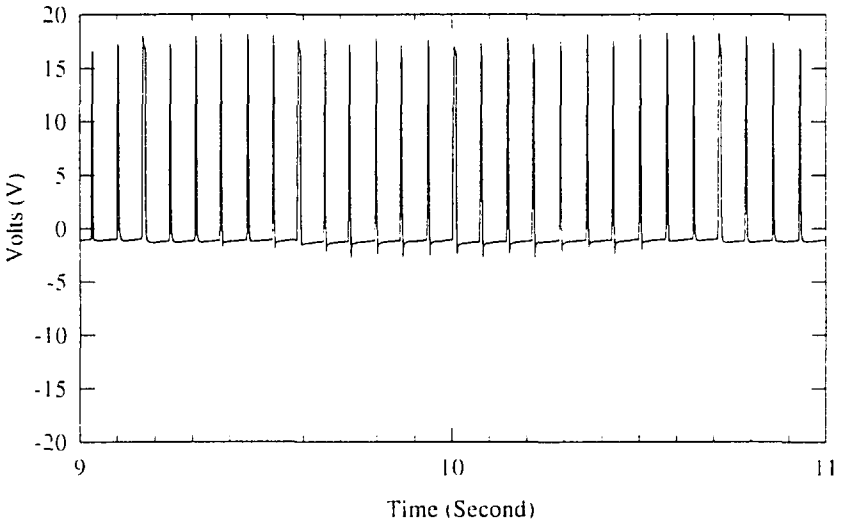

(a) Photocell signal (three pulse per revolution)

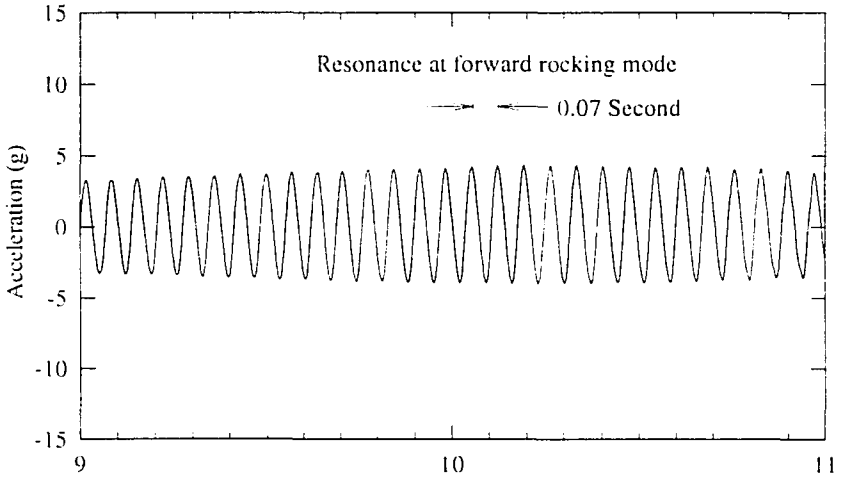

(b) Accelerometer signal

Figure 6-30: The coast down test of test unit #1 on four-leg frame with 1/4 HP motor and circular disk, cutting off at 1060 RPM, 9 - 11 second zoom record

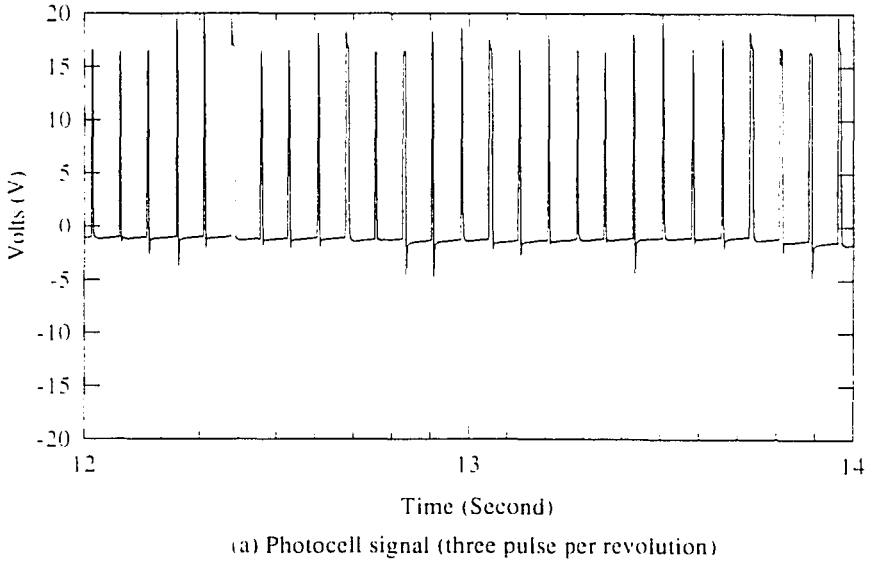

(a) Photocell signal (three pulse per revolution)

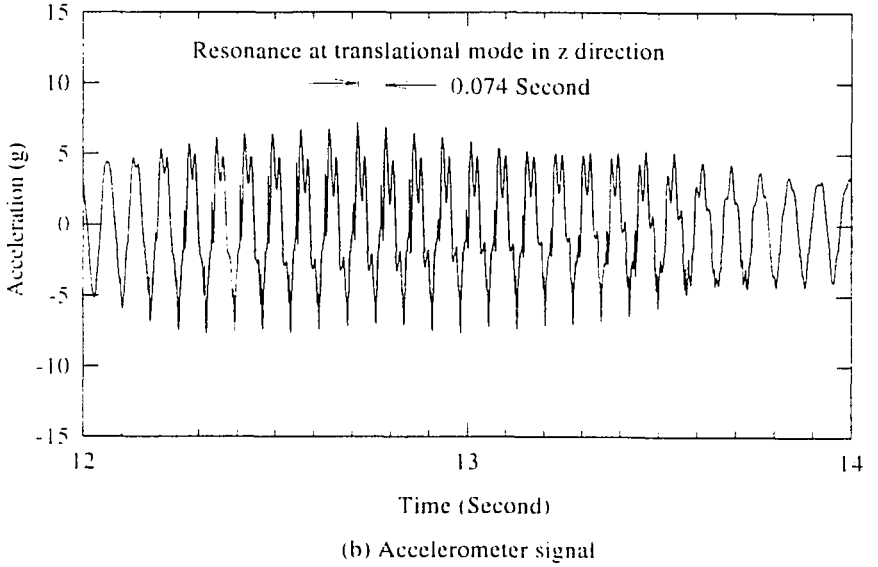

(b) Accelerometer signal

Figure 6-31: The coast down test of test unit #1 on four-leg frame with 1/4 HP motor and circular disk, cutting off at 1060 RPM, 12 - 14 second zoom record

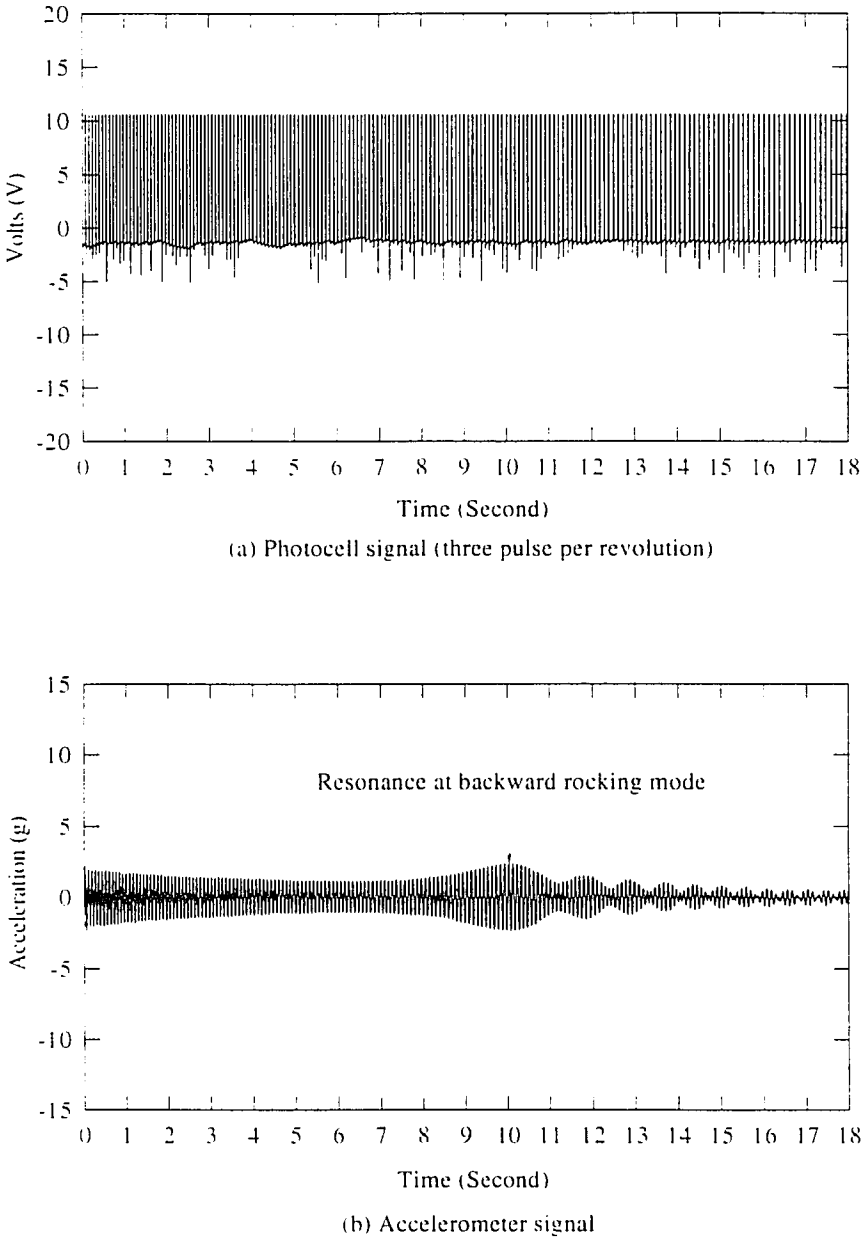

Figure 6-32: The coast down test of test unit #1 on four-leg frame with 1/4 HP motor and circular disk, cutting off at 750 RPM, 18 second record

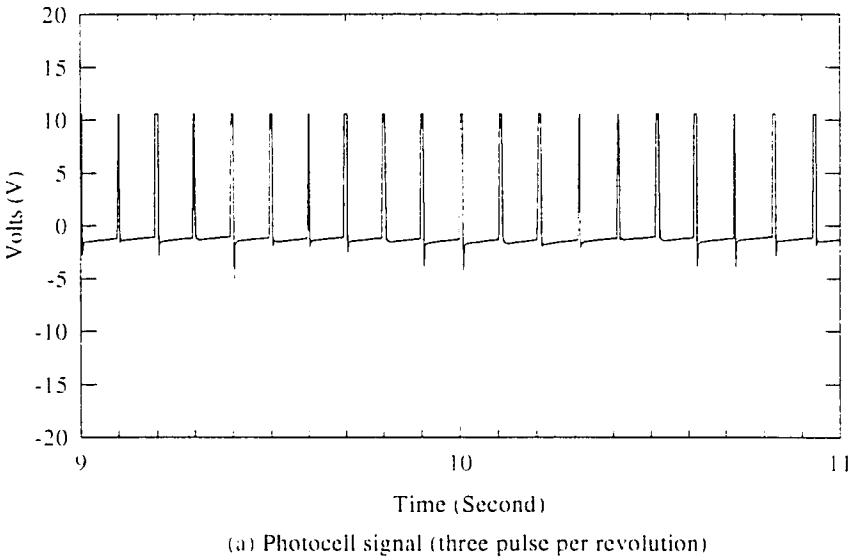

(a) Photocell signal (three pulse per revolution)

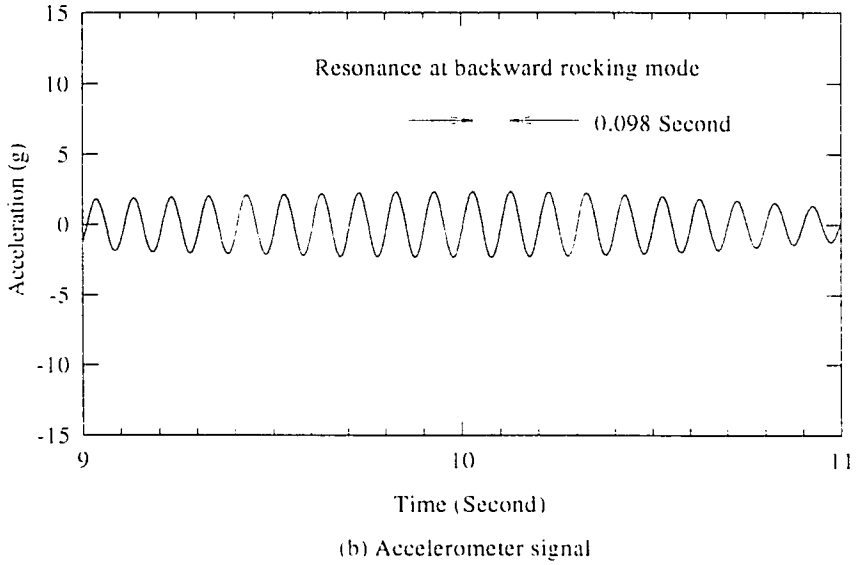

(b) Accelerometer signal

Figure 6-33: The coast down test of test unit #1 on four-leg frame with 1/4 HP motor and circular disk, cutting off at 750 RPM, 9 - 11 second zoom record

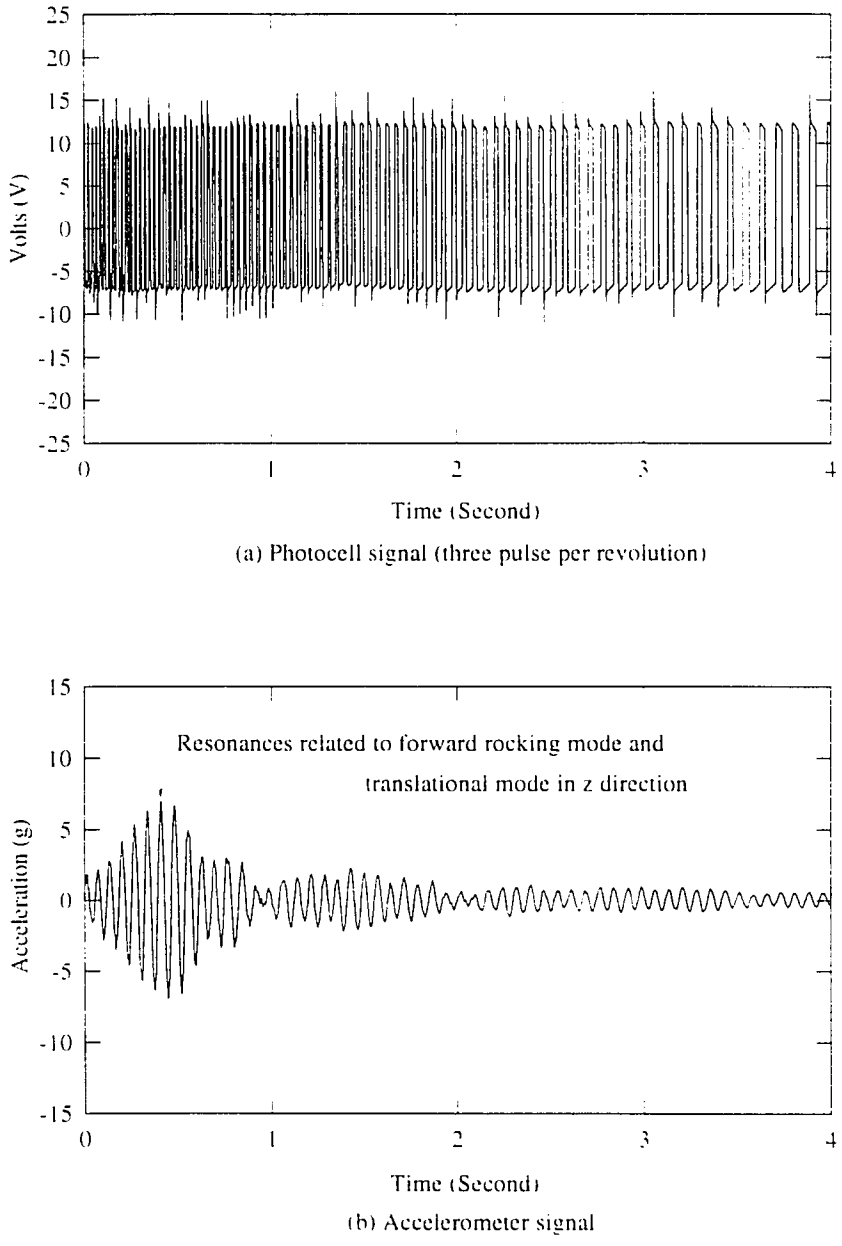

Figure 6-34: The coast down test of test unit #1 on four-leg frame with 1/4 HP motor and No. 60799501 fan impeller, cutting off at 1010 RPM, 4 second record

CHAPTER 7

CONCLUSIONS

Based on both the analytical and experimental works on the vibration modes associated with fan impeller, motor and motor mount system that are excited by fan impeller unbalance, taking into account the gyroscopic effect of the rotating fan impeller, the following conclusions were obtained for test units #1 and #2:

(1) The test procedures, both non-rotating tests and rotating tests, developed in this project can be used to identify and qualify the vibration modes associated with the fan impeller, motor and motor mount systems in the investigated air-conditioning units.

(2) The gyroscopic effect of the rotating fan impeller do have significant effects on both the rocking modes and the swaying modes in the investigated air-conditioning units. This gyroscopic effect forces the resonance frequencies associated with the two non-rotating rocking modes and two non-rotating swaying modes to separate as the rotating speed is increased.

(3) The three dimensional analytical models, in which the gyroscopic effect of the rotating fan impeller was included, show that one of the non-rotating modes will increase in frequency, which is called the forward mode, and the other will decrease in frequency, which is called backward mode. The rotating mobility tests proved that the forward modes and the backward modes happened simultaneously in the investigated air-

conditioning units.

(4) The forward modes can be excited by the fan impeller unbalance and it is a resonance phenomenon. The forward rocking modes caused the vibration problems in the two test units. The backward modes can not be excited by the fan impeller unbalance. They are only important when the aeroelastic stability is considered based on the studies in NASA and Lockheed. In the peak hold spectrum tests conducted in this project, both the forward and backward rocking modes were measured in test units #1 and #2.

(5) Both classical approach, in which the gyroscopic effect of the rotating fan impeller was treated as the additional external moments and their virtual work was included in the system equations, and the energy approach, in which the gyroscopic effect of the rotating fan impeller was treated as an additional kinetic energy and was included in the system equations, were used to develop the three dimensional models. Model 1 from classical approach and model 2 from energy approach gave very good predictions both for the forward and backward modes. The calculated results from model 1 and model 2 matched very well with the experimental data from the rotating mobility tests.

(6) A circular disk was needed to conduct the coast down tests, which gave the same information as the peak hold tests.

(7) The analytical model parameter estimation techniques used in this project gave fairly good results.

APPENDIX A

THE MEASURES STATIC STIFFNESS

OF TEST UNIT #1 ON CASE

In this Appendix, the static stiffness measurement data of test unit #1 on case are presented.

Tables 12 and 13 give the measured data for static stiffness in x direction, K_x. In Table 12, the force was applied at point 3 and displacement was measured at point 1, as shown in Figure 2-1. In Table 13, the force was applied at point 1 and displacement was measured at point 3. The average static stiffness in the x direction was calculated by:

$$K_x = \frac{K_x' + K_x''}{2} \qquad \text{(B-1)}$$

The average static stiffness in the x direction was K_x = 2526.00 lbf/in = 442,000.00 N/m.

Tables 14 and 15 give the measured data for static stiffness in y direction, K_y. In Table 14, the force was applied at point 4 and displacement was measured at point 2, as shown in Figure 2-1. In Table 15, the force was applied at point 2 and displacement was measured at point 4. The average static stiffness in the x direction was calculated by:

$$K_y = \frac{K_y' + K_y''}{2} \qquad \text{(B-2)}$$

The average static stiffness in the y direction was K_y = 2824.00 lbf/in = 494,000.00 N/m.

Table 12: The static stiffness measurement data in the x direction, K_x, for test unit #1 on case, force at point 3 and displacement at point 1

Force (lbf)	10	15	20	25
Displacement (1/1000 in)	4.0	6.0	8.3	10.9
	3.9	6.0	8.0	10.5
	4.0	6.0	8.1	10.3
	4.0	5.8	7.9	10.3
Average Displacement	3.975	5.950	8.075	10.500
Stiffness (lbf/in)	2516.00	2521.00	2477.00	2381.00
Average Stiffness (lbf/in)	K'_x = 2474.00			

Table 13: The static stiffness measurement data in the x direction, K_x, for test unit #1 on case, force at point 1 and displacement at point 3

Force (lbf)	10	15	20	25
Displacement (1/1000 in)	4.0	5.9	7.1	10.1
	3.9	5.9	7.9	10.4
	4.0	5.4	7.5	9.5
	3.8	5.8	7.7	10.0
Average Displacement	3.925	5.750	7.550	10.000
Stiffness (lbf/in)	2548.00	2609.00	2649.00	2500.00
Average Stiffness (lbf/in)	K''_x = 2577.00			

Table 14: The static stiffness measurement data in the y direction, K_y, for test unit #1 on case, force at point 4 and displacement at point 2

Force (lbf)	10	15	20	25
Displacement (1/1000 in)	4.0	5.9	7.6	10.0
	3.9	5.5	7.2	9.2
	3.9	5.2	7.0	9.0
	3.9	5.9	7.9	10.0
Average Displacement	3.925	5.625	7.425	9.550
Stiffness (lbf/in)	2548.00	2667.00	2694.00	2618.00
Average Stiffness (lbf/in)	$K'_y = 2632.00$			

Table 15: The static stiffness measurement data in the y direction, K_y, for test unit #1 on case, force at point 2 and displacement at point 4

Force (lbf)	10	15	20	25
Displacement (1/1000 in)	3.0	4.9	6.3	8.5
	3.2	5.0	6.7	8.7
	3.1	4.9	6.8	8.9
	3.2	5.0	7.0	9.0
Average Displacement	3.125	4.950	6.700	8.775
Stiffness (lbf/in)	3200.00	3030.00	2985.00	2849.00
Average Stiffness (lbf/in)	$K''_y = 3016.00$			

APPENDIX B

THE MEASURED STIFFNESS OF

TEST UNIT #1 ON FOUR LEG FRAME

In this Appendix, the static stiffness measurement data of test unit #1 on four leg frame are presented.

Tables 16 gives the measured data for static stiffness in x direction, K_x. In Table 16, the force was applied at point 1 and displacement was measured at point 3, as shown in Figure 5-1. The average static stiffness in the x direction was calculated by:

$$K_x = K_x' \tag{C-1}$$

The average static stiffness in the x direction was K_x = 1732.00 lbf/in = 303,000.00 N/m.

Tables 17 and 18 give the measured data for static stiffness in y direction, K_y. In Table 17, the force was applied at point 4 and displacement was measured at point 2, as shown in Figure 5-1. In Table 18, the force was applied at point 2 and displacement was measured at point 4. The average static stiffness in the x direction was calculated by:

$$K_x = \frac{K_x' + K_x''}{2} \tag{C-2}$$

The average static stiffness in the y direction was K_y = 2824.00 lbf/in = 494,000.00 N/m.

Table 16: The static stiffness measurement data in the x direction, K_x, for test unit #1 on four leg frame, force at point 1 and displacement at point 3

Force (lbf)	10	15	20	25
Displacement (1/1000 in)	5.5	9.0	11.5	14.5
	5.5	8.5	11.5	14.5
	5.5	8.5	11.5	15.0
	6.0	9.0	11.5	15.0
Average Displacement	5.625	8.750	11.500	14.750
Stiffness (lbf/in)	1778.00	1714.00	1739.00	1695.00
Average Stiffness (lbf/in)	K'_x = 1732.00			

Table 17: The static stiffness measurement data in the y direction, K_y, for test unit #1 on four leg frame, force at point 4 and displacement at point 2

Force (lbf)	10	15	20	25
Displacement (1/1000 in)	5.0	8.5	11.0	14.0
	5.0	8.0	11.0	13.0
	5.0	7.5	11.0	13.5
	5.0	8.0	11.0	13.5
Average Displacement	5.000	8.000	11.000	13.500
Stiffness (lbf/in)	2000.00	1875.00	1818.00	1852.00
Average Stiffness (lbf/in)	K'_y = 1886.00			

Table 18: The static stiffness measurement data in the y direction, K_y, for test unit #1 on four leg frame, force at point 2 and displacement at point 4

Force (lbf)	10	15	20	25
Displacement (1/1000 in)	6.0	9.1	12.1	15.3
	5.3	8.2	11.2	15.0
	5.9	8.9	11.9	15.3
	5.9	9.0	12.1	15.3
Average Displacement	5.775	8.800	11.825	15.225
Stiffness (lbf/in)	1731.00	1705.00	1691.00	1642.00
Average Stiffness (lbf/in)	$K''_y = 1963.00$			

APPENDIX C

THE MATLAB PROGRAMS

In this appendix, the Matlab programs used in this thesis are presented. These programs were used to solve standard and non-standard eigenvalue problems given in the three dimension non-rotational model and the three dimension rotational models.

In the Matlab program, the system response, which are mobilities in the xz and yz planes and the mobility in the z direction, are plotted and the frequency data and mobility data are saved in an user named text file, for example: "datafile.dat". To locate the resonance frequencies of the system, this user named text file must be checked by using a text editor, for example: DOS Editor. At any resonance frequency, the mobility will have maximum amplitude.

For the non-rotational case, because that motions in the xz plane and motions in the yz plane are uncoupled from each other, both mobility data from the xz and yz planes must be checked separately to obtain the rocking modes and swaying modes in different planes.

For the rotating case, motions in the xz plane and motions in the yz plane are coupled from each other. Only the mobility data from the xz or yz planes needs to be checked to obtain the both forward and backward rocking modes and swaying modes.

D.1 The Matlab program for model 1

In the three dimension rotational model 1, which was developed in Section 3.2, the forward and backward modes are given simultaneously by the model. To obtain the forward and backward modes at different speed, the parameter "Speed" in the program must be changed in each calculation.

The followings are Matlab program.

```
clc, clg, clear
%  This is Matlab file for calculating the frequency response function (FRF) of five degree
% of freedom system of test unit #1 and #2 including the gyroscopic effect of the rotating
% fan impeller.
*************************************************************************************
disp('This is test unit #1 with 1/4 HP motor & 60799501 fan on four-leg frame')
disp('including gyroscopic effect of the rotating fan impeller')
*************************************************************************************
% Input the system parameters (in SI units)
%-------------------------------------------------------------------------------
% Mass in Kg: M3 - Motor; M4 - Fan; Mx, My & Mz - Equivalent masses in the
%                                   x, y, z directions;
M3 = 5.9;     M4 = 1.45;    Mx = 18.1;    My = 17.6;   Mz = 2.03;
%-------------------------------------------------------------------------------
%
%-------------------------------------------------------------------------------
% Mass Moment of Inertia in Kg-m^2: I3 - Motor; I4 - Fan; Ia - Fan Impeller along the
% rotating axis; Ix & Iy - Equivalent mass moment of inertia in xz and yz planes;
```

```
I3 = 0.0138;   I4 = 0.0205;   Ia = 0.0378;   Ix = 0.00927;  Iy = 0.00858;
%-------------------------------------------------------------------------
%
%-------------------------------------------------------------------------
% Mass Center to Unit Top in meter: L3 - Motor:  L4 - Fan;
L3 = 0.059;    L4 = 0.14;
%-------------------------------------------------------------------------
%
%-------------------------------------------------------------------------
% Equivalent Translational Stiffness of System in N/m: Kx, Ky & Kz
Kx = 303000.0;  Ky = 313000.0;  Kz = 70000.0;
%-------------------------------------------------------------------------
%
%-------------------------------------------------------------------------
% Equivalent Rocking Stiffness of System in N-m: Kqx and Kqy
Kqx = 546.0;   Kqy = 601.0;
%-------------------------------------------------------------------------
% End of input system parameters.
% Mass Matrix of system [M] ---------------------------------------------
M(1,1)=Mx+M3+M4;  M(1,2)=M3*L3+M4*L4;  M(1,3)=0;  M(1,4)=0;  M(1,5)=0;
M(2,1)=M3*L3+M4*L4; M(2,2)=Ix+I3+I4+M3*L3^2+M4*L4^2; M(2,3)=0;
M(2,4)=0; M(2,5)=0;
M(3,1)=0;  M(3,2)=0;  M(3,3)=My+M3+M4;  M(3,4)=M3*L3+M4*L4;  M(3,5)=0;
M(4,1)=0; M(4,2)=0; M(4,3)=M3*L3+M4*L4; M(4,4)=Iy+I3+I4+M3*L3^2+M4*L4^2;
M(4,5)=0;
M(5,1)=0;  M(5,2)=0;  M(5,3)=0;  M(5,4)=0;  M(5,5)=Mz+M3+M4;
%-------------------------------------------------------------------------
```

```
%
% Non-Rotational Stiffness Matrix of system [K] ----------
K(1,1)=Kx;  K(1,2)=0 ;  K(1,3)=0 ; K(1,4)=0  ; K(1,5)=0 ;
K(2,1)=0 ;  K(2,2)=Kqx;  K(2,3)=0 ; K(2,4)=0  ; K(2,5)=0 ;
K(3,1)=0 ;  K(3,2)=0  ;  K(3,3)=Ky; K(3,4)=0  ; K(3,5)=0 ;
K(4,1)=0 ;  K(4,2)=0  ;  K(4,3)=0 ; K(4,4)=Kqy; K(4,5)=0 ;
K(5,1)=0 ;  K(5,2)=0  ;  K(5,3)=0 ; K(5,4)=0  ; K(5,5)=Kz;
%----------
Itx = Ix+I3+I4+M3*L3^2+M4*L4^2;
Ity = Ix+I3+I4+M3*L3^2+M4*L4^2;
jj = sqrt(-1);
Speed = 900.0                    % Rotating Speed of the fan impeller in RPM.
SS=Speed*2*pi/60;                % Speed = 0 gives the non-rotating case;
% Prepare data for ploting the Dynamic Compliance, Mobility and Accelerance;
df = 0.1;                        % frequency resolution in Hz;
ffinal = 50.0;                   % frequency range in Hz
for i = 1:(ffinal/df-9)          % frequency range
 f(i) = (i+9)*df;
 w = 2*pi*f(i);                  % angular frequency
% Dynamic Stiffness Matrix [Kd] ----------
Kd(1,1)=K(1,1)-w^2*M(1,1); Kd(1,2)=K(1,2)-w^2*M(1,2);
Kd(1,3)=K(1,3)-w^2*M(1,3); Kd(1,4)=K(1,4)-w^2*M(1,4);
Kd(1,5)=K(1,5)-w^2*M(1,5);
Kd(2,1)=K(2,1)-w^2*M(2,1); Kd(2,2)=K(2,2)-w^2*M(2,2);
Kd(2,3)=K(2,3)-w^2*M(2,3); Kd(2,4)=K(2,4)-w^2*M(2,4)+(Ia*SS*w)*jj;
Kd(2,5)=K(2,5)-w^2*M(2,5);
Kd(3,1)=K(3,1)-w^2*M(3,1); Kd(3,2)=K(3,2)-w^2*M(3,2);
```

```
Kd(3,3)=K(3,3)-w^2*M(3,3); Kd(3,4)=K(3,4)-w^2*M(3,4);
Kd(3,5)=K(3,5)-w^2*M(3,5);
Kd(4,1)=K(4,1)-w^2*M(4,1); Kd(4,2)=K(4,2)-w^2*M(4,2)-(Ia*SS*w)*jj;
Kd(4,3)=K(4,3)-w^2*M(4,3); Kd(4,4)=K(4,4)-w^2*M(4,4);
Kd(4,5)=K(4,5)-w^2*M(4,5);
Kd(5,1)=K(5,1)-w^2*M(5,1); Kd(5,2)=K(5,2)-w^2*M(5,2);
Kd(5,3)=K(5,3)-w^2*M(5,3); Kd(5,4)=K(5,4)-w^2*M(5,4);
Kd(5,5)=K(5,5)-w^2*M(5,5);
%-----------------------------------------------------------------------
% Dynamic Compliance Matrix [DC]
    DC = inv(Kd);
    Cxz(i) = abs(DC(2,2));    % Compliance in xz plane
    Mxz(i) = w*Cxz(i);        % Mobility in xz plane
    Cyz(i) = abs(DC(4,4));    % Compliance in yz plane
    Myz(i) = w*Cyz(i);        % Mobility in yz plane
    Cz(i) = abs(DC(5,5));     % Compliance in z direction
    Mz(i) = w*Cz(i);          % Mobility in z direction
    out(i,1) = f(i);          % Save frequency data and mobility data to array OUT
    out(i,2) = Mxz(i);
    out(i,3) = Myz(i);
    out(i,4) = Mz(i);
end
%
% Write the rotating speed, frequency and mobility data to a text file <<datafile.dat>>,
% user can change this ftext file name with his own name.
save datafile.dat Speed out /ascii;
% Plot the mobility of the system in the xz and yz planes and in the z direction.
```

```
loglog(f, Mxz, ':', f, Myz, '—', f, Mz, '-.'),
title(' The mobility plot of the system in the xz and yz planes and in the z direction'),
xlabel('Frequency (Hz)'), ylabel('Mobility m/s*N'),
pause
quit
```

D.2 The Matlab program for model 2

In the three dimension rotational model 2 developed in Section 3.3, to calculate the forward modes, the parameter "Speed" in the Matlab file must be positive. For a given "Speed", the system will give four peaks (the system response in the z direction is not affected by rotational fan impeller, this peak is unchanged and not included). Among these four peaks, there will be two peaks which are not changed with the changes of "Speed". They are not the modes of interest. The other two peaks will increase in frequency smoothly with the increases of "Speed". These two peaks correspond to the forward rocking mode and forward swaying mode. Because that the motions in the xz plane and motions in the yz plane are coupled from each other, the mobility in the xz plane and mobility in the yz plane will give same peaks.

To calculate the backward modes, the parameter "Speed" in the Matlab file must be negative. For a given "Speed", the system will give four peaks (the system response in the z direction is not affected by rotational fan impeller, this peak is unchanged and not included). Among these four peaks, there will be two peaks which will decrease in frequency with increases of "-Speed" sharply. They are not the modes of interest. The other two peaks will decrease in frequency smoothly with the increases of "-Speed". These two peaks correspond to the backward rocking mode and backward swaying mode.

The difference between the Matlab programs for model 1 and model 2 is that they have different Dynamic Stiffness Matrix. Followings are different part of Matlab program used by model 2.

```
Speed = 900.0                    % Rotating Speed of the fan impeller in RPM.
SS=Speed*2*pi/60;                % Speed = 0 gives the non-rotating case;
if abs(Speed) > 0.0              % If capital Omiga is not equal zero, small Omiga
   As = 1.0;                     % is not equal zero too.
   else                          % If capital Omiga is equal to zero, small Omiga
   As = 0.0;                     % is equal zero too.
end;
% Prepare data for ploting the Dynamic Compliance, Mobility and Accelerance;
df = 0.1;                        % frequency resolution in Hz;
ffinal = 50.0;                   % frequency range in Hz
for i = 1:(ffinal/df-9)          % frequency range
 f(i) = (i+9)*df;
 w = 2*pi*f(i);                  % angular frequency
% Dynamic Stiffness Matrix [Kd] ----------------------------------------------------
Kd(1,1)=K(1,1)-w^2*M(1,1); Kd(1,2)=K(1,2)-w^2*M(1,2);
Kd(1,3)=K(1,3)-w^2*M(1,3); Kd(1,4)=K(1,4)-w^2*M(1,4);
Kd(1,5)=K(1,5)-w^2*M(1,5);
Kd(2,1)=K(2,1)-w^2*M(2,1); Kd(2,2)=K(2,2)+Ia*SS*w+As*(Ia-Itx)*w^2-w^2*M(2,2);
Kd(2,3)=K(2,3)-w^2*M(2,3); Kd(2,4)=K(2,4)+Ia*SS*w+As*Ia*w^2-w^2*M(2,4);
Kd(2,5)=K(2,5)-w^2*M(2,5);
Kd(3,1)=K(3,1)-w^2*M(3,1); Kd(3,2)=K(3,2)-w^2*M(3,2);
Kd(3,3)=K(3,3)-w^2*M(3,3); Kd(3,4)=K(3,4)-w^2*M(3,4);
Kd(3,5)=K(3,5)-w^2*M(3,5);
Kd(4,1)=K(4,1)-w^2*M(4,1); Kd(4,2)=K(4,2)+Ia*SS*w+As*Ia*w^2-w^2*M(4,2);
Kd(4,3)=K(4,3)-w^2*M(4,3); Kd(4,4)=K(4,4)+Ia*SS*w+As*(Ia-Ity)*w^2-w^2*M(4,4);
Kd(4,5)=K(4,5)-w^2*M(4,5);
```

```
Kd(5,1)=K(5,1)-w^2*M(5,1); Kd(5,2)=K(5,2)-w^2*M(5,2);
Kd(5,3)=K(5,3)-w^2*M(5,3); Kd(5,4)=K(5,4)-w^2*M(5,4);
Kd(5,5)=K(5,5)-w^2*M(5,5);
%-----------------------------------------------------------------------
```

D.3 The Matlab program for model 3

All the discussions for model 2 are applicable for model 3. The difference between the Matlab programs for model 2 and model 3 is the different Dynamic Stiffness Matrix. Followings are different part of Matlab program used by model 3.

```
% Dynamic Stiffness Matrix [Kd] ----------------------------------------
Kd(1,1)=K(1,1)-w^2*M(1,1); Kd(1,2)=K(1,2)-w^2*M(1,2);
Kd(1,3)=K(1,3)-w^2*M(1,3); Kd(1,4)=K(1,4)-w^2*M(1,4);
Kd(1,5)=K(1,5)-w^2*M(1,5);
Kd(2,1)=K(2,1)-w^2*M(2,1); Kd(2,2)=K(2,2)+Ia*SS*w+(Ia-Itx)*SS^2-w^2*M(2,2);
Kd(2,3)=K(2,3)-w^2*M(2,3); Kd(2,4)=K(2,4)+Ia*SS*w+Ia*SS^2-w^2*M(2,4);
Kd(2,5)=K(2,5)-w^2*M(2,5);
Kd(3,1)=K(3,1)-w^2*M(3,1); Kd(3,2)=K(3,2)-w^2*M(3,2);
Kd(3,3)=K(3,3)-w^2*M(3,3); Kd(3,4)=K(3,4)-w^2*M(3,4);
Kd(3,5)=K(3,5)-w^2*M(3,5);
Kd(4,1)=K(4,1)-w^2*M(4,1); Kd(4,2)=K(4,2)+Ia*SS*w+Ia*SS^2-w^2*M(4,2);
Kd(4,3)=K(4,3)-w^2*M(4,3); Kd(4,4)=K(4,4)+Ia*SS*w+(Ia-Ity)*SS^2-w^2*M(4,4);
Kd(4,5)=K(4,5)-w^2*M(4,5);
Kd(5,1)=K(5,1)-w^2*M(5,1); Kd(5,2)=K(5,2)-w^2*M(5,2);
Kd(5,3)=K(5,3)-w^2*M(5,3); Kd(5,4)=K(5,4)-w^2*M(5,4);
Kd(5,5)=K(5,5)-w^2*M(5,5);
%-----------------------------------------------------------------------
```

REFERENCE

1. "Papers Presented at the Symposium on Propeller Fan Vibration," ASHRAE Annual Meeting, Louisville, Kentucky, June 24-28, 1973.

2. D. D. Reynolds and T. N. Cranes, "Propeller Fan Dynamics I: Static Vibration Test Procedure (ASHRAE RP 266)," ASHRAE Transactions, Vol. 90, Part 1, 1984.

3. D. D. Reynolds and T. N. Cranes, "Propeller Fan Dynamics II: Dynamic Vibration Test Procedure (ASHRAE RP 266)," ASHRAE Transactions, Vol. 90, Part 1, 1984.

4. ASHRAE Standard 87.1 - 1992: Method of Testing Fan Vibration - Blade Vibrations and Critical Speeds," 1992.

5. D. D. Reynolds, J. M. Bledsoe, W. Culbreth, and S. G. Ladkany, "Vibration Response of Propeller Fans under Actual Operating Conditions: I. Operational Tests of Four-Bladed Fans (ASHRAE RP 477)," ASHRAE Transactions, Vol. 95, Part 2, 1989.

6. S. G. Ladkany, D. D. Reynolds, M. S. Rouas, and P. K. Baade, "Vibration Response of Propeller Fans under Actual Operating Conditions: II. Finite Element Studies of the Vibration Response of Propeller Fans under Centrifugal Stiffening (ASHRAE RP 477)," ASHRAE Transactions, Vol. 96, Part 1, 1990.

7. S. G. Ladkany, D. D. Reynolds, and M. S. Rouas, "Vibration Response of Propeller Fans under Actual Operating Conditions: III. Finite Element Studies of the Influence of Welded and Riveted Connections on the Vibration Response of Propeller Fans (ASHRAE RP 477)," ASHRAE Transactions, Vol. 95, Part 2, 1989.

8. S. G. Ladkany, M. S. Rouas, and D. D. Reynolds, "Vibration Response of Propeller Fans under Actual Operating Conditions: IV. Automatic Generation of Curved and Twisted Propeller Fan Surfaces by Finite Elements (ASHRAE RP 477)," ASHRAE Transactions, Vol. 95, Part 2, 1989.

9. Den Hartog, Mechanical Vibrations, McGraw-Hill Co., New York, 1972.

10. "Report S-1 from Joy Manufacturing Cooperation," 1976.

11. Peter Rogers, "Genuine Modal Testing of Rotating Machinery," Sound and Vibration, January, 1988, pp. 36-42.

12. W. T. Thomson, F. C. Younger, and H. S. Gordon, "Whirl Stability of the Pendulously Supported Flywheel System," Transaction of the ASME, Journal of Applied Mechanics, June 1977, pp. 322-328.

13. D. R. Chivens and H. D. Nelson, "The Natural Frequencies and Critical Speeds of a Rotating, Flexible Shaft-Disk System," Transaction of the ASME, Journal of Engineering for Industry, August 1975, pp. 881-886.

14. D. J. Salamone and E. J. Gunter, "Synchronous Unbalance Response of an Overhung Rotor with Disk Skew," Transaction of the ASME, Journal of Engineering for Power, October 1980, pp. 749-755.

15. N. Hagwara and H. Ijima, "Coupled Whirling Dynamics of Flexible Bladed Disk/ Shaft System Considering Coriolis Effects," Rotating Machinery Dynamics, Vol. 12, ASME, New York, 1987, pp. 305-317.

16. F. Sisto, A. Chang and M. Sutcu, "The Influence of Coriolis Forces on Gyroscopic Motion of Sinning Blades," ASME Paper 82-GT-163.

17. S. H. Crandall and J. Dugundji, "Forced Backward Whirling of Aircraft Propeller-Engine Systems," Second International Conference on Vibration in Rotating Machinery, Institute of Mechanical Engineers, U. K., 1980, pp. 265-270.

18. S. H. Crandall and J. Dugundji, "Resonant Whirling of Aircraft Propeller-Engine Systems," Transactions of ASME, Journal of Applied Mechanics, December 1981, pp. 929-935.

19. R. O. Fehr and D. F. Muster, "Electric-Motor and Generator Noise," Chapter 30, Handbook of Noise Control, C. Harris, editor, McGraw-Hill Co., New York, 1957.

20. T. Yokozuka, "Effects of Rotor Slot Shape on the Alternating Torque Characteristics of Condenser Motors," Electrical Engineering in Japan, Vol. 95, No. 6, 1975, pp. 61-69.

21. S. Williamson, D. Pearson, and A. M. Rugege, "Acoustic Noise and Pulsating Torques in a Triac-Controlled Permanent-Split-Capacitor Fan Motor, IEEE Proceedings, Vol. 128, Part B, No. 4, July 1981, pp. 201-206.

22. T. M. Holdsworth and R. D. Morris, "The Use of Induction Motors as Vibration Generators," Sound and Vibration, November 1976, pp. 24-28.

23. C. M. Harris and C. E. Crede, Shock and Vibration Handbook, Vol. 1, McGraw-Hill, 1961.

24. E. R. Collins, "Torque and Slip Behavior of Single-Phase Induction Motors Driven from Variable-Frequency Supplies," IEEE Transactions on Industry Applications, Vol. 28, No. 3, May/June 1992.

25. C. G. Veinott, How to Design a Single-Phase Motor on a Personal Computer,

3rd edition, 1992, C. G. Veinott Publisher.

26. R. Belmans, K. J. Binns, W. Geysen, and A. Vandenput, Vibrations and Audible Noise in Alternating Current Machines, Kluwer Academic Publications, 1988.

27. H. H. Woodsen, "Possible Errors in Measurement of Air-Gap Torque Pulsations in Induction Motors," IEEE Transaction on Energy Conversion, Vol.7, No. 1, 1992.

28. ANSI S2.34-1984, "American National Standard Guide to the Experimental Determination of Rotational Mobility Properties and the Complete Mobility Matrix," Standards Secretariat of the Acoustical Society of American, New York, 1984.